Saint Petersburg State University

Manuscript copy

Kostin Mikhail Aleksandrovich

NMR AND IR SPECTRAL DIAGNOSTICS OF HYDROGEN BONDS INVOLVING P=O GROUP

Specialization 1.3.6. Optics

Dissertation is submitted

for the degree of Candidate of Physical and Mathematical Sciences

Translation from Russian

Scientific supervisor:

Doctor in Chemical Sciences, professor

Peter M. Tolstoy

Saint Petersburg

2024

Table of contents

Introduction

Relevance of the research topic

Hydrogen bonds are a special group of non-covalent interactions due to their extraordinary abundance and, in many cases, high strength. These interactions are found in many low molecular weight substances (water, ammonia, alcohols, carboxylic acids and *etc.*) and high molecular weight substances (many polymers, the DNA double helix, secondary and tertiary structure of proteins and *etc.*). Hydrogen bonds often determine the physical and chemical properties of substances: boiling and melting points; solubility, extensibility, plasticity and strength of materials; electrical conductivity; affect lipophilicity, permeability and binding of drug compounds to proteins and *etc.* Increased interest in studying properties of hydrogen bonds is associated with a possibility of their practical application, for example, for a development of new materials and medicines, for a self-assembly of supramolecular structures, for determination and prediction of a biological activity of compounds.

The main characteristics of hydrogen bonds include their strength and geometry, which determine the potential use of hydrogen bonds in practice. Therefore, many studies of hydrogen bonds are aimed at determining the numeric values of these characteristics. Experimentally, direct measurement of the strength or geometry of hydrogen bonds is often unavailable or difficult, especially for disordered media (liquid, amorphous). In these cases, the observed spectral characteristics of hydrogen bonds are often used as descriptors of strength and geometry. Such informative spectral parameters include, for example, chemical shifts, spin-spin interaction constants in NMR spectra, frequencies and intensities of vibrations of proton acceptor and proton donor groups in vibrational spectra, and others. Quantum chemistry methods can also be used to determine the spectral characteristics of hydrogen bonds. However, the solution to the inverse spectral problem, *i.e.* determining the values of the strength and geometry of hydrogen bonds using spectral characteristics becomes possible only with the preliminary establishment of correlations

(or functional dependencies in some cases) connecting the spectral and energetic, geometric parameters with each other. Determining the most informative spectral characteristics, establishing their dependencies between the strength and geometry of hydrogen bonds, and estimating the universality of the obtained dependencies remain an urgent task.

For example, phosphine oxides with the general formula $R_3P{=}O$ can act as probe molecules – electron donors (proton acceptors). Phosphine oxides have proven themselves as partners in the formation of intermolecular complexes with Lewis acids. A number of studies have noted the high sensitivity of IR and NMR spectral characteristics of P=O group (the stretching vibration band of P=O group in IR spectra and the ^{31}P chemical shift in NMR spectra) to the properties of hydrogen bonds. Thus, it can be expected that correlations between the spectral characteristics of a selected phosphine oxide and the properties of hydrogen bonds could potentially be used to estimate hydrogen bond strength and geometry. However, studies that establish such correlations are quite rare, and the set of selected proton donor molecules has been often limited and covers a small range of changes in the strength (geometry) of hydrogen bond.

The aim and objectives of the study

The general aim of the studies presented in this work is to establish correlations between the spectral characteristics of phosphine oxides and the strength of hydrogen bonds in complexes with various proton donors theoretically using quantum chemistry methods and experimentally using IR and NMR spectroscopy.

The following tasks were identified:

1. Perform quantum mechanical modeling of geometry of complexes with one hydrogen bond between trimethylphosphine oxide and a wide range of proton donors in a polar aprotic medium. Calculate the strength of hydrogen bonds, IR and NMR spectral characteristics of the complexes. To evaluate the possibility of using IR and NMR spectral

characteristics of trimethylphosphine oxide to estimate the strength and geometry of the hydrogen bonds.

2. Perform quantum mechanical calculations of geometry and spectral characteristics of complexes with two hydrogen bonds between triphenylphosphine oxide and the same set of proton donors. Establish general correlations between geometry, strength and spectral parameters of complexes with one and two hydrogen bonds. Evaluate the cooperativity (anticooperativity) effects on the same parameters.

3. Using experimental low-temperature ^{1}H and ^{31}P NMR spectroscopy, establish the stoichiometry of complexes formed by triphenylphosphine oxide and a set of substituted phenols in the mixture of liquefied deuterated freons CDF_3/CDF_2Cl, build a correlation between the enthalpy of formation of complexes and the ^{31}P NMR chemical shift. Determine the factors influencing the ^{31}P NMR chemical shift during the complexation.

4. Using experimental IR spectroscopy measurements, study complexes of triphenylphosphine oxide, tri-*n*-butylphosphine oxide, hexamethylphosphoramide and substituted phenols in CCl_4 solution: estimate the complexation enthalpy and establish a correlation between the frequency of the stretching vibration of P=O group of phosphine oxide and the enthalpy of complexation.

Methods of research

The study results presented in this work were obtained using the following physical and chemical methods, both theoretical and experimental:

1. Quantum chemical calculations of geometry and spectral characteristics of complexes using density functional theory (DFT);

2. Topological analysis of electron density in complexes, calculation of electron density parameters at critical points;

3. Low-temperature ^{1}H and ^{31}P NMR spectroscopy for solutions in the mixture of liquefied deuterated freons CDF_3/CDF_2Cl;

4. IR spectroscopy for CCl_4 solutions at room temperature.

The research methods used and additional experimental details are described in detail in each chapter of this work.

Scientific novelty and theoretical, practical application of research findings

As the main result of the work, the set of correlations is presented that are proposed to be used to estimate the strength of hydrogen bonds in complexes using the IR and NMR spectral characteristics of phosphine oxides when direct measurement of the strength by other methods is unavailable or difficult. Supposedly, these correlations will hold under similar conditions for other acids over a wide range of their proton-donating abilities. The use of phosphine oxides as spectral probes for estimating the proton-donating abilities of acids represents the next stage in the development of research devoted to the spectral diagnostics of hydrogen bonds.

The reliability of the results obtained.

The reliability of the experimental results obtained is ensured by the use of modern instrument base. The selected conditions and details of experiments performed by IR and NMR spectroscopy methods have proven themselves well for studying the geometric, energetic and spectral characteristics of complexes with hydrogen bonds, which is confirmed by a significant number of publications and the volume of accumulated data. The obtained results are also confirmed by additional test studies performed with the replacement of the used solvent or phosphine oxide. The reliability of the results of quantum chemical calculations is additionally ensured by test calculations at different levels of theory and under different conditions. Both experimental and theoretical results have been internationally peer-reviewed and published in the first quartile journal Physical Chemistry Chemical Physics.

Approbation.

The main results of this work were presented at the following conferences: the XX Symposium on High Resolution Molecular Spectroscopy (Russia, Irkutsk, 2023), 2nd International Symposium “Noncovalent Interactions in Synthesis, Catalysis, and Crystal Engineering” (Russia, Moscow, 2022), 16th International School-Conference “Spinus. Magnetic resonance and its applications” (Russia, Saint Petersburg, 2020), International Polymer Characterization Forum POLY-CHAR-2019 (Nepal, Kathmandu, 2019).

Publications on the research topic

1. Kostin M.A., Pylaeva S.A., Tolstoy P.M., “Phosphine oxides as NMR and IR spectroscopic probes for the estimation of the geometry and energy of PO···H–A hydrogen bonds”, Physical Chemistry Chemical Physics, 2022, 24, 7121−7133
2. Kostin M.A., Alkhuder O., Xu L., Krutin D.V., Asfin R.E., Tolstoy P.M., “Complexes of phosphine oxides with substituted phenols: hydrogen bond characterization based on shifts of P=O stretching bands”, Physical Chemistry Chemical Physics, 2024, 26, 10234–10242

Other publication

1. Tupikina E.Yu., Titova A.A., Kaplanskiy M.V., Chakalov E.R., Kostin M.A., Tolstoy P.M., “Estimations of OH···N hydrogen bond length from positions and intensities of IR bands”, Spectrochimica Acta Part A: Molecular and Biomolecular Spectroscopy, 2022, 275, 121172
2. Tupikina E.Yu., Tolstoy P.M., Titova A.A., Kostin M.A., Denisov G.S., “Estimations of FH···X hydrogen bond energies from IR intensities: Iogansen's rule revisited”, The Journal of Computational Chemistry, 2021, 42(8), 564–571
3. Melnikova D.L., Badrieva Z.F., Kostin M.A., Maller C., Stas M., Buczek A., Broda M.A., Kupka T., Kelterer A.-M., Tolstoy P.M., Skirda V.D., “On Complex Formation between 5-Fluorouracil and β-Cyclodextrin in Solution and in the Solid State: IR Markers and Detection of Short-Lived Complexes by Diffusion NMR”, Molecules, 2020, 25, 5706
4. Mulloyarova V.V., Giba I.S., Kostin M.A., Denisov G.S., Shenderovich I.G., Tolstoy P.M., “Cyclic trimers of phosphinic acids in polar aprotic solvent: Symmetry, chirality and H/D isotope effects on NMR chemical shifts”, Physical Chemistry Chemical Physics, 2018, 20, 4901–4910

The results of the research presented in these publications are not included in the text of the dissertation.

The main scientific results.

1. The geometry and strength of hydrogen bonds in the set of 140 complexes (1:1 and 1:2 complexes), formed by trimethylphosphine oxide and one or two OH, CH, NH and NH^+ proton donors, were studied using quantum chemistry methods. It has been established that the IR and NMR spectral characteristics of trimethylphosphine oxide correlate well with the strength of one hydrogen bond and the total strength of two hydrogen bonds in the complex over the wide range of their energies and

geometries. Correlations were determined between the anticooperativity effects on the strength, geometry and spectral parameters of hydrogen bonds in 1:2 complexes and the strength of hydrogen bonds in 1:1 complexes [1] (pp. 7127–7129; the results of the study of complexes 1:2 are being prepared for publication). Personal contribution of the author: all the main results were obtained personally by the author or as the result of collaboration with other researchers, which is explicitly stated in appropriate chapters.

2. For complexes of triphenylphosphine oxide, tri-*n*-butylphosphine oxide, hexamethylphosphoramide with the set of nine substituted phenols and one alcohol in solution in CCl_4, the power correlation between the frequency of stretching vibration of P=O group of the phosphine oxide and the strength of hydrogen bond in the complexes was experimentally found using IR measurements. IR spectroscopy has been proposed as the fast and accurate method for estimating hydrogen bond strength in complexes using obtained correlation [2] (pp. 10240–10241). Personal contribution of the author: all the main results were obtained personally by the author or as the result of collaboration with other researchers, which is explicitly stated in appropriate chapters.
3. Using low-temperature NMR spectroscopy in solution in the liquefied deuterated freons CDF_3/CDF_2Cl at a temperature of 100 K, the complexation of triphenylphosphine oxide with various substituted phenols was experimentally studied. The formation of complexes of both 1:1 and 1:2 stoichiometries has been proven. For the first time, the formation of triphenylphosphine oxide complex with three hydrogen bonds (complex 1:3) was found. The power correlation has been proposed between the ^{31}P NMR chemical shift and hydrogen bond strength, which is common for complexes of different stoichiometries (the results of this study are being prepared for publication). Personal contribution of the author: all the main results were obtained personally by the author or as the result of collaboration with other researchers, which is explicitly stated in appropriate chapters.

Statements put forward for defense.

1. Phosphine oxides may be involved in formation complexes with one, two and three hydrogen bonds between P=O group and proton donors in solution.

2. The chemical shift of phosphorus and the frequency of P=O stretching vibration correlate with interatomic distances and hydrogen bond strengths in hydrogen-bonded complexes. The correlations are nonlinear and universal for complexes of various stoichiometry over a wide range of hydrogen bond strengths.

3. Hydrogen bonds formed by one P=O group and two proton donors interact anticooperatively. Anticooperativity effects were found on the strength and geometry of hydrogen bonds. The values of these effects are determined by the proton donor ability of the molecules involved in the formation of hydrogen bonds and may be assessed from the spectral characteristics of P=O group: ^{31}P NMR chemical shift and stretching vibrations frequency.

Chapter 1. Hydrogen bond: characteristics, main research methods

This chapter contains information about the basic properties of hydrogen bonds, the most commonly used and informative physical and chemical methods for studying hydrogen bonds, as well as an overview of the possibility of using probe molecules to determine the main characteristics of hydrogen bonds.

1.1. Definition of hydrogen bond

The first hypotheses about the existence of hydrogen bonds appeared at the beginning of the last century [3–6]. Attempts to give a generalized definition of hydrogen bonds and to clarify their physical nature began to be made with the development of the theory of valency, quantum mechanics and ideas about the structure of atoms and molecules [7–12]. The accumulation of significant experimental and computational material made it possible to present the most general definition of hydrogen bonds, given by IUPAC in 1997 and refined in 2011 [13]. The latter definition is supplemented by criteria for the formation of a hydrogen bond and is generally accepted.

According to IUPAC [13], a hydrogen bond is the interaction between a hydrogen atom, free or covalently bound to an electronegative atom X, and another atom Y, which has an excess of electron density. A typical hydrogen bond, formed between hydrogen atom and X, Y atoms, is denoted as X–H···Y, where the dots represent the bond; X is called a proton donor, and Y is called an acceptor. Hydrogen bonds are formed due to the action of several forces, including primarily forces of an electrostatic nature, charge transfer between atoms X and Y, and dispersion forces.

Among the main criteria for the formation of a hydrogen bond, geometric and energetic features stand out, such as elongation of X–H bond; proximity of X–H···Y angle to linear (180°); the increase in the strength of H···Y bond with the increase in electronegativity of X atom.

A hydrogen bond is called homonuclear if X and Y are atoms of the same chemical element, or heteronuclear if they are atoms of different elements. If the donor X and the acceptor Y are located in the same molecule, then the hydrogen bond X–H···Y formed between them is called intramolecular; on the contrary, if X and Y are part of different molecules, then the bond formed between them is called intermolecular.

The proton donor X–H fragment may be involved in the formation of one, two or three hydrogen bonds with an acceptors Y as shown in Figure 1.1. The most common are hydrogen bonds with one Y acceptor – classical hydrogen bonds (Figure 1.1a), bifurcate hydrogen bonds (Figure 1.1b) with two Y acceptors are much less common [14,15], and hydrogen bonds with three acceptors – trifurcate (Figure 1.1c) – was observed only in the number of examples [16,17].

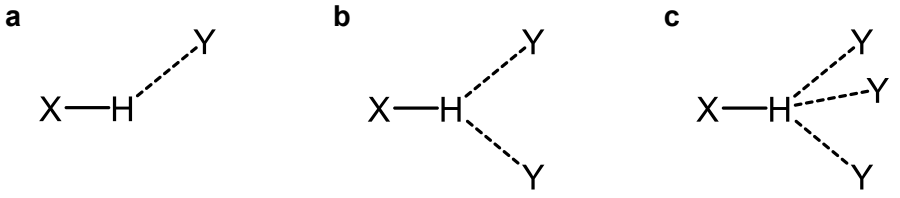

Figure 1.1. The types of hydrogen bonds: a) classical hydrogen bond (proton donor fragment X–H forms the hydrogen bond with one acceptor Y), b) bifurcate hydrogen bond (fragment X–H forms two hydrogen bonds with two acceptors Y), c) trifurcate hydrogen bond (X–H associated by three Y acceptors, three hydrogen bonds).

The proton acceptor Y, in addition to the formation of classical hydrogen bond X–H···Y, may also participate in the formation of two or more hydrogen bonds with several proton donor fragments X–H as shown in Figure 1.2 [14,15].

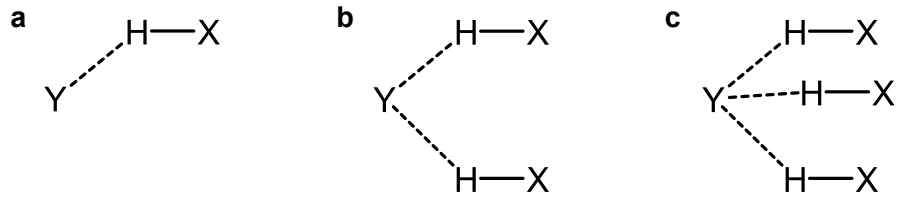

Figure 1.2. The types of hydrogen bonds formed by one acceptor Y and a) one, b) two c) three proton donor fragments X–H.

If one molecule contains both proton donor fragments X–H and acceptors Y, the formation of several classical hydrogen bonds is possible between fragments of one molecule (intramolecular hydrogen bond is formed) or between different molecules (intermolecular hydrogen bonds are formed). In the latter case, molecules associate with the formation of dimers [18,19], trimers [19], tetramers [20], chains and *etc*. The examples of such associates are shown in Figure 1.3.

Hydrogen bonds may influence the main characteristics of each other – length and strength, when several hydrogen bonds are formed within one complex. The mutual influence of hydrogen bonds can be accompanied by the shortening of the distance between heavy atoms X, Y and the increase in the strength of bonds (cooperativity) or, conversely, the increase in the distance between X, Y and the decrease in the strength (anticooperativity).

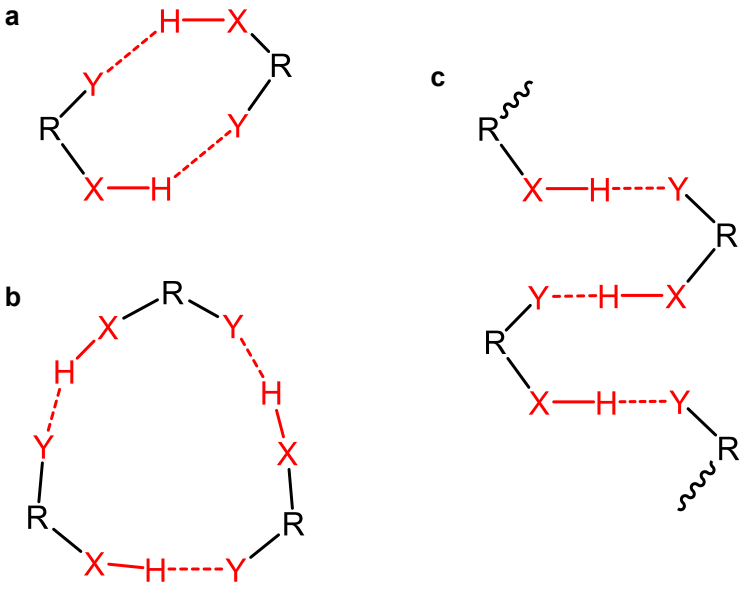

Figure 1.3. The examples of the association of molecules with the formation of several hydrogen bonds: a) cyclic dimers, b) cyclic trimers, c) infinite chains.

1.2. Main methods of study of hydrogen bonds

The description of systems with hydrogen bonds usually includes establishing the number of hydrogen bonds in the complex, determining the main geometric and energetic characteristics – the lengths and strengths of hydrogen bonds and, if hydrogen bonds interact with each other, estimating the power of their mutual influence on each other (cooperativity, anticooperativity).

The most informative and accurate experimental method for studying each of these characteristics is selected taking into account the temperature, aggregation state of the medium and its physical and chemical properties (viscosity, spectral transparency, polarizability and *etc*.), and also taking into account the chemical nature of the interacting fragments, as well as possible dynamic processes in the system, including processes of breaking and formation of hydrogen bonds and proton transitions in them. Methods for study of hydrogen bonds may refer to direct methods, when the necessary characteristics of systems with hydrogen bonds are determined directly from experimental data, or indirect methods, when the numerical values of characteristics are determined based on correlations with other quantities directly measured in an experiment. The simplest and most accurate correlations used to indirectly estimate the geometry and strength of hydrogen bonds may be obtained using observed spectral parameters, such as chemical shifts of signals in NMR spectra, location and intensities of absorption bands in spectra in IR and UV regions. Some of these correlations are described in this and following subsections.

Direct methods of study geometry and energy

Geometry. The main geometric characteristics of hydrogen bond are: hydrogen bond angles α, β and the hydrogen bond distances, r_1, r_2 and r_{XY}, shown schematically in Figure 1.4. The most accessible direct methods for measuring the lengths and angles of hydrogen bonds are the methods of X-ray diffraction and the methods of neutron scattering on single crystals.

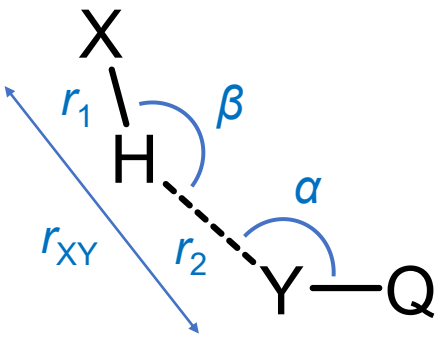

Figure 1.4. The main geometric characteristics of hydrogen bond: angles α, β and distances r_1, r_2 and r_{XY}.

X-ray scatter at the electrons of atomic shells. Analysis of the resulting diffraction pattern makes it possible to determine the position of the atoms of heavy elements and, therefore, to calculate the distance between the electronegative atoms X and Y involved in the formation of X–H···Y hydrogen bond, *i.e.* distance r_{XY}. The typical length of a hydrogen bond r_{XY} ranges from 2.6 Å to 3.0 Å, which is more than the length of a covalent bond and is less than the sum of the van der Waals radii of the X and Y atoms. Hydrogen bonds with the length of less than 2.6 Å are short, and more than 3.0 Å are long [21] (although this classification seems relative). The position of the hydrogen atom in a single crystal may be determined using ultra-high-resolution electron density maps [22–24] or approximately, for example, using so called riding model [25]. The hydrogen bond angle β, as a rule, is close to linear (primarily for intermolecular complexes), which is one of the criteria for the formation of the hydrogen bond [13].

Unlike X-rays, neutrons are scattered by atomic nuclei. Protons and deuterons have the largest scattering cross sections. Neutron scattering experiments can be used to precisely determine the position of the hydrogen atom in hydrogen bond. For such studies, it is necessary to produce a significant amount of study compounds (up to several grams), and in addition, an intense neutron flux in the beam is required to conduct experiments. Producing the required amount of material containing hydrogen-bonded complexes is a laborious task. The neutron flux in the beam required for the experiment is provided by nuclear reactors. In contrast, X-ray scattering experiments are almost always not required a large amount of study compounds and are carried out using X-ray diffractometer, so X-ray diffraction analysis remains the most accessible and most often used experimental method for studying hydrogen bond geometry.

To describe the position of the bridging proton in a hydrogen bond, the distances r_1 and r_2 are used (see Figure 1.4). For linear hydrogen bonds, the length r_{XY} can be calculated as the algebraic sum of the distances r_1 and r_2. Often, instead of r_1 and r_2, equivalent natural coordinates are used, which are defined as $q_1 = ½(r_1 – r_2)$ и $q_2 = r_1 + r_2$. For a linear hydrogen bond, q_1 shows the distance between the proton and geometric center of the hydrogen bond, and q_2 shows the total hydrogen bond length r_{XY}. For a nonlinear hydrogen bond, q_1 and q_2 are simply another way of specifying r_1 and r_2. The distances r_1 and r_2 (or q_1 and q_2) are interdependent, as observed in many experimental and computational studies of hydrogen-bonded complexes [26,27]. Their interdependence can be expressed within the parametric model [28,29] containing addition parameters (1.1)–(1.2):

$$p_1 = \exp\left(-\frac{r_1 - r_1^0}{b_1}\right) \qquad (1.1)$$

$$p_2 = \exp\left(-\frac{r_2 - r_2^0}{b_2}\right) \qquad (1.2)$$

In these equations, the distances r_1^0 and r_2^0 are the length of X–H bond in a free proton donor molecule and the length of H–Y bond in protonated proton acceptor molecule, respectively. The values p_1 and p_2 are the so-called “bond orders”, changing from 1 for

X–H bond in the free proton donor molecule (or for H–Y bond in protonated proton acceptor molecule) to 0 for an infinitely long bond. Parameters b_1 and b_2 describe the rate of change of "bond orders" when the bond is lengthened. The numerical values of b_1 and b_2 are obtained as the result of fitting of data points for each pair of heavy atoms X and Y so that for experimental data, on average, the equation (1.3) is holds, describing the dependence between the coordinates r_1 and r_2.

$$p_1 + p_2 = 1 \qquad (1.3)$$

As an example, Figure 1.5 shows the correlation between q_2 and q_1 coordinates determined from structural analysis by neutron scattering for OHO hydrogen bonds. The general pattern is observed: the closer the proton is to the center of the hydrogen bond (smaller $|q_1|$), the shorter the hydrogen bond (smaller q_2). The solid line in Figure 1.5 corresponds to correlation curve built using equations (1.1)–(1.3) with the parameters given in Table 1 and taken from [29]. The data points correspond to experimental values of q_2 are slightly higher than this curve, which may be explained by the presence of zero-point energy [29].

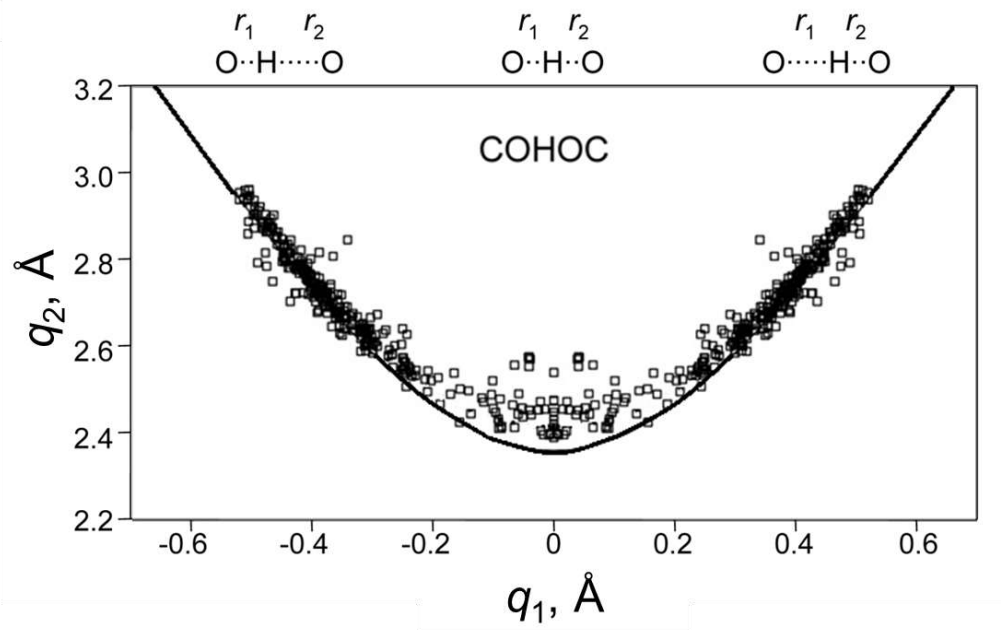

Figure 1.5. Interdependence between natural coordinates q_2 and q_1 for OHO hydrogen bonds [29].

Energy. Experimentally, direct measurement of the strength of intermolecular hydrogen bonds consists of measuring the enthalpy of complexation [30–32]. Most of these studies are carried out for molecular systems in the gas phase. For example, in ref.[31] the enthalpies of dimers formation of three phosphinic acids R_2POOH (R_2 = CH_2Cl, Ph, Me) in the gas phase were measured using IR spectroscopy. Figure 1.6 shows the temperature dependence of logarithm of the equilibrium constant obtained for dimerization reaction of each of these acids. The approximation equations for each of these dependences contain the dimerization enthalpies ΔH of each of three studied phosphinic acids in the gas phase:

$$\ln\left(\frac{B_M^2(T)}{B_D(T)}\right) = -\frac{\Delta H}{kT} + const \qquad (1.4)$$

The equilibrium constants at each temperature T (see equation (1.4)) were determined as the ratio of squared intensity of OH stretching vibrations band in IR spectra corresponding to monomers, $B_M^2(T)$, to intensity of OH stretching vibrations band corresponding to dimers, $B_D(T)$.

In general, the strength of hydrogen bonds varies over a wide range from the natural minimum – zero, to the value of the strongest known hydrogen bond, ~180 kJ·mol^{-1}, found in the anion $(FHF)^-$ [33,34].

It should be noted that the definition of hydrogen bond energy as the enthalpy of complexation encounters difficulties for intramolecular bonds, complexes with multiple non-covalent interactions, complexes in condensed phases and complexes with proton transfer since in all these cases it is necessary to further determine the monomers forming the complex.

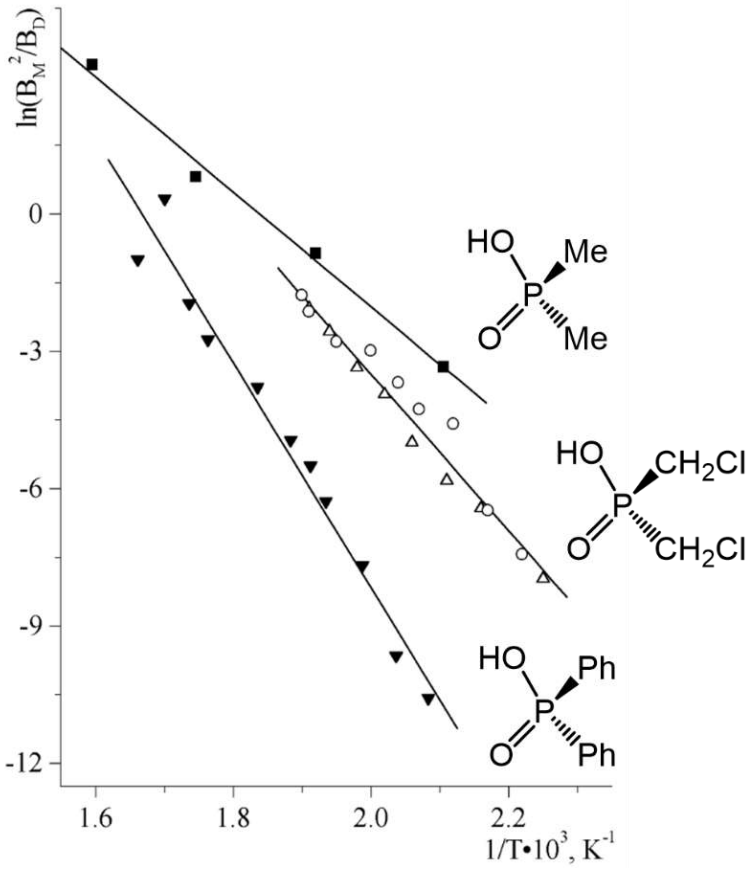

Figure 1.6. Dependences of logarithms of equilibrium constants $\ln\left(\frac{B_M^2(T)}{B_D(T)}\right)$, calculated from the intensities of monomers bands and dimers bands in IR spectra, on reverse temperature, T^{-1}. The dependences are taken from [31] and obtained for three phosphinic acids in the gas phase: Me_2POOH (filled squares), Ph_2POOH (filled triangles) and $(CH_2Cl)_2POOH$ (open triangles and circles), and approximated by linear functions.

In quantum mechanical methods, the strength of hydrogen bonds in complexes is assumed to be equal to the work required to separate interacting molecules over an infinite distance [35–39].

Indirect research methods: correlation between energy and geometry

Indirect measurement methods assume the presence of a correlation between the directly measured characteristics of hydrogen-bonded systems and the ones studied, such as the number of bonds, distances, energy, and values of cooperativity (anticooperativity). The set of indirect methods and the parameters measured in them is extensive and is selected individually for studying hydrogen-bonded system (or series of such systems).

The most frequently mentioned correlation is the correlation between the two main characteristics of a hydrogen bond – length and energy: as the length of X–H bond increases (decreases the distance between X and Y atoms), the strength of the hydrogen bond usually increases [40,41]. In the literature, the terms “short bond” and “strong bond” are often used interchangeably, and even the term SSHB (short strong hydrogen bond) is used. The type of correlation function depends on the studied hydrogen-bonded system, the features of the medium, and a number of other parameters.

The correlations between the strength of hydrogen bond and (a) the distance r_1, (b) the distance r_{NN}, calculated by quantum chemical methods is shown in Figure 1.7 as an example of N–H···N hydrogen bonds in aniline complexes with various NH proton donors [42]. The correlation function between hydrogen bond energy and hydrogen bond length r_1 described by the following equation:

$$E_{complex} = E_{max} \cdot \left(1 - \left(\frac{r_1 - r_1^{max}}{r_1^{min} - r_1^{max}}\right)^2\right) \quad (1.5)$$

In this equation r_1^{min} = 0.99 Å is the value of r_1 for free aniline molecule, and r_1^{max} = 1.26 Å is the length of the shortest hydrogen bond among all known complexes with aniline. The parameter E_{max} = 159 kJ·mol^{-1} indicate the maximum value of hydrogen bond strength and selected as fitting result. The solid curve shown in Figure 1.7a is plotted using these numerical parameter values. The solid line in Figure 1.7b corresponds to the approximation curve built according to the equation:

$$E_{complex} = E_{max} \cdot e^{-\frac{r_{NN} - r_{NN}^{min}}{b}} \qquad (1.6)$$

The parameter b in equation (1.6) describes the rate of decrease in the complexation energy with increasing r_{NN}; the value of r_{NN}^{min} was taken equal to 2.52 Å for all NHN hydrogen bonds. The value of E_{max} is given above and the value b = 0.338 Å was obtained by fitting the data points shown in Figure 1.7b.

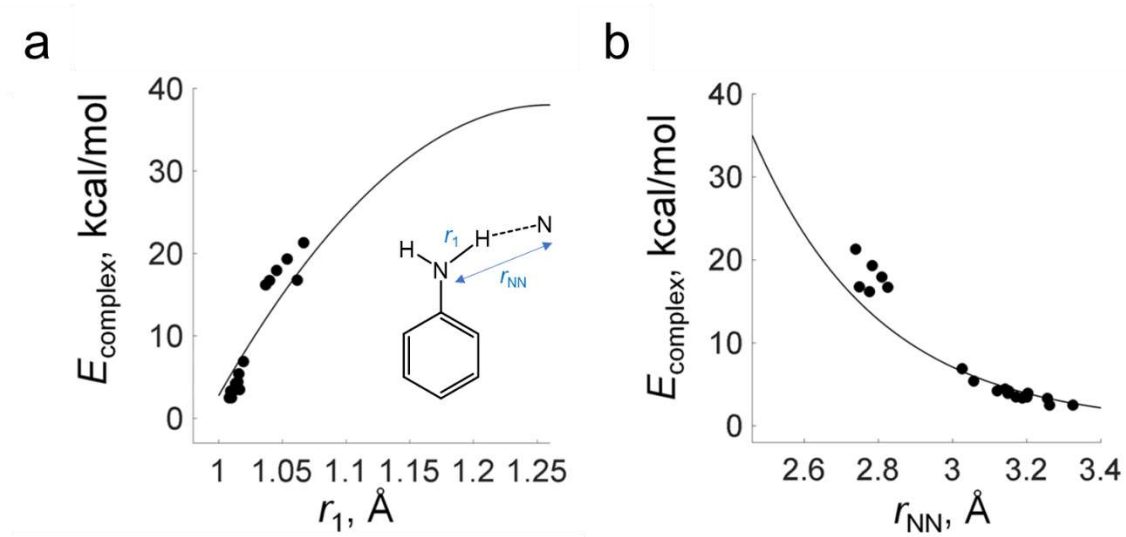

Figure 1.7. Correlation between the strength of NHN hydrogen bond, $E_{complex}$, and (a) distance r_1, (b) distance r_{NN} for aniline complexes with various NH proton donors [42].

The relationship between hydrogen bond strength and geometry may be described using the "bond order" model. For example, the relationship between energy and bond orders for complexes with F–H···F hydrogen bond was described in [42] according to the equation: $E = E^0 \cdot (4p_1 \cdot p_2)^m$, in which the values of parameters E^0 and m were obtained as the result of approximation.

It is also possible to estimate hydrogen bond energy indirectly from the properties of electron density [43]. Analysis of electron density distribution may be performed using the quantum theory of atoms in molecules (QTAIM) [44–46] or experimentally by measuring the electron density in X-ray scattering experiments in crystals [47,48]. In QTAIM method, a hydrogen bond is characterized by a bond path connecting the bridging

proton and the acceptor atom, the bond critical point (BCP) located along this path and electron density properties calculated at this critical point: electron density ρ, Laplacian of the electron density $\nabla^2\rho$, as well as local densities of kinetic (G) and potential (V) energies of electrons [44–46].

Indirect research methods: NMR spectroscopy

To describe the properties of hydrogen bonds using NMR spectra, the spectral characteristics of the bridging particle are primarily used. Shift of the proton signal to a weak field, *i.e.* an increase in chemical shift is the most characteristic sign of hydrogen bond formation [13]. It seems natural that the absolute value of the change of bridging proton chemical shift, $\Delta\delta$H, upon formation of the hydrogen bond indicates both proton-donating and proton-accepting abilities of the groups involved in the formation of hydrogen bond. Therefore, among all the experimentally available spectral NMR parameters, the values of $\Delta\delta$H are considered as a descriptor of the strength (geometry) of hydrogen bonds before others [49–55].

Geometry. In many of the works listed above, the general trend observed: as the length of the hydrogen bond decreases, as well as strength increases, the chemical shift increases and reaches a maximum when the proton moves to the center of hydrogen bridge; after the proton passes through the center of hydrogen bridge, the value of δH decreases. The example of the relationship between proton position in hydrogen bond q_1 and chemical shift δH is shown in Figure 1.8 for a wide range of complexes with OHO hydrogen bond [29]. The dashed lines in Figure 1.8 correspond to the correlation curves obtained separately for hydrogen bonds formed by aliphatic OH groups (filled circles) and formed by OH groups bound to an unsaturated carbon atom (open squares), both with (dashed lines) and without (dotted lines) effects caused by zero-point energy [29].

The dependence $\delta H(q_1)$ may be described using the parametric model of "bond orders", as was shown in [29], according to the equation:

$$\delta H = \delta H_{free} + \Delta \cdot (4 p_1 \cdot p_2)^m \qquad (1.6)$$

The value δH_{free} in this equation corresponds to the chemical shift of the bridging proton of proton donor group in free proton donor molecule, and $m = 1.2$ is the empirical parameter determined by the results of approximation. The parameter Δ reports the maximum value of proton chemical shift and is also determined by the result of approximation. Note that the dependence presented in Figure 1.8 obtained to homonuclear hydrogen bonds and is therefore symmetrical relative to $q_1 = 0$. The dependence is not symmetrical for heteronuclear hydrogen bonds.

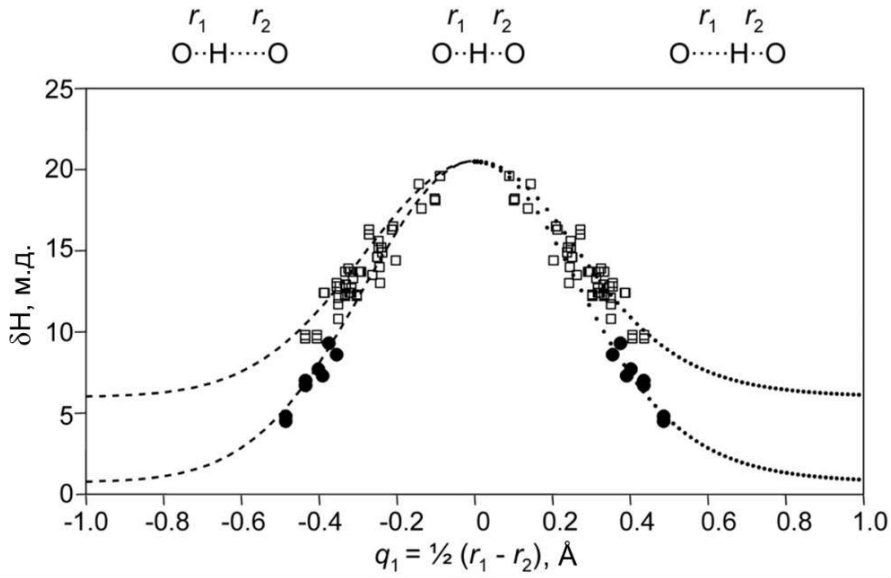

Figure 1.8. Correlation between chemical shift of bridging proton δH and q_1 coordinate for OHO hydrogen bonds [29]. Data points are obtained from the result of neutron scattering and solid-state NMR spectroscopy measurements. Filled circles refer to aliphatic OH groups, open squares refer to OH groups bonded to unsaturated carbon atom (carboxylic acids, phenols and *etc.*). The dotted and dashed lines built by the result of approximations performed for two sets of data points as described in the text.

The number of observable spectral parameters, which may be potentially used to study of hydrogen bonds, is large. Among them, for example, chemical shifts of nuclei close to the hydrogen bridge ^{19}F, ^{15}N, ^{13}C, ^{31}P [56–61], spin-spin interaction constant between nuclei involved in formation of hydrogen bond as well as close to ones [29,42,56,62–66] and H/D isotope effects on these parameters [19,29,67–72].

As an example, the correlation between ^{15}N chemical shift, $\delta^{15}N$, and q_1 shown in Figure 1.9 for hydrogen-bonded complexes formed by 2,4,6-trimethylpyriline and different acids in solution and solid [58].

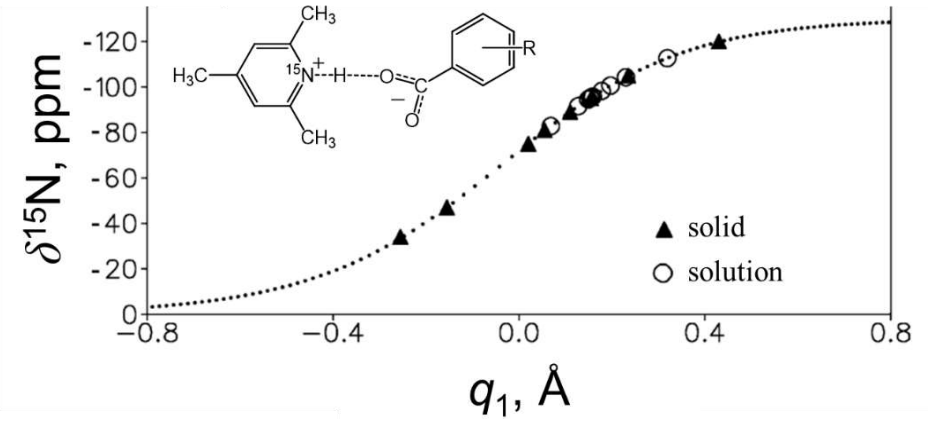

Figure 1.9. Correlation between ^{15}N chemical shift and q_1 for OHN hydrogen bonds formed by 2,4,6-trimethylpyridine and the set of different acids [58].

The correlation $\delta^{15}N(q_1)$ is well described using the parametric "bond orders" model according to the equation:

$$\delta^{15}N = \delta N^{inf} - (\delta N^{inf} - \delta(HN)^0) \cdot p_{HN} \qquad (1.7)$$

The parameters $\delta(HN)^0$ and δN^{inf} in equation (1.7) refer to ^{15}N NMR chemical shifts for isolated molecules of protonated collidine and non-protonated (free) collidine, respectively. The parameter p_{HN} is the order of bond between nitrogen atom and the bridging proton.

Another example of the possibility of describing the geometry of hydrogen bonds using NMR spectral parameters is the correlation between parameter q_1 and ^{31}P chemical shift, $\delta^{31}P$, shown in Figure 1.10a,b and presented in [61], where complexes with

intermolecular hydrogen bonds between substituted pyridines and dimethylphosphinic, phenylphosphinic acids were studied. As can be seen, the correlation $\delta^{31}\mathrm{P}(q_1)$ is well described by the curve built according to equation:

$$\delta^{31}\mathrm{P} = \frac{\delta(\mathbf{P}\mathrm{OOH}) - \delta(\mathbf{P}\mathrm{OO}^-)}{1 + e^{\frac{q_1 - q_1^0}{c}}} + \delta(\mathbf{P}\mathrm{OO}^-) \qquad (1.8)$$

The parameters δ(**P**OOH) and δ(**P**OO$^-$) in this equation specify ^{31}P chemical shifts in limiting cases: for the complex with extremely weak hydrogen bond and for the complex with complete proton transition. The parameter δ(**P**OOH) equal to 44.90 ppm and 12.87 ppm, and the parameter δ(**P**OO$^-$) equal to 30.35 ppm and 6.94 ppm for complexes with dimethylphosphinic acid and phenylphosphinic acid, respectively (numerical values obtained as the analysis of additional quantum chemical calculations). The values of parameters c and q_1^0 were obtained as the result of approximation of the data points: c = 0.037 and q_1^0 = –0.314 Å, the values of these parameters are the same for two sets of complexes: with dimethylphosphinic acid and with diphenylphosphinic acid.

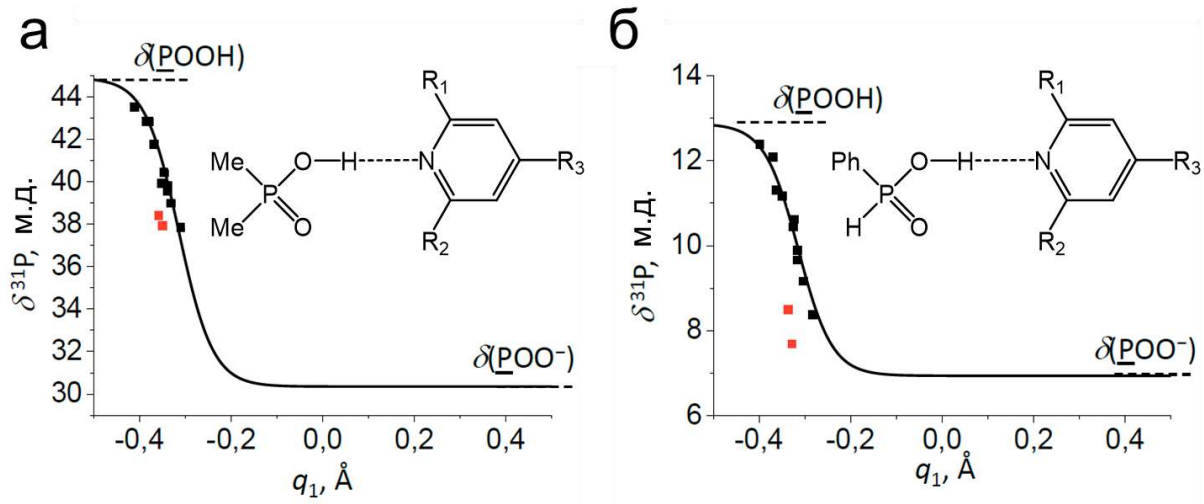

Figure 1.10. Correlations between ^{31}P chemical shift, δ^{31}P, and parameter q_1 for complexes of substituted pyridines with a) dimethylphosphinic acid b) phenylphosphinic acid. The correlations taken from [61]. Red dots refer to complexes of phosphinic acids with pyridines with substituents in *ortho* position. Solid curves correspond to correlation curves built according to equation (1.8).

The red dots in Figure 1.10 deviate significantly from the correlation curve and correspond to complexes with pyridines with substituents in *ortho* positions. The deviation of these points from correlation was explained by the presence of additional interactions between these substituents and phosphinic acid.

Energy. The strength of hydrogen bonds may also be studied using NMR parameters, primarily the ^{1}H chemical shift. In a number of studies [53–55,73,74] linear correlations between hydrogen bond strength, ΔE, and the change of ^{1}H NMR chemical shift of bridging proton upon hydrogen bond formation, $\Delta\delta$H, were demonstrated, the general equation of these correlations:

$$\Delta E = a \cdot \Delta\delta\mathrm{H} + b \qquad (1.8)$$

The values of the coefficients a and b in equation (1.8) are slightly different for each set of complexes and were selected empirically. The presence in equation (1.8) of the term b with the value different from zero, seems to contradict the physical meaning of the equation. Nevertheless, taking this term into account leads to the most accurate description of the linear correlation $\Delta E(\Delta\delta\mathrm{H})$ for most hydrogen bonds.

Indirect research methods: IR spectroscopy

Informative IR spectral markers used to quantitatively describe the geometry and strength of hydrogen bonds include, first of all, stretching vibrations of proton donor group X–H [75–82].

The largest number of studies of the dependence of X–H group vibration frequency, ν_{XH}, on the length of hydrogen bridge, r_{XY}, was carried out for OHO and OHN hydrogen bonds. One of the most famous works devoted to establishing this correlation is ref. [83],

in which several functional dependencies $v_{OH}(r_{XY})$ were proposed for specific ranges of IR spectrum. The functional dependence $v_{OH}(r_{XY})$ is not given explicitly in this study.

The change in the frequency of stretching vibration of X–H group may also be associated with the change in the length of XH bond, $\Delta r_{XH} = r_{XH} - r_{XH}^{free}$. For example, the following correlation between Δv_{OH}, ν_{OH}^{free} (in cm^{-1}) and Δr_{OH} (in Å) was established for OHO hydrogen bonds [83]:

$$\Delta v_{OH}/\nu_{OH}^{free} = 3.6 \cdot \Delta r_{OH} \qquad (1.9)$$

IR characteristics of proton donor group are also informative parameters for estimating the strength of hydrogen bond. In ref. [84], the correlation between Δv_{OH} and complexation enthalpy, ΔH, was first demonstrated on the example of OHO hydrogen bonds. This correlation is described by the linear equation:

$$\Delta H = a \cdot \Delta v_{OH} + b \qquad (1.10)$$

The coefficients in equation (1.10) are individual for each proton donor group X–H and are determined by the result of approximation. It is interesting that two equations, namely equation (1.10), obtained by IR spectroscopy, and equation (1.8), obtained from the results of NMR studies, indicate the linear correlation between the enthalpy of hydrogen bond formation and IR, NMR spectral characteristics of proton donor group. However, some deviations from linearity observed in some studies [85,86]. The correlations $\Delta H(\Delta v_{OH})$ and $\Delta H(\Delta \delta H)$ will be used in this work to obtain numeric values of complexation enthalpy using recorded IR and NMR spectra, as will be demonstrated in the following section.

Other IR spectral characteristics may also be sensitive to hydrogen bond properties. The set of these spectral characteristics include, for example, the frequency of stretching vibrations of C=O group, $v_{C=O}$ [87–90], band intensities [91–95], frequencies of deformation vibrations [96–98]. However, there are few studies devoted to detailed study of correlations between spectral changes of characteristics of proton acceptor groups due to the formation of hydrogen bonds and the geometry, strength of hydrogen bonds.

1.3. P=O group. Phosphine oxides

The proton acceptor group P=O is present in the structure of phosphine oxides, phosphorus-containing acids (for example, phosphinic, phosphonic, phosphorous and hypophosphorous acids) and their anions. The P=O group of these compounds is often used to synthesize polymers that have excellent flame retardancy and good mechanical properties [99–102] or can be used as biomaterials [100]. The P=O group is also present in phosphates, which can participate in proton transfer processes in polymer membranes of fuel cells [103–105]. The P=O group in phosphine oxides is particular uses. For example, metal complexes of secondary phosphine oxides are popular ligands for homogeneous catalysts [106–109]. Another example is long-chain phosphine oxides, such as trioctylphosphine oxide, which are important components used for the synthesis and stabilization of semiconductor quantum dots, including applications as bright fluorescent probes for tracking individual molecules in living organisms [110,111]. In spectroscopic studies, the characteristics of P=O group may be used to establish the properties of intermolecular complexes with compounds containing this group [19,61,112–121].

Among all compounds with P=O group, phosphine oxides are among the strongest donors of electron density. The chemical bond between phosphorus and oxygen atoms in phosphine oxides is semi-polar, *i.e.* this bond may be represent as a single P^{+}–O^{-} bond with an excess negative charge on the oxygen atom and an excess positive charge on the phosphorus atom, as shown in Figure 1.11a. Near the oxygen atom of P=O group, there are three maxima of electron localization function (ELF), located symmetrically relative to P=O bond, as demonstrated in Figure 1.11b for isolated trimethylphosphine oxide molecule. Consequently, phosphine oxides can act as electron donors for several acceptor molecules. For example, hexamethylphosphoramide in the solid (crystals) tends to form two hydrogen bonds with two molecules of phosphoric acid [114] or two molecules of water [38], and triarylphosphine oxides can also form bonds with two proton donor molecules in the solid [122]. In addition, in the solid, the formation of two hydrogen

bonds is possible between the P=O group of phosphine oxides and two proton donor groups of the same proton donor molecule [123]. Spectral manifestations of the formation of complexes formed by phosphine oxide and several proton donor molecules were also recorded in solutions, for example, the formation of complexes with two hydrogen bonds with the P=O group was demonstrated for solutions of triethylphosphine oxide and strong Brønsted acids in chloroform [124].

There are few studies that study the cooperativity (anticooperativity) effects for such complexes. For example, in [114], it was shown that two strong hydrogen bonds with the P=O group in model complexes formed by phosphine oxides $H_3P{=}O$ and $(Me_2N)_3P{=}O$ with two HF molecules apparently interact anticooperatively, but the anticooperativity effects are is very weak (the strength of one hydrogen bond decreases by 10% when the second hydrogen bond is formed). Therefore, one of the objectives of this work is to determine the values of cooperativity effects on the strength and lengths

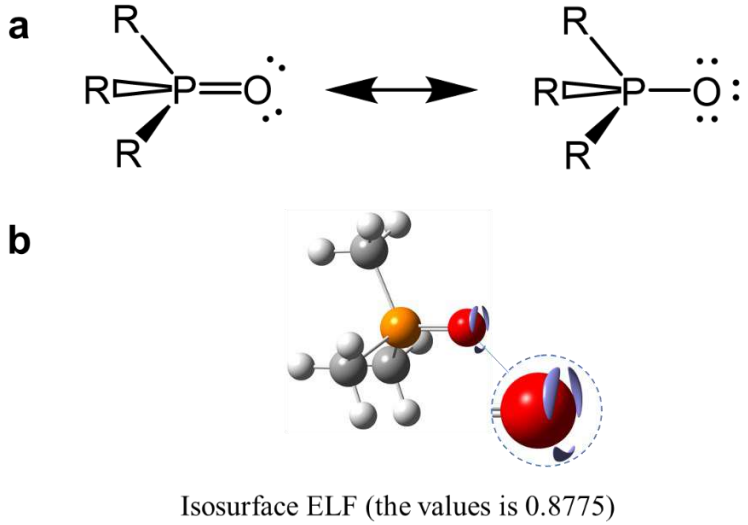

Figure 1.11. (a) The structures demonstrating resonance between the double and polar P=O bond in phosphine oxides, (b) isosurface of electron localization function (the values equal to 0.8775) near the oxygen atom of isolated trimethylphosphine oxide (the inset of figure part is shown on the right for greater clarity; the geometry of trimethylphosphine oxide is obtained by quantum chemical calculations at the level of theory B3LYP/6-311++G(d,p) in the gas phase).

of hydrogen bonds in a wide range of proton donor abilities of partner molecules, as well as to evaluate the possibility of estimating these effects using spectral characteristics (see Section 2.4 and Section 3.6).

Interest in the use of phosphine oxides to describe non-covalent interactions by NMR markers of the P=O group is associated with the presence in the P=O group of the phosphorus atom, the nucleus of which characterized by ½ spin, high gyromagnetic ratio (~40.5% of gyromagnetic ratio for ^{1}H) and wide range of chemical shifts [125–127]. NMR chemical shifts of ^{31}P may be informative in the case of non-covalent interactions [116–121]. The range of changes in ^{31}P NMR chemical shift for the P=O group of phosphine oxides is relatively wide (about 50 ppm) and depends primarily on the chemical structure of phosphine oxides, solvating shell (or crystal packing) and the properties of interactions between the P=O group with other molecules [116,128]. Phosphine oxides are used in ^{31}P NMR spectroscopy to characterize the electron-acceptor properties of solvents [129] and other compounds with Lewis acidity [130–132] (so-called Guttman-Beckett acceptor number scale, AN). New works devoted to this aim appear from time to time [118,133,134], including one review [128]. The first report on using ^{31}P NMR of phosphine oxides for hydrogen bond characterization was published in 1982 [135]. After that probing of proton donor ability of Brønsted acids by phosphine oxides was mentioned only occasionally, often in combination with studies of Lewis acidity [133,134]. However, over the last years several experimental papers appeared devoted to Brønsted acidity exclusively [124,136–138]. In these works, the ^{31}P chemical shift (or the change of δ^{31}P) of triethylphosphine oxide [124,136,137] or tri-*n*-butylphosphine oxide [138] is used to describe the properties of the series of proton donor molecules in solutions in dichloromethane or chloroform (most often this works report correlations with pK_a of the proton donor). As the concentration of proton donor molecules in solutions increases, the equilibrium shifts to the formation of complexes with phosphine oxide. The phosphorus chemical shift is sensitive to formation of complex and shifts downfield, typically to 15–20 ppm [136–138] for molecules with medium and strong proton donor ability (alcohols, phenols, carboxylic acids), and up to 40 ppm for

the strongest proton donors (for example, trifluoromethanesulfonic acid and methanesulfonic acid) [124].

In addition, several theoretical works have been published recently [118,139] that report studies studied of the spectral, geometric and energetic characteristics of halogen bonds on a wide series of intermolecular complexes with trimethylphosphine oxide. These studies report correlations between the change of ^{31}P NMR chemical shift of phosphine oxide during complexation and the length, strength of halogen bonds, electron density parameters calculated at critical points. In addition, the sensitivity of stretching vibration frequency of P=O group to halogen bond strength was demonstrated in [118].

The stretching vibrations of P=O group demonstrate characteristic bands in the range from 1100 cm^{-1} to 1250 cm^{-1} in IR spectra [140–143]. The value of the shift of P=O stretching vibration band in IR spectra during complexation may be used for determining the properties of non-covalent interactions with phosphine oxides [118,144]. One of the first attempts to find a correlation between the characteristics of hydrogen bond (strength primarily) and the shift of P=O stretching vibration band during complexation was made in 1979 [144]. Thereafter, the development of such studies has been almost unreported with the exception of a few publications describing solvent-solute interactions [145–147]. This is probably due to the fact that P=O vibrational bands located in the same range of spectra as bands of many other vibrations, and can potentially overlap with these bands.

Studies carried out using IR and NMR spectroscopy methods indicate great potential for using the spectral characteristics of P=O group of phosphine oxides (^{31}P NMR chemical shift and P=O stretching vibration band in IR spectra) to describe the properties of non-covalent interactions in complexes involving them. However, attempts to find a correlation between spectral characteristics of P=O group and the energy or geometry of hydrogen bond formed by Brønsted acid with selected phosphine oxide were rarely made, although such correlations may be used to compare the proton donor abilities of acids or to predict the strength and geometry of hydrogen bonds in complexes formed by selected phosphine oxide and specific proton donor molecule. Therefore, in this work

we study hydrogen bond characteristics in complexes with several selected phosphine oxides and the set of different proton donors over a wide range of their proton donor abilities.

Chapter 2. Quantum chemistry calculations of Me_3PO complexes with proton donors

2.1. Introduction and problem statement

In this chapter, we report the results of quantum chemistry investigation of complexes with one or two hydrogen bonds, formed by trimethylphosphine oxide (Me_3PO) with various proton donors either in an aprotic medium (chloroform, modelled as a polarizable continuum). We study 70 complexes with one hydrogen bond, 1:1 complexes, and 70 complexes with two hydrogen bonds, 1:2 complexes, by the DFT calculations – 140 complexes without proton transfer in general. Each proton donor molecule in the series used is assigned to one of the four classes: OH (Figure 2.1), NH (Figure 2.2), NH^+ (Figure 2.3) and CH (Figure 2.4). Thus, we consider four types of hydrogen-bonded complexes: $Me_3PO\cdots HO$, $Me_3PO\cdots HC$ and $Me_3PO\cdots HN$ (electroneutral complexes) and $Me_3PO\cdots HN^+$ (cationic complexes).

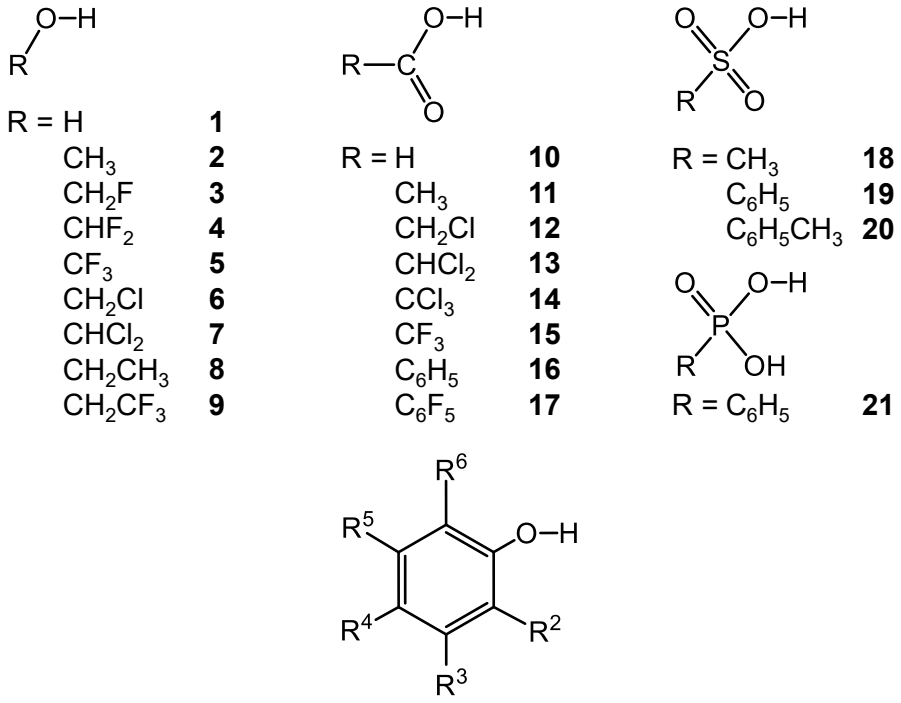

R^2	R^3	R^4	R^5	R^6	
H	H	H	H	H	**22**
NO_2	H	H	H	H	**23**
H	**NO_2**	H	H	H	**24**
H	H	**NO_2**	H	H	**25**

Figure 2.1. The set of OH proton donors (**1**–**25**), forming complexes of $Me_3PO\cdots HO$ type with Me_3PO.

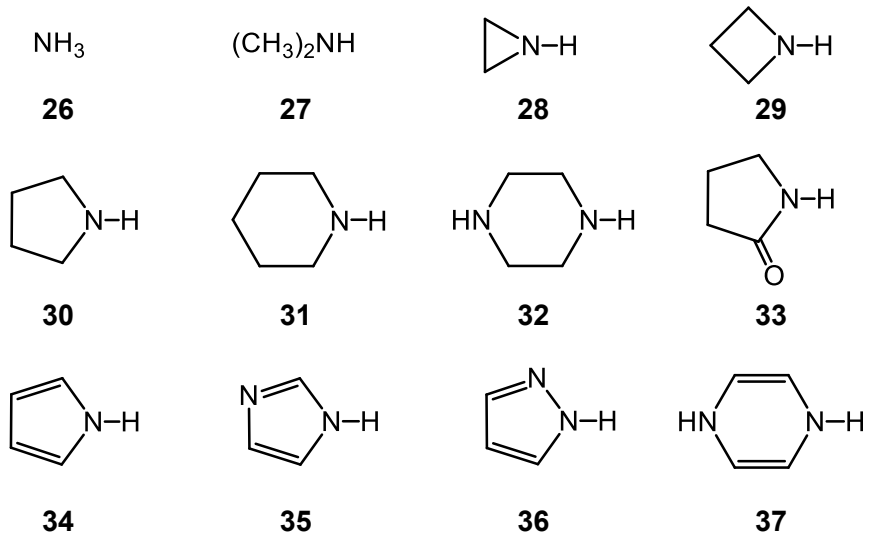

Figure 2.2. The set of NH proton donors (**26**–**37**), forming complexes of $Me_3PO\cdots HN$ type with Me_3PO.

38

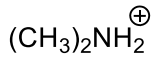

39

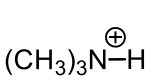

40

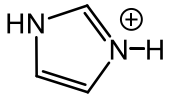

41

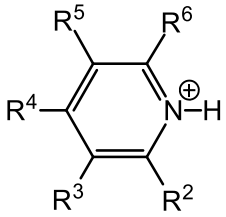

R^2	R^3	R^4	R^5	R^6	
H	H	H	H	H	**42**
Me	H	H	H	H	**43**
H	**Me**	H	H	H	**44**
H	H	**Me**	H	H	**45**
H	**Me**	H	**Me**	H	**46**
Me	H	H	H	**Me**	**47**
Me	H	**Me**	H	**Me**	**48**
NMe_2	H	H	H	H	**49**
H	**NMe_2**	H	H	H	**50**
H	H	**NMe_2**	H	H	**51**
H	**NMe_2**	H	**NMe_2**	H	**52**
H	**OMe**	**OMe**	**OMe**	H	**53**
H	**F**	**F**	**F**	H	**54**
H	**Cl**	**Cl**	**Cl**	H	**55**
H	**NH_2**	H	**NH_2**	H	**56**

Figure 2.3. The set of NH^+ proton donors (**38**–**56**), forming complexes of $Me_3PO\cdots HN^+$ type with Me_3PO.

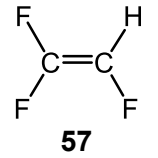

57

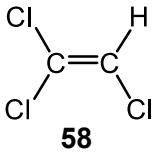

58

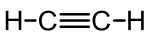

59

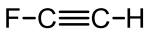

60

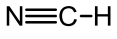

61

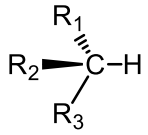

R_1	R_2	R_3	
NO_2	NO_2	NO_2	**62**
NO_2	NO_2	Me	**63**
NO_2	Me	Me	**64**
Cl	Cl	Cl	**65**
Cl	Cl	H	**66**
Cl	H	H	**67**
H	H	H	**68**
F	F	F	**69**
Br	Br	Br	**70**

Figure 2.4. The set of CH proton donors (**57**–**70**), forming complexes of $Me_3PO\cdots HC$ type with Me_3PO.

The set of study parameters calculated for 1:1 and 1:2 complexes is shown in Figure 2.5, the notation for the energy, geometric and spectral parameters discussed below is also given there. Within the set of investigated complexes complexation energy ΔE (for 1:1 complexes) and the energy of the second of formed hydrogen bonds ΔE^a (for 1:2 complexes) vary over a wide range from natural zero to ~85 kJ·mol^{-1} and to ~65 kJ·mol^{-1} respectively. The total complexation energy of 1:2 complexes, $\Delta E^t = \Delta E + \Delta E^a$, ranges up to ~120 kJ·mol^{-1}. Hydrogen bond strength was also estimated using local electron kinetic G^a, G and potential V^a, V energy densities calculated at (3, –1) bond critical point according to QTAIM analysis [148]. The hydrogen bond length varies as well: 1.41 Å < r_2 < 2.75 Å (for 1:1 complexes) and 1.53 Å < r_2^a < 2.96 Å (for 1:2 complexes). All these changes are reflected in IR and NMR spectral characteristics of complexes. For 1:2 complexes P=O stretching frequency $\nu^t_{P=O}$ changes up to ~110 cm^{-1}; ^{1}H and ^{31}P NMR chemical shifts δH^a and δP^t change up to ~8 ppm and ~30 ppm respectively. For 1:1 complexes spectral manifestations of hydrogen bond formation are comparable: $\nu_{P=O}$ changes up to ~80 cm^{-1}; δH and δP change up to ~11 ppm and ~20 ppm

respectively. The mutual influence of hydrogen bonds in 1:2 complexes was considered in this chapter as cooperativity (anticooperativity) effects on the following parameters: energy, $\Delta\Delta E$ and $\Delta\Delta E/\Delta E$; geometry, Δr_2 and $\Delta r_2/r_2$; ^{1}H and ^{31}P NMR chemical shifts, $\Delta\Delta\delta$H and $\Delta\Delta\delta$P; stretching vibration frequency, $\Delta\Delta\nu_{P=O}$ (see equations in Figure 2.5, bottom).

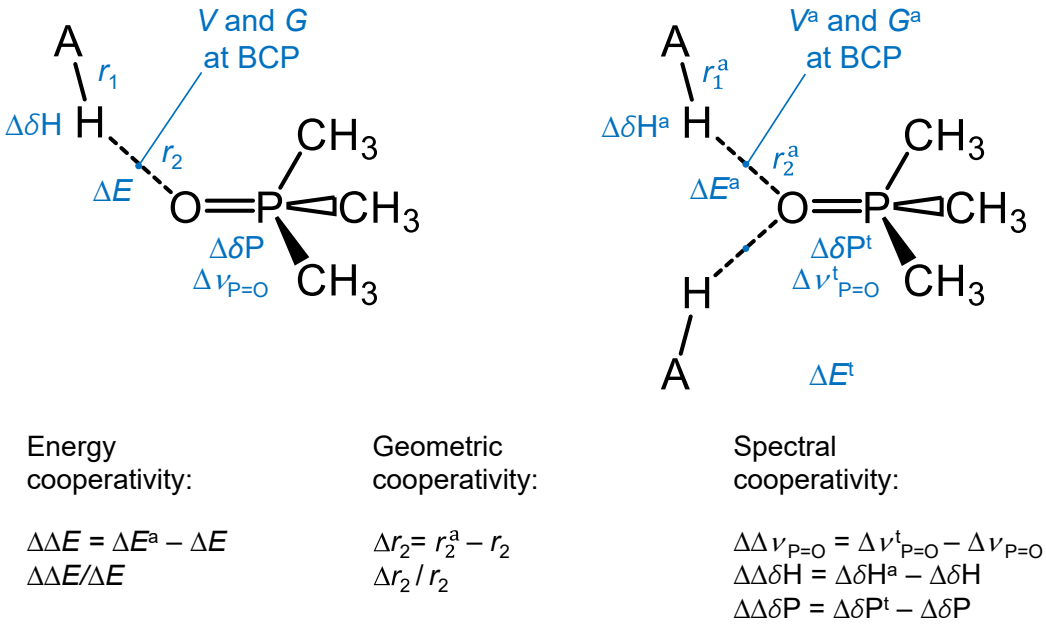

Figure 2.5. General structures of 1:1 and 1:2 complexes formed by Me_3PO and AH proton donor molecules, as well as geometric, energetic and spectral parameters considered in this work: the lengths of hydrogen bond r_1, r_2, r_1^a, r_2^a, hydrogen bond energies ΔE and ΔE^a, total hydrogen bonds energy $\Delta E^t = \Delta E + \Delta E^a$, local electron kinetic G, G^a and potential V and V^a energy densities calculated at bond critical point (BCP), changes of ^{1}H and ^{31}P chemical shifts $\Delta\delta$H and $\Delta\delta H^a$, $\Delta\delta$P and $\Delta\delta P^t$, changes of P=O stretching vibration frequencies $\Delta\nu_{P=O}$ and $\Delta\nu^t_{P=O}$ upon complexation, cooperative (anticooperative) effects on energy ($\Delta\Delta E$ and $\Delta\Delta E/\Delta E$), geometry (Δr_2 and $\Delta r_2/r_2$) and spectral parameters ($\Delta\Delta\delta$H, $\Delta\Delta\delta$P and $\Delta\Delta\nu_{P=O}$).

The goal of this part of work is a) to find correlations between spectral parameters and energy (geometry) of hydrogen bonds in 1:1 complexes, b) to expand this correlations to the more complicated case of 1:2 complexes and c) to estimate the cooperativity (anticooperativity) effects on energy, geometry, IR and NMR spectral characteristics of 1:2 complexes of Me_3PO with proton donors. Correlations between spectral

characteristics and energy (geometry) of hydrogen bond are presented in Section 2.3 for 1:1 complexes and are expanded in Section 2.4 for the case of 1:2 complexes, cooperativity (anticooperativity) effects are discussed in Section 2.4.

2.2. Computational details

The calculations were performed using Gaussian 16 software package [149]. Optimized geometries ("tight" convergence criteria), energies and harmonic vibration frequencies were calculated using the density functional theory (DFT) at the B3LYP/6–311++G(d,p) level [150–153]. The aprotic medium was modelled as polarizable continuum (PCM; chloroform, ε = 4.7) [154]. The complexation energy ΔE was computed including the relaxation energy of monomers. The complexation energy ΔE^a of 1:2 complexes was computed in this work as the difference between the full electron energy of 1:2 complex and the sum of the energies of corresponding 1:1 complex ($Me_3PO\cdots HA$) and isolated AH species. Both ΔE and ΔE^a were calculated at the same level of theory without the dispersion correction and the correction for the basis set superposition error. The absolute and relative cooperativity effects on hydrogen bond energy upon transition from 1:1 to 1:2 complexes were defined as $\Delta\Delta E = \Delta E^a - \Delta E$ and $\Delta\Delta E/\Delta E$, respectively. In a similar way, the absolute and relative cooperativity effects on hydrogen bond geometry were defined as $\Delta r_2 = r_2^a - r_2$ and $\Delta r_2/r_2$ respectively.

The set of NMR parameters was calculated using the GIAO approach at the same level of theory. The NMR shielding constants σ_{free} were calculated for the isolated proton donor (for ^1H) or isolated Me_3PO (for ^{31}P) in their relaxed geometries. The NMR shielding constants $\sigma_{complex}$ were computed for the proton donors and Me_3PO in 1:1 and 1:2 complexes. Changes of ^1H and ^{31}P NMR chemical shifts upon complexation, $\Delta\delta H$, $\Delta\delta H^a$ and $\Delta\delta P$, $\Delta\delta P^t$, were calculated as $\Delta\delta = \sigma_{free} - \sigma_{complex}$. The values of cooperativity effects on NMR parameters were defined as $\Delta\Delta\delta H = \Delta\delta H^a - \Delta\delta H$ and $\Delta\Delta\delta P = \Delta\delta P^t - \Delta\delta P$ using NMR parameters of 1:1 and 1:2 complexes of Me_3PO with the same AH proton donor.

The P=O stretching vibration frequencies are reported relative to those calculated at the same level of theory for isolated Me_3PO molecule ($\nu_{P=O}$ = 1153.39 cm^{-1}). The values of cooperativity effects on P=O stretching frequencies, $\Delta\Delta\nu_{P=O}$, were calculated as a difference between $\Delta\nu^t_{P=O}$ and $\Delta\nu_{P=O}$.

The QTAIM analysis was implemented using Multiwfn software [155,156]. Visualization of complex structures was performed using GaussView 6.0 software [157]. The graphical representation of the data was performed using a script written in Python 2.7.

2.3. Me_3PO complexes with one hydrogen bond

The calculated geometric, energetic and spectral parameters calculated for each of 70 hydrogen-bonded intermolecular 1:1 complexes formed by Me_3PO with proton donors **1**–**70** in chloroform are listed in Table 2.1, while some additional parameters are given in Table A1 (see Appendix A). Below we discuss the interrelations between these parameters.

Typical examples of the structures of complexes 1:1 are shown in Figure 2.6 for $Me_3PO\cdots HO$ (Figure 2.6a), $Me_3PO\cdots HN$ (Figure 2.6b), $Me_3PO\cdots HN^+$ (Figure 2.6c) and $Me_3PO\cdots HC$ (Figure 2.6d) types of complexes. Some complexes have additional hydrogen bonds, which can be detected as close contacts between heavy atoms (the distance between atoms less than the sum of their van der Waals radii) and confirmed by analysis of electron density (QTAIM analysis) as the presence of the corresponding bon critical points (BCP). Such additional hydrogen bonds could be classified into two types shown in Figure 2.7 on the examples of $Me_3PO\cdots HN$ and $Me_3PO\cdots HO$ complexes. Type 1 is the interaction between one or two protons of methyl group in Me_3PO with one electronegative atom of AH molecule. Type 2 is the interaction between electron lone pairs of the oxygen atom in Me_3PO and CH proton in the AH molecule. Type 1 occurs mainly in complexes with carboxylic acids and halogenated alcohols. Type 2 is found in complexes with phenols and almost all *ortho*-substituted pyridine cations. All additional interactions are much weaker than the main intermolecular hydrogen bond, though they might affect complex's geometry and thus its spectral parameters. To visually indicate the presence of additional interactions, throughout Section 2.3 the corresponding data points will be plotted as open symbols, while the data points for the complexes without additional interactions will be plotted as filled symbols. Besides, throughout the Section 2.3 the data points corresponding to different types of proton donors will be shape- and color-coded: red circles for $Me_3PO\cdots HO$, blue triangles for $Me_3PO\cdots HN$, black stars for $Me_3PO\cdots HN^+$ and green diamonds for $Me_3PO\cdots HC$.

Table 2.1. The calculated geometric, energetic and spectral parameters for hydrogen-bonded intermolecular 1:1 complexes formed by Me_3PO with proton donors **1**–**70** (PCM, $\varepsilon = 4.7$). The numerical values are given in the following units: ΔE in kJ·mol^{-1}, V and G in kJ·mol^{-1}·Bohr^{-3}, $q_1 = 0.5\cdot(r_1 - r_2)$ and $q_2 = r_1 + r_2$ in Å, α and β in degrees, $\Delta\delta$H and $\Delta\delta$P in ppm and $\Delta\nu_{P=O}$ in cm^{-1}. The last column indicates the type of additional non-covalent interaction in the complex (see Figure 2.7 and the text for more details).

No	Proton donor	ΔE	G	V	q_1	q_2	α	β	$\Delta\delta$H	$\Delta\delta$P	$\Delta\nu_{P=O}$	Type of add. int.
OH proton donors												
1	Water	30.08	84.29	84.18	–0.391	2.746	132.2	179.1	4.9	5.7	–18.1	–
2	Methanol	29.68	85.97	86.19	–0.390	2.740	134.3	178.7	5.3	5.9	–16.5	–
3	Fluoromethanol	42.27	112.79	125.71	–0.329	2.643	133.9	176.6	6.5	8.9	–27.8	–
4	Difluoromethanol	49.20	136.54	166.97	–0.274	2.577	133.9	176.0	8.3	11.0	–37.7	1
5	Trifluoromethanol	62.80	170.43	231.10	–0.216	2.501	136.0	176.8	9.7	13.5	–50.1	1
6	Chloromethanol	46.24	124.88	145.04	–0.305	2.608	134.4	176.8	7.8	10.0	–35.4	1
7	Dichloromethanol	53.58	155.97	201.21	–0.242	2.531	137.0	174.4	9.8	12.1	–47.1	1
8	Ethanol	28.06	83.32	82.54	–0.396	2.751	135.8	178.2	5.4	5.1	–16.0	–
9	2,2,2-Trifluoroethanol	40.35	108.13	118.25	–0.339	2.657	134.9	176.9	6.2	8.3	–18.8	1
10	Formic acid	49.41	140.12	175.02	–0.266	2.572	128.3	175.8	8.1	12.9	–47.2	1
11	Acetic acid	45.26	130.12	157.47	–0.285	2.596	127.4	175.2	7.6	12.1	–42.6	1
12	Chloroacetic acid	53.22	151.70	196.19	–0.245	2.544	129.2	175.2	8.8	13.5	–51.7	1
13	Dichloroacetic acid	59.39	164.86	222.64	–0.221	2.517	129.4	176.1	9.3	15.5	–63.3	1
14	Trichloroacetic acid	63.16	176.97	248.87	–0.200	2.493	130.0	176.1	10.0	16.4	–69.3	1
15	Trifluoroacetic acid	64.79	181.39	259.15	–0.191	2.486	130.4	176.3	10.1	16.7	–74.1	1
16	Benzoic acid	46.79	134.86	165.78	–0.277	2.584	127.4	175.0	8.1	12.6	–46.7	1
17	Pentafluorobenzoic acid	56.36	160.31	213.33	–0.229	2.527	129.6	175.5	9.1	14.7	–58.1	1
18	Methanesulfonic acid	65.10	187.50	276.06	–0.179	2.476	128.5	177.0	8.7	18.4	–35.1	1
19	Benzenesulfonic acid	64.42	186.23	273.13	–0.180	2.478	128.5	176.3	10.4	17.7	–27.0	1
20	p-Toluenesulfonic acid	61.34	188.26	279.14	–0.174	2.474	130.6	175.6	10.8	17.1	–54.5	1
21	Phenylphosphonic acid	54.06	149.00	191.91	–0.251	2.547	129.2	178.8	8.9	14.5	–51.0	1
22	Phenol	40.42	107.85	118.34	–0.337	2.657	136.8	177.7	6.5	7.1	–27.1	2
23	2-Nitrophenol	52.55	129.06	153.17	–0.294	2.596	134.1	178.0	7.7	10.3	–40.8	2
24	3-Nitrophenol	48.99	121.78	139.32	–0.310	2.614	142.7	177.9	7.1	8.5	–27.0	2
25	4-Nitrophenol	52.03	128.37	150.93	–0.296	2.596	139.1	179.5	7.4	9.5	–39.9	2
NH proton donors												
26	Ammonia	12.00	41.64	35.30	–0.513	3.071	130.6	177.0	2.9	2.2	–8.6	–
27	Dimethylamine	11.90	43.84	37.27	–0.506	3.052	137.9	179.0	3.0	1.9	–7.9	–
28	Aziridine	15.62	50.30	44.06	–0.479	3.004	133.2	175.9	3.2	3.2	–9.4	–
29	Azetidine	11.70	42.41	36.26	–0.513	3.066	132.4	177.7	2.8	2.1	–7.4	–
30	Pyrrolidine	12.00	41.31	35.41	–0.518	3.080	130.4	177.2	2.7	2.0	–8.0	–
31	Piperidine	11.55	42.00	35.80	–0.515	3.068	133.1	179.0	2.9	2.0	–7.7	–
32	Piperazine	11.83	41.31	35.15	–0.517	3.077	134.0	176.5	3.0	1.7	–7.8	–
33	2-Pyrrolidone	26.94	69.32	66.78	–0.409	2.873	121.8	174.1	4.7	8.0	–25.7	1
34	Pyrrole	28.06	77.45	74.03	–0.387	2.826	142.3	179.7	4.3	4.9	–14.5	–
35	Imidazole	33.68	88.12	87.70	–0.359	2.779	147.2	178.9	4.7	5.7	–16.0	–
36	Pyrazole	33.35	87.87	89.42	–0.359	2.781	139.0	177.2	4.5	6.1	–19.3	–
37	1,4-Dihydropyrazine	20.18	64.69	58.51	–0.427	2.896	142.2	179.8	4.5	3.6	–11.5	–
NH^+ proton donors												
38	Ammonium	77.43	157.15	210.79	–0.205	2.582	151.2	175.5	9.8	14.1	–47.6	–
39	Dimethylammonium	69.12	137.33	166.42	–0.253	2.633	159.6	174.6	7.6	12.6	–33.8	–
40	Trimethylammonium	67.45	134.39	159.89	–0.263	2.642	160.7	175.7	7.2	12.7	–34.1	–
41	Imidazolium	66.29	142.22	178.05	–0.240	2.608	150.1	176.0	7.6	12.5	–33.3	–

42	Pyridinium	70.04	148.19	186.87	–0.233	2.600	154.4	175.9	7.3	13.5	–39.3	–
43	2-Picolinium	66.30	136.95	165.52	–0.255	2.627	157.9	177.3	6.9	11.8	–36.7	2
44	3-Picolinium	68.16	144.79	180.06	–0.240	2.608	155.5	174.9	7.1	12.8	–37.3	–
45	4-Picolinium	67.11	142.46	176.39	–0.244	2.613	153.8	176.8	7.2	12.7	–40.0	–
46	3,5-Lutidinium	66.80	142.76	176.62	–0.244	2.613	153.5	177.0	7.0	12.5	–39.4	–
47	2,6-Lutidinium	61.13	126.52	147.81	–0.274	2.656	158.1	175.7	6.7	10.7	–34.7	–
48	2,4,6-Collidinium	58.65	124.70	144.13	–0.278	2.661	160.1	175.3	6.6	10.3	–27.1	2
49	2-(Dimethylamino)pyridinium	55.79	109.71	120.29	–0.309	2.705	158.8	164.0	5.8	10.6	–34.2	2
50	3-(Dimethylamino)pyridinium	64.44	137.12	166.46	–0.254	2.627	153.2	174.2	6.8	12.1	–35.2	–
51	4-(Dimethylamino)pyridinium	57.36	123.90	144.06	–0.279	2.658	152.5	177.2	6.6	10.8	–28.8	–
52	3,5-(Dimethylamino)pyridinium	60.35	130.32	154.27	–0.267	2.644	153.8	177.4	6.5	11.4	–36.1	–
53	3,4,5-(Trimethoxy)pyridinium	63.57	136.19	162.33	–0.258	2.626	164.6	176.3	6.9	11.1	–28.3	–
54	3,4,5-Trifluoropyridinium	85.05	183.05	257.61	–0.171	2.535	153.4	175.5	8.9	16.8	–58.7	–
55	3,4,5-Trichloropyridinium	81.76	177.11	244.30	–0.182	2.546	151.1	176.2	8.7	16.3	–72.4	–
56	3,5-Diaminopyridinium	63.92	137.72	167.75	–0.253	2.625	153.3	176.9	6.8	12.0	–37.3	–
CH proton donors												
57	Trifluoroethylene	14.86	44.54	36.38	–0.468	3.107	148.7	176.1	2.7	2.0	–7.3	–
58	Trichloroethylene	14.78	45.53	37.63	–0.463	3.102	145.5	172.4	2.6	2.1	–8.4	–
59	Acetylene	14.84	47.83	39.08	–0.453	3.061	149.2	179.9	3.2	1.6	–7.7	–
60	Fluoroacetylene	15.87	49.54	40.27	–0.444	3.042	150.2	179.5	3.5	1.6	–7.6	–
61	Hydrogen cyanide	30.77	81.55	77.71	–0.340	2.872	149.5	179.4	4.8	4.9	–18.2	–
62	Trinitromethane	41.71	102.36	108.31	–0.293	2.818	144.9	179.3	5.3	8.6	–31.8	1
63	1,1-Dinitroethane	25.38	61.08	54.30	–0.408	3.012	141.4	165.5	3.3	4.7	–19.5	–
64	2-Nitropropane	9.82	27.02	23.03	–0.576	3.334	120.9	173.8	1.8	2.8	–7.8	1
65	Trichloromethane	22.11	61.64	54.65	–0.408	2.997	147.8	179.3	2.8	4.1	–11.6	–
66	Dichloromethane	14.94	45.22	38.10	–0.469	3.114	141.7	178.4	2.6	2.5	–9.0	–
67	Chloromethane	7.34	28.67	23.42	–0.558	3.292	142.2	178.1	2.0	1.0	–4.3	–
68	Methane	0.19	8.62	7.13	–0.825	3.832	153.2	178.7	0.8	0.5	–0.2	–
69	Trifluoromethane	18.89	53.51	45.21	–0.435	3.053	156.1	177.2	2.4	2.8	–7.8	–
70	Tribromomethane	19.29	59.47	52.31	–0.413	3.008	147.1	179.3	2.6	4.2	–11.4	–

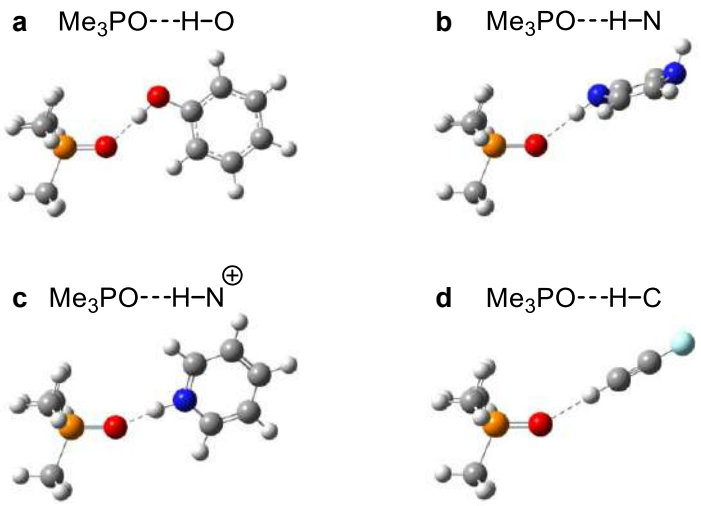

Figure 2.6. Typical structures of complexes with (**a**) $Me_3PO\cdots HO$, (**b**) $Me_3PO\cdots HN$, (**c**) $Me_3PO\cdots HN^+$ and (**d**) $Me_3PO\cdots HC$ hydrogen bonds. The complexes with phenol (**22**), 1,4-dihydropyrazine (**37**), pyridinium (**42**) and fluoroacetylene (**60**) are taken as examples.

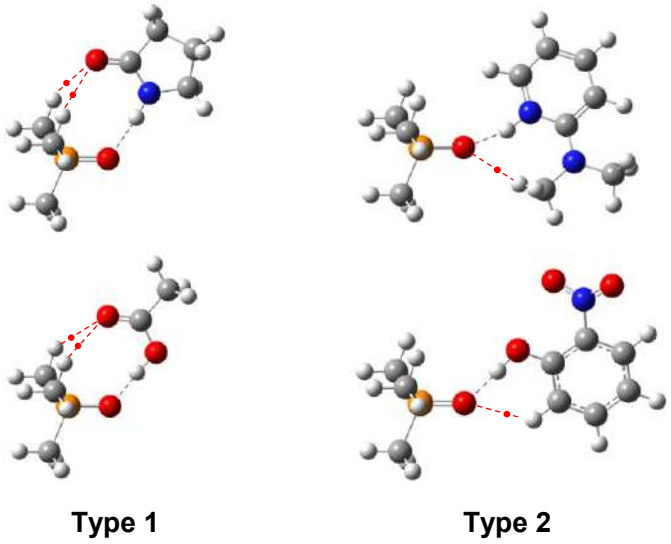

Figure 2.7. Examples of $Me_3PO\cdots HN$ and $Me_3PO\cdots HO$ complexes with additional hydrogen bonds (indicated by red dotted lines). Type 1: the interaction between one or two protons of Me_3PO with an electronegative atom in AH molecule. Type 2: the interaction between lone pairs of oxygen atom of Me_3PO with CH proton in AH molecule. The positions of BCP (3, –1) are shown by red dots. The complexes with 2-pyrrolidone (**33**), 2-(dimethylamino)pyridinium (**49**), acetic acid (**11**), and 2-nitrophenol (**23**) are taken as examples.

Hydrogen bond geometry: angles

Distribution diagrams of angles PO···H (α) and AH···O (β) are shown in Figure 2.8a and Figure 2.8b respectively. The angles are plotted as circular histograms with the step size of 10°: the bar direction indicates the range of angles and the bar length shows the number of such complexes. The distribution of angles α (Figure 2.8a) indicates the existence of two types of complexes. The first distribution maximum is close to 135° (with the span from 120° to 150°), meaning that the hydrogen bond is formed along the direction of the oxygen atom lone pair localization in Me_3PO. Almost all neutral complexes belong to this group with the exception of three complexes of Me_3PO with weak CH proton donors: fluoroacetylene (**60**) methane (**68**), and trifluoromethane (**69**).

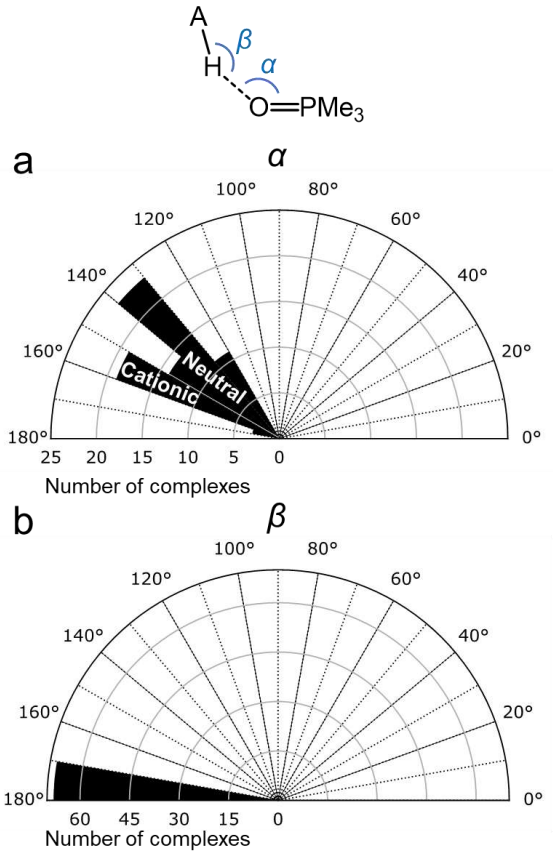

Figure 2.8. Distribution diagrams of angles α (a) and β (b) in the investigated 1:1 complexes.

The second distribution maximum of angles α is close to 155° (spanning from 150° to 165°), and it includes all complexes with cationic proton donors. The angle β is close to linear for the majority of complexes (Figure 2.8b). Some of the largest deviations from linearity are observed for complexes with additional interactions, for example complexes with proton donors **7**, **33**, **49**, **64**.

Hydrogen bond geometry: correlation between r_1 and r_2

The coordinates r_1 and r_2 (see the definition in Figure 2.5, left) are interdependent, which was observed in many experimental and computational studies of hydrogen-bonded complexes [26,27]. Often, instead of r_1 and r_2 distances, it is more convenient to use equivalent natural coordinates q_1, q_2 (see Section 1.2). The correlation between q_1 and q_2 is shown in Figure 2.9 for studied 1:1 complexes. Solid lines are built according to equations (1.1)–(1.3) (see Section 1.2) using numerical parameters taken from refs. [28,29] and listed in Table 2.2. The lines have the same color coding as the data points. A general pattern is observed: the closer the proton to the hydrogen bond center (smaller $|q_1|$) the shorter the bond (smaller q_2). This rule also holds for the complexes with additional interactions. It can be seen that bond order model well describes the results of calculations: all data points lie almost perfectly on the correlation curves.

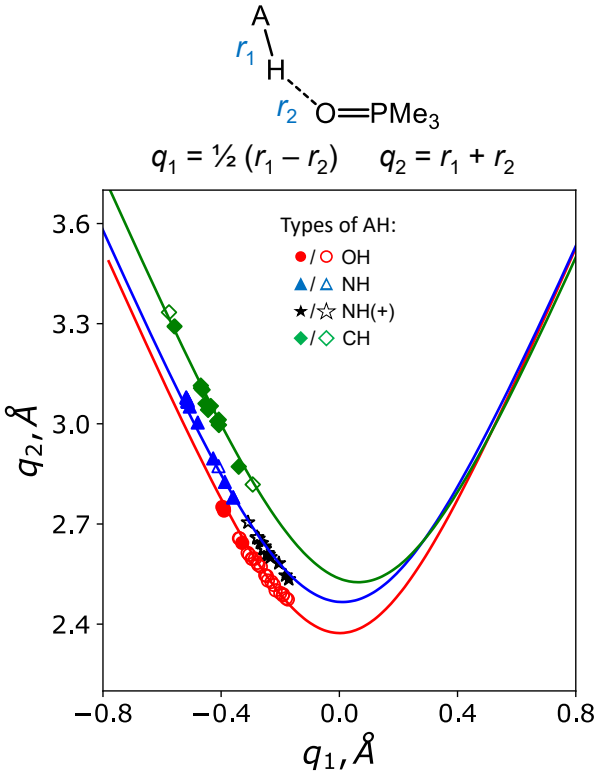

Figure 2.9. Correlation between q_2 and q_1 natural coordinates of hydrogen bond in the studied 1:1 complexes. The solid lines correspond to correlation curves obtained from Eqs. (1.1)–(1.3) given in Section 1.2. The curve parameters were taken from refs. [28,29] and are given in Table 2.2.

Table 2.2. The values of coefficients r_1^0, r_2^0, b_1 and b_2 (in Å) in Eqs. (1.1)–(1.3) were taken from refs. [28,29] and used to plot the solid lines in Figure 2.9.

Coefficient	Type of hydrogen bond		
	O···HO	O···HN	O···HC
r_1^0	0.960	0.985	1.070
r_2^0	0.960	0.960	0.942
b_1	0.322	0.381	0.370
b_2	0.322	0.371	0.371

Hydrogen bond energy: ΔE and G, V

The existence of a bond critical point between two atoms indicates an attractive interaction between them, *i.e.* chemical bonding. A series of works [44,45,79] is devoted to establishing correlations between bond strength and electronic parameters calculated at the BCP. The local densities of electron kinetic G and potential V energies are perhaps the most widely used among such parameters. Figure 2.10 shows the correlation between ΔE and G for 1:1 complexes of Me_3PO with proton donors **1**–**70**. Similar plot for V is shown in Appendix A, Figure A1. Hydrogen bond strength ΔE in the studied series of 1:1 complexes varies over a wide range (from 0 to 85 kJ·mol^{-1}). The total variation of G spans approximately 200 kJ·mol^{-1}·Bohr^{-3}. The correlation between ΔE and G seems to be

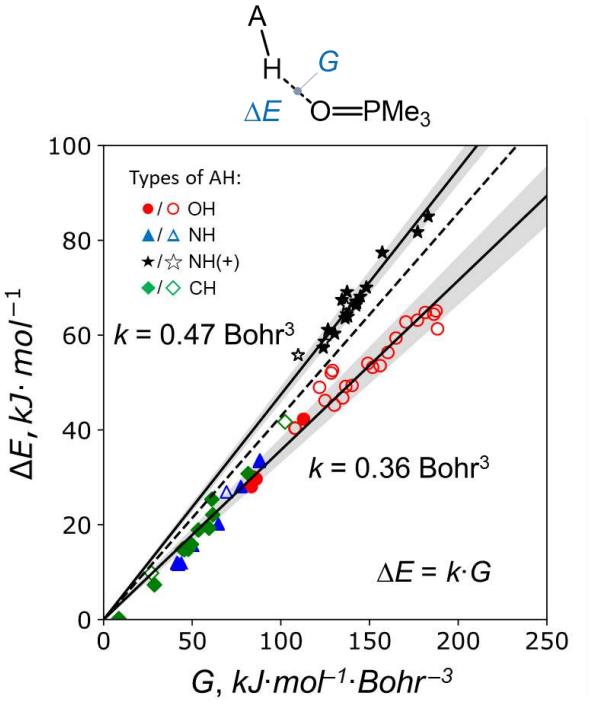

Figure 2.10. Correlation between hydrogen bond energy ΔE and local electron kinetic energy density G. Solid lines correspond to equation $\Delta E = k \cdot G$. Coefficients k differ for complexes with cationic (k = 0.47 Bohr^3) and electroneutral (k = 0.36 Bohr^3) proton donors AH. Grey areas indicate the standard error of the fitted k values. Dashed line (k = 0.43 Bohr^3) is built according to the results obtained in refs. [44,45].

linear, $\Delta E = k \cdot G$, while the values of the proportionality coefficients k, obtained by least squares fitting, differ for the complexes with neutral AH molecules ($k = 0.36 \pm 0.02$ Bohr^3) and with cationic AH molecules ($k = 0.47 \pm 0.01$ Bohr^3). This phenomenon was previously reported for various complexes with hydrogen bonds [42,158]. The presence of additional interactions does not seem to influence the $\Delta E(G)$ correlation significantly. Note, that an intermediary value of the proportionality coefficient $k = 0.43$ Bohr^3 was previously reported in refs. [44,45] for a wide set of complexes.

Figure 2.11 shows a very good nonlinear correlation $G(V)$ for complexes with neutral as well as cationic molecules. The correlation holds for complexes with additional interactions too. The correlation in Figure 2.11 is well described by the power function $G = 3.62 \cdot V^{0.71}$. Previously, a similar correlation between G and V was reported in ref. [46]. However, more recent works [44,45] suggest the linear correlations between ΔE, V and G, where the deviation from the linearity could be seen only for the strongest hydrogen bonds.

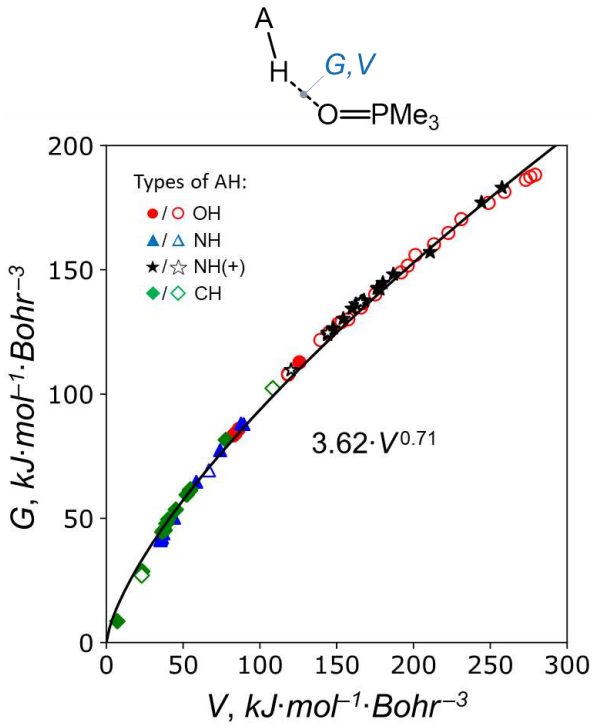

Figure 2.11. Correlation between local electrons kinetic G and potential V energy densities. Solid line corresponds to equation $G = 3.62 \cdot V^{0.71}$.

Hydrogen bond energy and P=O vibration frequency

The change of stretching vibration frequency of the proton accepting group is potentially one of the most useful parameters in IR spectroscopy for detecting hydrogen bonding [87–90]. One of the advantages of IR marker bands is that in almost any realistic situation relatively short lifetime of complexes does not lead to the band averaging, in contrast to NMR markers discussed in the following sections.

For the studied series of 1:1 complexes, the P=O stretching frequency decreases upon complexation and the absolute value of its change, $|\Delta\nu_{P=O}|$, ranges from 0.2 cm^{-1} to 74 cm^{-1} (see Table 2.1). Figure 2.12a,b shows the correlations between ΔE, G and $|\Delta\nu_{P=O}|$ respectively. A power function correlation between energy and stretching vibration frequency was previously reported in ref. [86] for FHF complexes. We also used a power function for the least square fitting of the correlation between G and $\Delta\nu_{P=O}$, giving $G = 14.02 \cdot |\Delta\nu_{P=O}|^{0.62}$ (see the solid line in Figure 2.12b).

Correlations between ΔE and $|\Delta\nu_{P=O}|$ (see Figure 2.12a) differ for complexes with neutral and cationic proton donors. As the correlation $\Delta E(G)$ is linear (Figure 2.10) and the correlation $G(|\Delta\nu_{P=O}|)$ is a power function, the $\Delta E(|\Delta\nu_{P=O}|)$ should also be described by a power function. By keeping the power value fixed at 0.62, we obtained $\Delta E = 4.87 \cdot |\Delta\nu_{P=O}|^{0.62}$ for the complexes with neutral molecules and $\Delta E = 7.09 \cdot |\Delta\nu_{P=O}|^{0.62}$ for the complexes with cationic molecules (see solid lines in Figure 2.12a). We note that $\Delta\nu_{P=O}$ is more responsive to the formation of stronger hydrogen bond. Hence the precision of ΔE estimates decreases for weaker complexes.

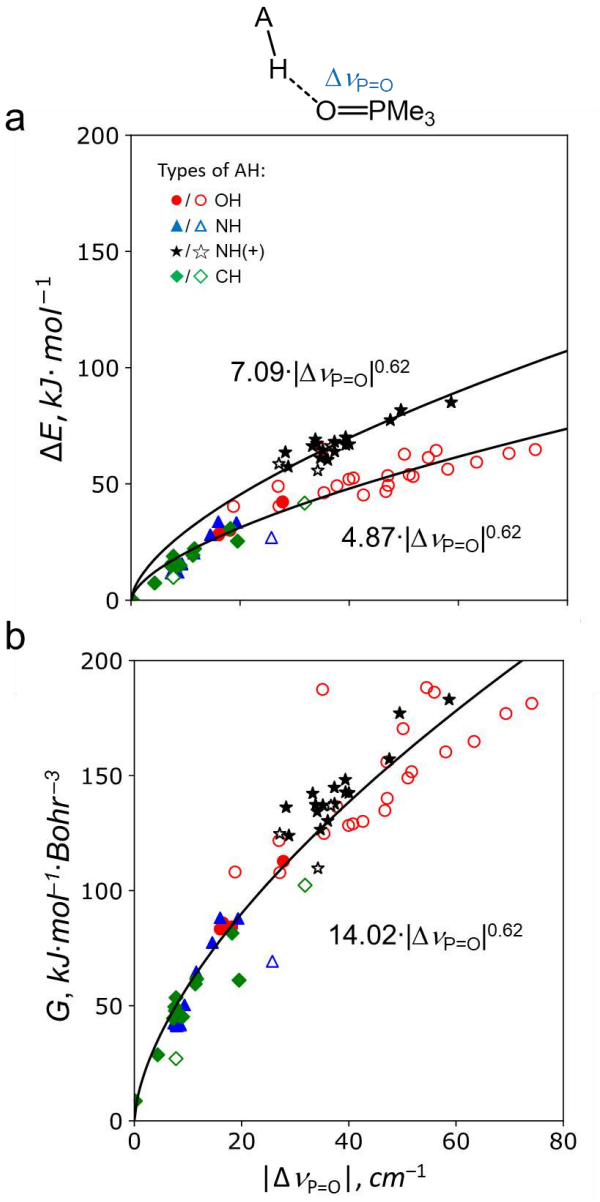

Figure 2.12. Correlations between (a) the hydrogen bond energy ΔE and the change of the stretching frequency $|\Delta\nu_{P=O}|$ and (b) the local electron kinetic energy density G and $|\Delta\nu_{P=O}|$. Solid lines correspond to the results of least squares fitting.

Hydrogen bond energy and ^{1}H NMR chemical shifts

The bridging proton chemical shift increases upon complexation: the stronger the complex the more deshielded is the proton (see Figure 2.13a).

For 1:1 complexes with proton donors **1**–**70** the overall span of ^{1}H NMR chemical shifts is *ca.* 11 ppm. The correlation between the bond energy ΔE and proton signal shift upon complexation $\Delta\delta$H differ for complexes with cationic and neutral molecules: for charged complexes (with NH^+ proton donors) the correlation coefficient is 9.2 ± 0.5 kJ·mol^{-1}·ppm^{-1}, while for neutral complexes (with OH, CH, NH proton donors) it is 6.1 ± 0.7 kJ·mol^{-1}·ppm^{-1}; this difference is absent in the correlation between G and $\Delta\delta$H (Figure 2.13b): correlation coefficient 17.9 ± 1.6 kJ·mol^{-1}·Bohr^{-3}·ppm^{-1} is valid for all complexes. Some scattering of the data points might be associated with the presence of additional non-covalent interactions, but in general it does not break the overall linear dependence.

The linearity of the correlation between hydrogen bond energy and the bridging proton chemical shift was previously reported for various hydrogen-bonded complexes [42,85,159–161], though the reported proportionality coefficients differ rather significantly, depending on the set of complexes considered. Very roughly, for neutral complexes the majority of these coefficients lie in the range 4–11 kJ·mol^{-1}·ppm^{-1}, which matches well the value 6.1 kJ·mol^{-1}·ppm^{-1} found here.

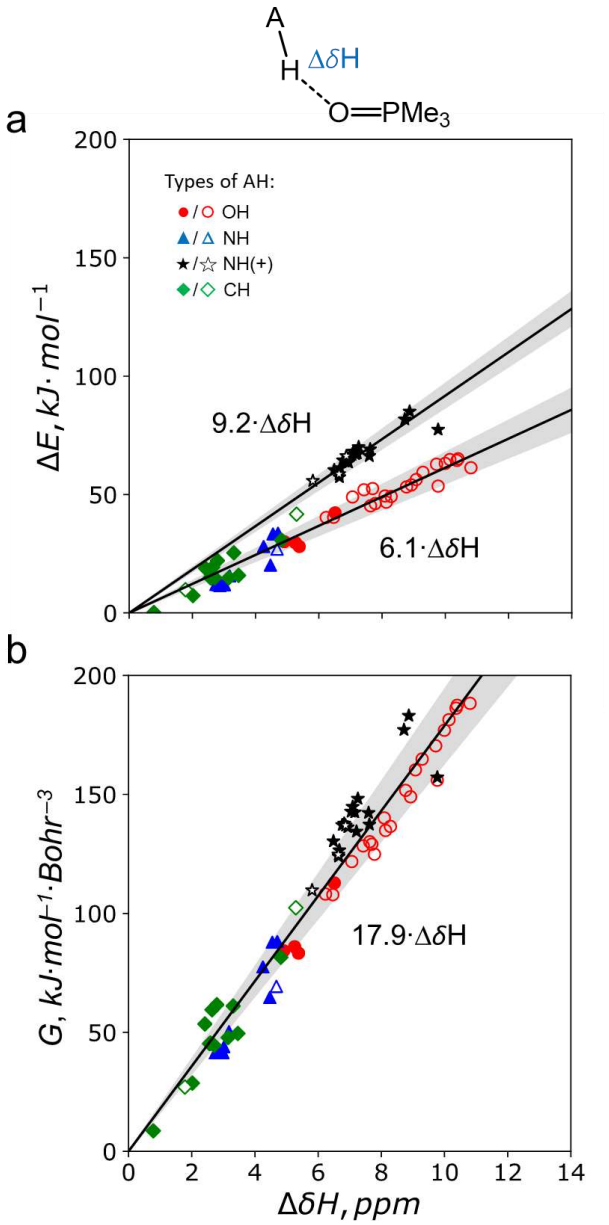

Figure 2.13. The correlations between ΔE and (a) the change of bridging proton chemical shift $\Delta\delta$H, (b) local electron kinetic energy density G and $\Delta\delta$H for studied 1:1 complexes. Solid lines correspond to the results of least squares fitting. Grey areas indicate the standard error of fitting.

Hydrogen bond energy and ^{31}P NMR chemical shifts

Another potentially informative parameter for estimating the hydrogen bond energy is the change of ^{31}P NMR chemical shift upon complexation, $\Delta\delta$P. The estimation of the information content (usefulness) of this parameter was one of the main goals of this work. Recently several attempts to employ δP for the hydrogen bond characterization were published [124,128,136,137]. Practically in every case the authors saw significant potential in δP, but in order to estimate the robustness of this parameter and establish the limits of its applicability further studies seem to be necessary. In case of complexes studied in this chapter, as can be seen in Figure 2.14, δP is sensitive to the hydrogen bond formation and $\Delta\delta$P varies over a wide range from 0 to 20 ppm.

The correlations between hydrogen bond energy ΔE, local electron kinetic energy density G and $\Delta\delta$P seems to be non-linear as shown in Figure 2.14a,b respectively. In contrast, the correlation between local electron potential energy density V and $\Delta\delta$P is quite linear (see Figure 2.14c) with correlation coefficient 14.51 ± 1.30 kJ·mol^{-1}·Bohr^{-3}·ppm^{-1} for 1:1 complexes with neutral as well as cationic proton donors. The non-linear correlations $\Delta E(\Delta\delta\text{P})$ and $G(\Delta\delta\text{P})$ could be fit by power functions with the fixed power value 0.71, as shown in Figure 2.14a,b: $\Delta E = 8.63\cdot\Delta\delta\text{P}^{0.71}$ for complexes of Me_3PO with neutral molecules, $\Delta E = 11.17\cdot\Delta\delta\text{P}^{0.71}$ for complexes with cationic molecules, $G = 23.87\cdot\Delta\delta\text{P}^{0.71}$ for all complexes. In summary, we evaluate the precision of energy estimation from the ^{31}P NMR chemical shift to be *ca.* 10%. The $\Delta\nu_{\text{P=O}}$ and $\Delta\delta$P spectral parameters seem to convey similar information (see their interdependence in Appendix A, Figure A2), though ΔE estimations from $\Delta\delta$P are somewhat more precise. On the one hand, the ^{31}P NMR spectra have a benefit of containing a single ^{31}P signal of $R_3P{=}O$, which makes the spectral assignment trivial.

On the other hand, it could be argued that experimentally IR spectroscopy might be a quicker way to estimate the complexation energy, as it does not require to measure a series of samples approaching an “infinite dilution” limit.

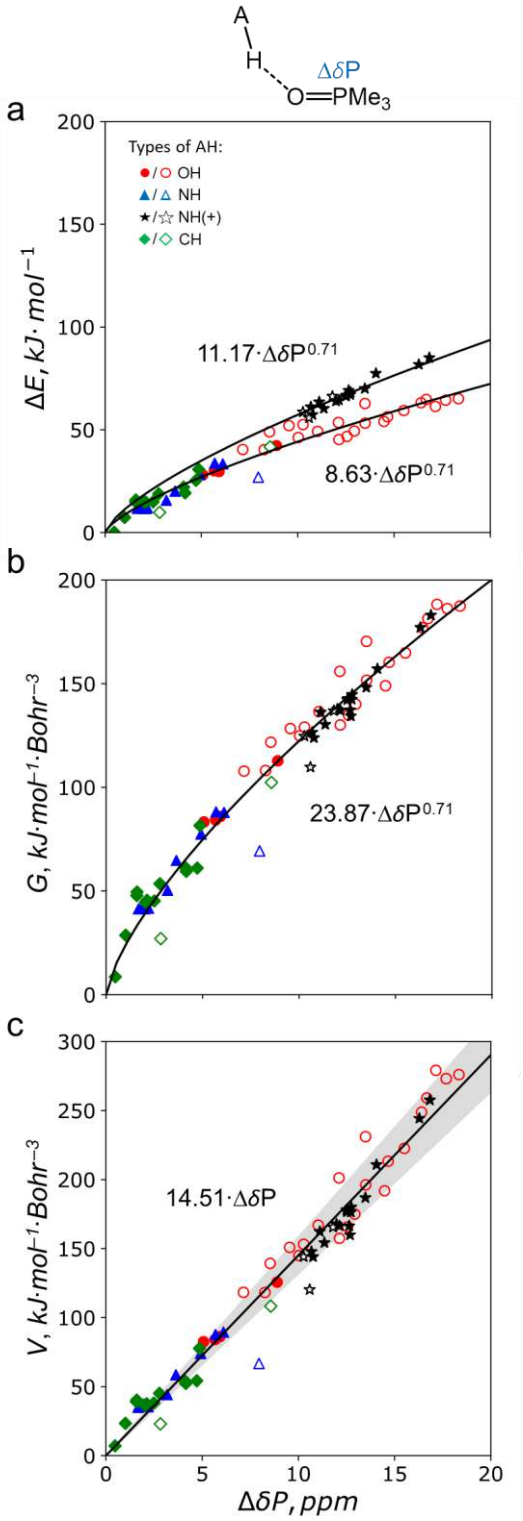

Figure 2.14. Correlations of $\Delta\delta$P and (a) hydrogen bond energy ΔE, (b) local electron kinetic energy density G and (c) local electron potential energy density V. Solid lines correspond to the results of least squares fitting. Grey area indicates the standard error of fitting.

Correlation between pK_a and $\Delta\delta$P

Yet another important characteristic parameter of proton donors is pK_a value. Previously in refs. [124,136,137] the complexes of triethylphosphine oxide with various OH Brønsted acids (phenols, alcohols, silanols, carboxylic acids, boronic acids, thioureas and *etc.*) in aprotic organic solvents were studied by ^{31}P NMR spectroscopy. In these publications linear correlations were proposed between δP and pK_a values of acids with different correlation coefficients for each of the chemical classes [136,137] and also separately for weak and strong acids [124]. In this part of the work, we test whether a similar correlation holds for the set of compounds **1**–**70**. The experimental pK_a values found in the literature for these proton donors (in water at 25 °C) are listed in Appendix A, Table A1. Figure 2.15 shows the correlations between $\Delta\delta$P and the pK_a values of phenols, alcohols, carboxylic acids and benzoic acids considered in this work (filled symbols) and collected from refs. [124,136,137] for OH acids with one OH group (open symbols). Though there is significant scattering of data points, a linear correlation is held for each class of proton donors. The slopes of the correlations found in this work and in the literature for alcohols match well, while in other cases there are certain deviations. However, the general trend is visible for all classes: $\Delta\delta$P decreases upon pK_a decrease within each class of chemical compound.

The average slopes for all kinds of OH proton donors are shown by dotted lines for the literature data and for 1:1 complexes considered in our study. The slopes are reasonably close, but the values of $\Delta\delta$P calculated in this part of work are 5–6 ppm higher in comparison with the experimental ones (this might be due to the $R_3P{=}O$ dimerization, the solvation effects as well as substituent effects in phosphine oxide: ethyls were used in the literature and methyls in this work). In general, for all complexes the δP values decrease by *ca.* 1 ppm per 1.0–1.3 pK_a units.

In the case of complexes formed by trimethylphosphine oxide with other types of proton donors (NH, NH^+ and CH) it is difficult to determine the overall trend due to large data point scattering (see Appendix A, Figure A3).

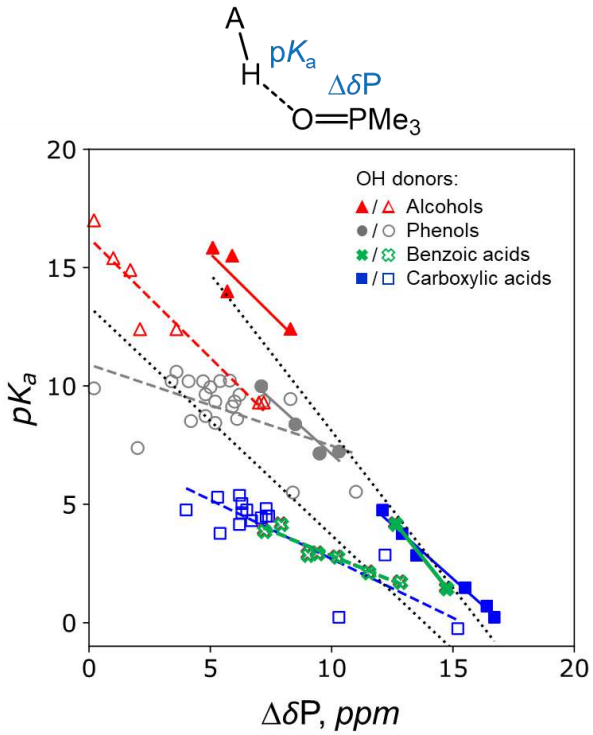

Figure 2.15. Correlation between $\Delta\delta$P and pK_a for 1:1 complexes with different OH acids: alcohols (red triangles), phenols (grey circles), benzoic acids (green cross) and carboxylic acids (blue squares), which were studied here (filled symbols) or collected from refs. [124,136,137] (open symbols). Solid lines correspond to fitting of data points (see text for more information).

2.4. Me_3PO complexes with two hydrogen bonds

In this section we discuss correlations between geometric, energetic, NMR and IR spectral characteristics of both 1:2 and 1:1 complexes and cooperativity (anticooperativity) effects on the same parameters.

The optimized structures of some 1:2 complexes with O···H–O (Figure 2.16a), O···H–N (Figure 2.16b), O···H–N^+ (Figure 2.16c) and O···H–C (Figure 2.16d) hydrogen bonds are shown on the examples of Me_3PO complexes with phenol (**22**), pyrrole (**34**), imidazolium (**41**) and fluoroacetylene (**60**). In all studied complexes hydrogen bonds are close to linear and formed in directions to localization of lone pairs of Me_3PO oxygen atom. The formation of each hydrogen bond was confirmed by the presence of bond critical point between Me_3PO oxygen atom and hydrogen atoms in both proton donor groups of two AH molecules.

The numeric values of the geometric, energetic, IR and NMR spectral parameters, as well as the cooperativity (anticooperativity) effects on them are collected in Table 2.3 for 1:2 complexes of Me_3PO with **1**–**70** proton donors in chloroform. Individual parameters for each hydrogen bond in the same 1:2 complex, such as hydrogen bonds lengths, chemical shifts of bridging protons and QTAIM parameters (calculated at bonds critical points) are close in value to each other (the spread of values is less than 5%) and listed in Table 2.3 for one of the hydrogen bonds. In other words, Me_3PO molecule forms two equivalent hydrogen bonds in 1:2 complexes in a symmetrical way. Some energetic and geometric parameters of the complexes 1:2 are listed in Appendix A, Table A2. Recall that all characteristics of 1:1 complexes formed by Me_3PO and the same proton donors **1**–**70** were taken from Table 2.1.

In the next sections we discuss the changes of energetic, geometric and spectral parameters as well as the changes in the electron localization function (ELF), the electrostatic potential (ESP) distributions near P=O acceptor group upon formation of hydrogen bonds.

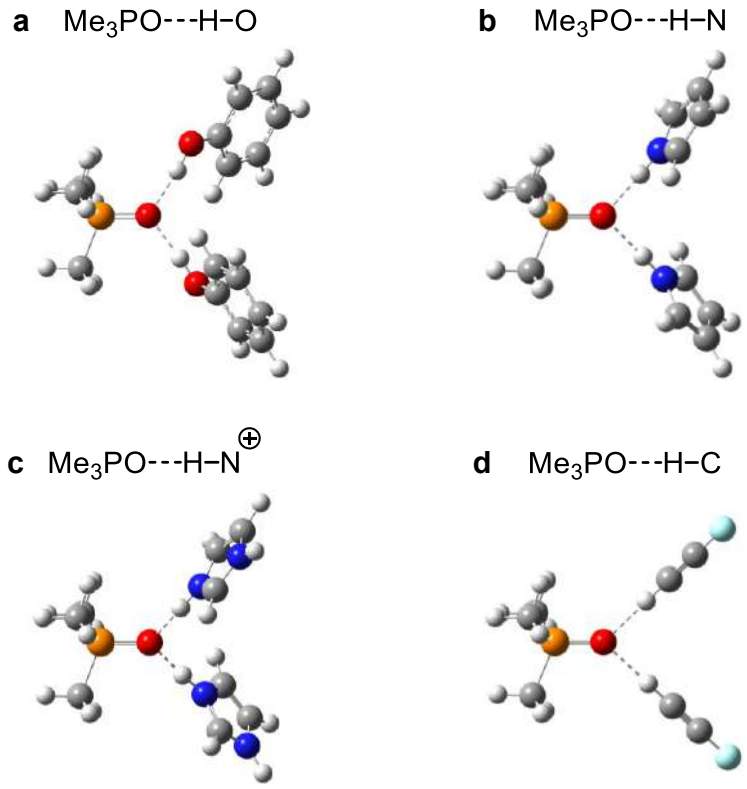

Figure 2.16. Typical structures of 1:2 complexes with (a) $Me_3PO\cdots HO$, (b) $Me_3PO\cdots HN$, (c) $Me_3PO\cdots HN^+$ and (d) $Me_3PO\cdots HC$ types of hydrogen bond. The complexes with (a) phenol (**22**), (b) pyrrole (**34**), (c) imidazolium (**41**) and (d) fluoroacetylene (**60**) are taken as examples.

Table 2.3. Energetic, geometric, IR and NMR spectral parameters of 1:2 complexes formed by Me_3PO with proton donors **1**–**70** in chloroform (PCM, ε = 4.7): hydrogen bond energy ΔE^a and total complexation energy ΔE^t (in kJ·mol^{-1}), interatomic distance r_2^a (in Å); changes of ^{1}H and ^{31}P NMR chemical shifts $\Delta\delta H^a$ and $\Delta\delta P^t$ (in ppm); P=O stretching vibrational frequency $\Delta\nu^t_{P=O}$ (in cm^{-1}) and also the values of cooperativity (anticooperativity) effects on energy $\Delta\Delta E/\Delta E$ ($\Delta\Delta E = \Delta E^a - \Delta E$), geometry $\Delta r_2/r_2$ ($\Delta r_2 = r_2^a - r_2$), NMR chemical shifts $\Delta\Delta\delta$H and $\Delta\Delta\delta$P (in ppm) and P=O stretching frequency $\Delta\Delta\nu_{P=O}$ (in cm^{-1}), which were calculated using the parameters of 1:1 complexes of Me_3PO with the same proton donors taken from Table 2.1. Some others energetic and geometric parameters of studied 1:2 complexes are given in Appendix A, Table A2.

No.	Proton donor	ΔE^a	ΔE^t	$\Delta\Delta E/\Delta E$	r_2^a	$\Delta r_2/r_2$	$\Delta\delta H^a$	$\Delta\Delta\delta H$	$\Delta\delta P^t$	$\Delta\Delta\delta P$	$\Delta\nu^t_{P=O}$	$\Delta\Delta\nu_{P=O}$
OH proton donors												
1	Water	27.39	57.47	–0.09	1.790	0.015	4.4	–0.5	12.2	6.6	–40.6	–22.4
2	Methanol	26.32	56.00	–0.11	1.793	0.019	4.7	–0.5	12.6	6.7	–41.6	–25.1
3	Fluoromethanol	36.48	78.75	–0.14	1.695	0.027	5.6	–0.9	19.4	10.5	–66.1	–38.3
4	Difluoromethanol	39.66	88.86	–0.19	1.638	0.048	6.8	–1.5	22.5	11.5	–75.2	–37.5
5	Trifluoromethanol	45.75	108.55	–0.27	1.576	0.075	7.4	–2.3	26.8	13.3	–97.7	–47.5
6	Chloromethanol	38.47	84.71	–0.17	1.669	0.038	6.7	–1.1	21.4	11.4	–75.5	–40.1
7	Dichloromethanol	39.54	93.12	–0.26	1.619	0.075	7.8	–2.0	24.0	11.9	–90.3	–43.3
8	Ethanol	23.96	52.02	–0.15	1.812	0.023	4.8	–0.5	12.3	7.3	–38.2	–22.1
9	2,2,2-Trifluoroethanol	35.15	75.50	–0.13	1.718	0.030	5.3	–0.9	17.5	9.3	–61.9	–43.2
10	Formic acid	40.15	89.56	–0.19	1.629	0.050	6.7	–1.4	24.4	11.5	–86.9	–39.8
11	Acetic acid	38.16	83.42	–0.16	1.651	0.043	6.5	–1.1	23.3	11.1	–80.3	–37.7
12	Chloroacetic acid	41.94	95.16	–0.21	1.607	0.059	7.2	–1.5	25.7	12.2	–94.6	–42.9
13	Dichloroacetic acid	45.73	105.12	–0.23	1.580	0.067	7.4	–1.9	28.3	12.8	–109.7	–46.3
14	Trichloroacetic acid	47.29	110.45	–0.25	1.561	0.079	7.8	–2.2	29.6	13.2	–108.9	–39.6
15	Trifluoroacetic acid	47.07	111.86	–0.27	1.553	0.082	7.8	–2.3	29.9	13.3	–110.5	–36.4
16	Benzoic acid	39.16	85.95	–0.16	1.641	0.046	7.0	–1.1	24.0	11.5	–84.5	–37.8
17	Pentafluorobenzoic acid	43.63	99.99	–0.23	1.591	0.066	7.4	–1.7	27.6	12.9	–96.9	–38.9
18	Methanesulfonic acid	49.99	115.12	–0.23	1.538	0.086	7.9	–2.5	30.6	12.3	–111.6	–76.5
19	Benzenesulfonic acid	50.59	115.01	–0.21	1.551	0.093	7.6	–2.7	29.6	11.9	–109.0	–53.1
20	*p*-Toluenesulfonic acid	51.45	112.79	–0.16	1.556	0.102	7.5	–3.3	29.3	12.2	–108.6	–54.1
21	Phenylphosphonic acid	45.36	99.42	–0.16	1.608	0.055	7.2	–1.8	27.7	13.3	–90.9	–39.9
22	Phenol	32.14	72.56	–0.20	1.731	0.039	5.7	–0.8	18.0	10.8	–64.0	–36.8
23	2-Nitrophenol	39.27	91.82	–0.25	1.661	0.043	6.5	–1.2	23.2	12.9	–80.8	–40.0
24	3-Nitrophenol	34.81	83.80	–0.29	1.697	0.050	6.0	–1.1	21.1	12.5	–72.6	–45.7
25	4-Nitrophenol	36.70	88.73	–0.29	1.674	0.050	6.3	–1.1	22.6	13.1	–79.6	–39.7
NH proton donors												
26	Ammonia	11.16	23.16	–0.07	2.062	0.007	2.8	–0.1	4.6	2.4	–19.1	–10.5
27	Dimethylamine	10.64	22.54	–0.11	2.066	0.017	2.8	–0.2	4.6	2.7	–17.8	–10.0
28	Aziridine	13.04	28.66	–0.16	2.013	0.016	2.8	–0.4	7.2	4.1	–23.8	–14.4
29	Azetidine	10.52	22.22	–0.10	2.071	0.012	2.7	–0.1	5.1	2.9	–18.8	–11.4
30	Pyrrolidine	7.61	19.61	–0.37	2.125	0.033	2.2	–0.5	3.4	1.4	–15.4	–7.4
31	Piperidine	10.46	22.01	–0.09	2.070	0.010	2.7	–0.1	4.4	2.4	–17.2	–9.5
32	Piperazine	8.81	20.64	–0.26	2.109	0.026	2.8	–0.2	5.0	3.4	–19.8	–12.0
33	2-Pyrrolidone	24.45	51.39	–0.09	1.867	0.011	4.5	–0.2	14.9	7.0	–50.0	–24.3
34	Pyrrole	22.54	50.60	–0.20	1.854	0.030	3.9	–0.4	12.2	7.3	–38.2	–23.7
35	Imidazole	25.54	59.22	–0.24	1.811	0.036	4.2	–0.5	14.5	8.8	–49.4	–33.4
36	Pyrazole	28.57	61.92	–0.14	1.785	0.020	4.4	–0.2	15.8	9.6	–50.4	–31.1
37	1,4-Dihydropyrazine	16.01	36.19	–0.21	1.922	0.025	3.9	–0.5	8.8	5.1	–30.7	–19.1
NH^+ proton donors												
38	Ammonium	–9.52	67.91	–1.12	1.638	0.095	–	–	–	–	–	–
39	Dimethylammonium	–12.94	56.18	–1.19	1.734	0.105	–	–	–	–	–	–
40	Trimethylammonium	–17.93	49.52	–1.27	1.806	0.140	–	–	–	–	–	–
41	Imidazolium	–0.19	66.10	–1.00	1.666	0.079	–	–	–	–	–	–
42	Pyridinium	–1.95	68.09	–1.03	1.651	0.077	–	–	–	–	–	–

43	2-Picolinium	−3.02	63.28	−1.05	1.657	0.057	–	–	–	–	–	–
44	3-Picolinium	−1.22	66.94	−1.02	1.659	0.074	–	–	–	–	–	–
45	4-Picolinium	−0.41	66.70	−1.01	1.678	0.082	–	–	–	–	–	–
46	3,5-Lutidinium	−0.44	66.36	−1.01	1.663	0.073	–	–	–	–	–	–
47	2,6-Lutidinium	−12.94	48.19	−1.21	1.760	0.099	–	–	–	–	–	–
48	2,4,6-Collidinium	−9.34	49.31	−1.16	1.763	0.096	–	–	–	–	–	–
49	2-(Dimethylamino)pyridinium	−11.44	44.35	−1.21	1.847	0.112	–	–	–	–	–	–
50	3-(Dimethylamino)pyridinium	1.08	65.52	−0.98	1.678	0.071	5.4	−1.3	28.1	15.9	−93.6	−58.4
51	4-(Dimethylamino)pyridinium	1.62	58.98	−0.97	1.710	0.063	5.4	−1.3	25.0	14.2	−79.3	−50.5
52	3,5-(Dimethylamino)pyridinium	2.94	63.29	−0.95	1.696	0.067	5.2	−1.3	26.0	14.7	−84.1	−48.0
53	3,4,5-(Trimethoxy)pyridinium	−2.23	61.34	−1.04	1.696	0.079	–	–	–	–	–	–
54	3,4,5-Trifluoropyridinium	−4.00	81.05	−1.05	1.587	0.103	–	–	–	–	–	–
55	3,4,5-Trichloropyridinium	−2.32	79.44	−1.03	1.608	0.105	–	–	–	–	–	–
56	3,5-Diaminopyridinium	2.16	66.08	−0.97	1.671	0.068	5.5	−1.3	28.3	16.3	−84.8	−47.5
CH proton donors												
57	Trifluoroethylene	12.93	27.79	−0.13	2.071	0.025	2.5	−0.2	5.2	3.2	−17.8	−10.5
58	Trichloroethylene	14.36	29.14	−0.03	2.052	0.019	2.6	0.0	4.9	2.8	−19.3	−10.9
59	Acetylene	12.70	27.54	−0.14	2.029	0.023	3.0	−0.2	5.1	3.5	−19.6	−12.0
60	Fluoroacetylene	13.65	29.52	−0.14	2.011	0.023	3.2	−0.2	5.3	3.7	−19.9	−12.3
61	Hydrogen cyanide	22.58	53.35	−0.27	1.846	0.039	4.2	−0.6	12.9	8.1	−48.0	−29.8
62	Trinitromethane	30.30	72.01	−0.27	1.822	0.071	4.0	−1.3	17.5	8.9	−66.7	−34.8
63	1,1-Dinitroethane	19.68	45.06	−0.22	2.009	0.050	2.8	−0.6	10.9	6.2	−43.1	−23.6
64	2-Nitropropane	7.88	17.70	−0.20	2.293	0.022	1.6	−0.2	5.2	2.4	−16.1	−8.3
65	Trichloromethane	19.14	41.25	−0.13	1.976	0.037	2.5	−0.3	8.9	4.8	−31.3	−19.6
66	Dichloromethane	13.87	28.81	−0.07	2.065	0.019	2.4	−0.2	5.5	3.0	−22.4	−13.4
67	Chloromethane	6.92	14.26	−0.06	2.260	0.026	1.8	−0.2	3.6	2.6	−12.0	−7.7
68	Methane	−0.56	−0.37	−3.94	2.962	0.081	–	–	–	–	–	–
69	Trifluoromethane	14.93	33.82	−0.21	2.020	0.030	2.2	−0.2	7.5	4.7	−18.2	−10.4
70	Tribromomethane	13.52	32.81	−0.30	1.997	0.042	2.4	−0.3	8.7	4.6	−33.0	−21.7

ELF and ESP distributions

In the Figures 2.17–2.18 the distributions of ELF and ESP near to oxygen atom of P=O group are shown for isolated Me_3PO and its 1:1 and 1:2 complexes on the example of complexes with methanol (**2**). The changes in ELF and ESP distributions upon complexation are visible: the formation of one hydrogen bond with methanol leads to localizations of ELF and ESP on the side of oxygen atom opposite to AH proton donor. The second hydrogen bond is formed in the directions of ELF and ESP localizations maxima. In complex with two hydrogen bonds ELF and ESP are redistributed relative to ones in 1:1 complex and localized in two (for ESP) or three (for ELF) separate species. These localizations of ELF and ESP may potentially indicate the most likely directions of formation third hydrogen bond with phosphine oxide.

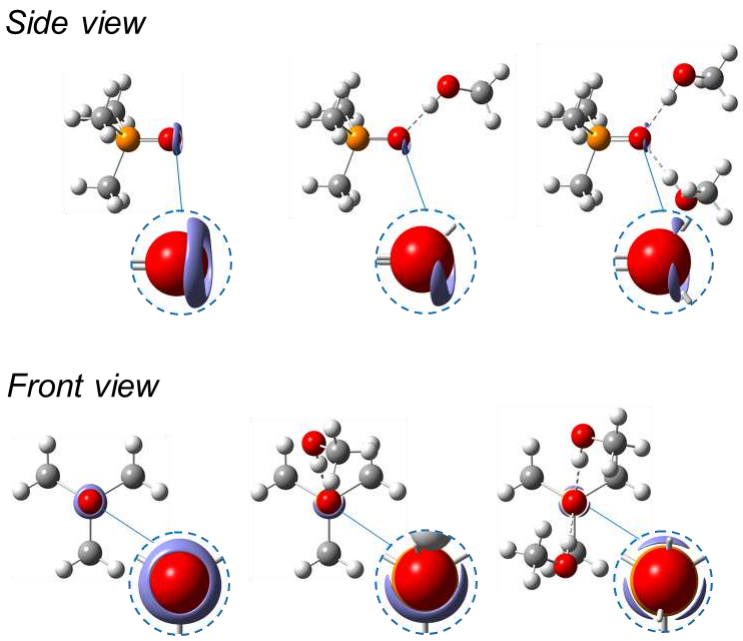

Figure 2.17. ELF isosurface (the value equal to 0.875) near oxygen atom for isolates Me_3PO, 1:1 complex and 1:2 complexes formed by Me_3PO and methanol (**2**).

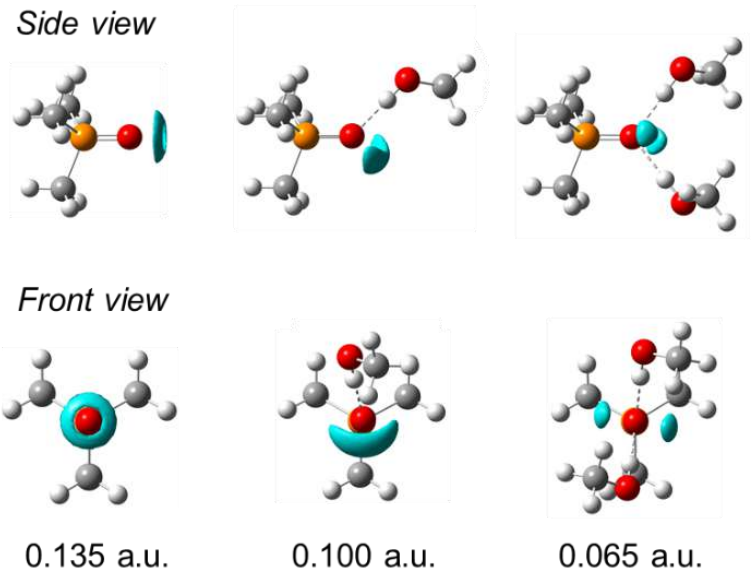

Figure 2.18. ESP isosurfaces near oxygen atoms for isolated Me_3PO molecule and its 1:1 and 1:2 complexes with methanol (**2**).

Hydrogen bond angles: α, β and γ

The distribution diagrams of hydrogen bond angles α (P=O···H), β (O···H–A) and dihedral angles γ (defined as described in the text below), for 1:2 complexes formed by Me_3PO with proton donors **1**–**70** are discussed in this section. The numeric values of these angles are given in Appendix A, Table A2.

The semicircle diagrams of α and β angles distributions are shown in Figure 2.19 and plotted for each hydrogen bond in 1:2 complexes (140 values in total). Semicircle axes of diagram indicate the range of angles changes with a step size of 10°. Horizontal axes correspond the number of complexes with the values of angles in according ranges.

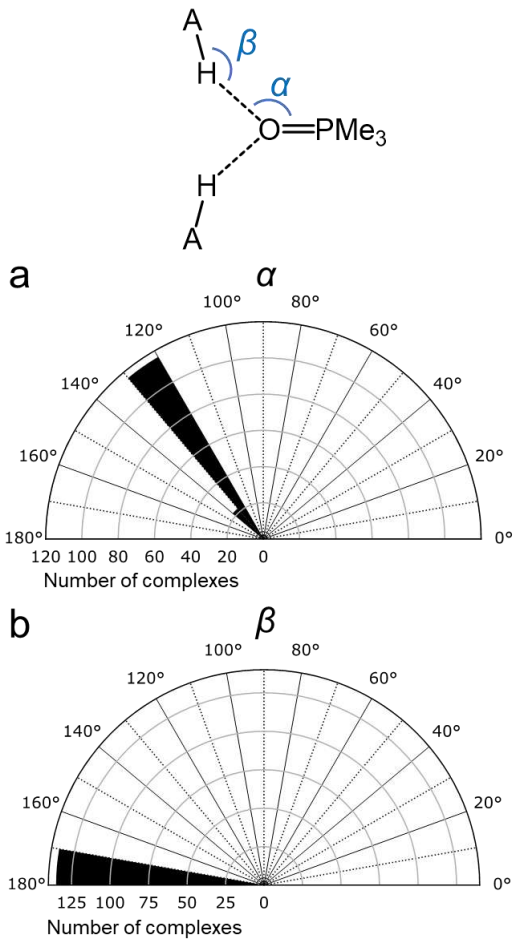

Figure 2.19. Distribution diagrams of angles (a) α and (b) β in 1:2 complexes of Me_3PO with proton donors (**1**–**70**).

The maximum of α distribution diagram is close to 125° (Figure 2.19a) with the span from 120° and 130°, indicating that the hydrogen bonds formed along lone pair of oxygen atom of Me_3PO. The angles β are close to linear for all hydrogen bonds in 1:2 complexes (Figure 2.19b).

The dihedral angle γ indicates the mutual positions of two hydrogen bonds in each of 1:2 complex relative to P=O bond of Me_3PO as schematically depicted in Figure 2.20, above. The diagram shown in Figure 2.20a indicates the distributions of numeric values of angles γ for 1:2 complexes studied here: the angle γ is close to 180° for the majority of complexes, in other words, two hydrogen bonds are formed approximately opposite each other. The values of γ significantly deviating from 180° correspond to Me_3PO complexes

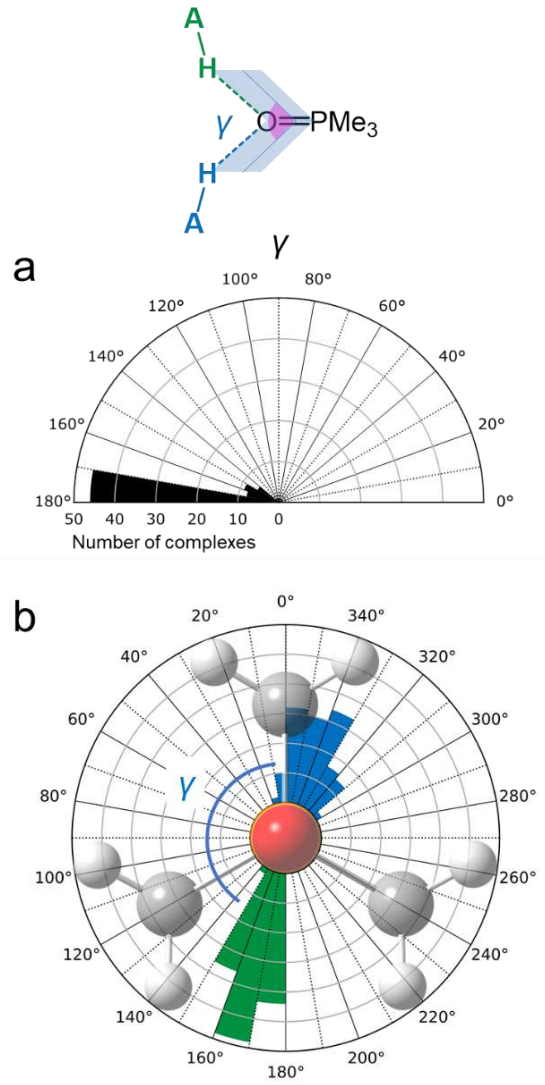

Figure 2.20. (a) Distribution diagram of angles γ values and (b) distribution diagram of AH proton donors positions in 1:2 complexes relative to Me_3PO.

with carboxylic acids (for example acetic acid (**11**), chloroacetic acid (**12**), benzoic acid (**16**), and phenylphosphonic acid (**21**)) or with AH molecules, in which substituent close to proton donor group (for example trinitromethane (**62**), 1,1- dinitroethane (**63**), 2-nitropropane (**64**)). In most of these complexes additional interactions may be appeared between the electronegative group of AH molecule (carboxyl group or substituents) and protons in methyl groups of phosphine oxide, which were obtained for the some 1:1 complexes (see additional interactions in 1:1 complexes in Figure 2.7) and may be influence in geometry of hydrogen bond in complexes.

The distribution diagram shown in Figure 2.20b demonstrates the mutual positions of two proton donors in 1:2 complexes relative to Me_3PO position (the P=O bond is directed perpendicular to the plane of the figure). The directions of the bars marked in blue correspond the deviation of one of the hydrogen bonds from the closest P–C bond (viewed in the plane of the figure), while the bars marked in green correspond the deviation of the other hydrogen bond from the same P–C bond of Me_3PO (with the step size of 10°). The length of each bar indicates the number of proton donors located in this direction. The angle between two directions of hydrogen bonds within the same complex correspond the angle γ discussed above. The maximum of distribution of "green" proton donor positions for 1:2 complexes is close to 160°, while the maximum for "blue" proton donors is located between 330° and 360° and is slightly deviate from 0° –the direction of the P–C bond. This deviation may be explained by the interaction of the "blue" proton donor with the methyl group of phosphine oxide. At the same time, there is the tendency for the formation of hydrogen bonds located opposite each other in each complex.

Hydrogen bond energy: correlations between ΔE, V, G

By analogy with section 2.3 for 1:1 complexes, in this section, in Figure 2.21a,b, the correlations between the energy of one hydrogen bond, ΔE^a and G^a, as well as between G^a and V^a, obtained for 1:2 complexes with OH (red circles), NH (blue triangles), NH^+ (black stars) and CH (olive diamonds) proton donors. For comparison, the data points corresponded to 1:1 complexes also shown in Figure 2.21 by open gray symbols (the shapes of symbols correspond the type of hydrogen bond as for 1:2 complexes).

The correlation $G^a(V^a)$ is general for both 1:1 and 1:2 complexes as well as for all electroneutral and cationic complexes. Besides, this correlation is certainly nonlinear and may be described by the power function $G = 3.6 \cdot V^{0.71}$ for all complexes in the wide range

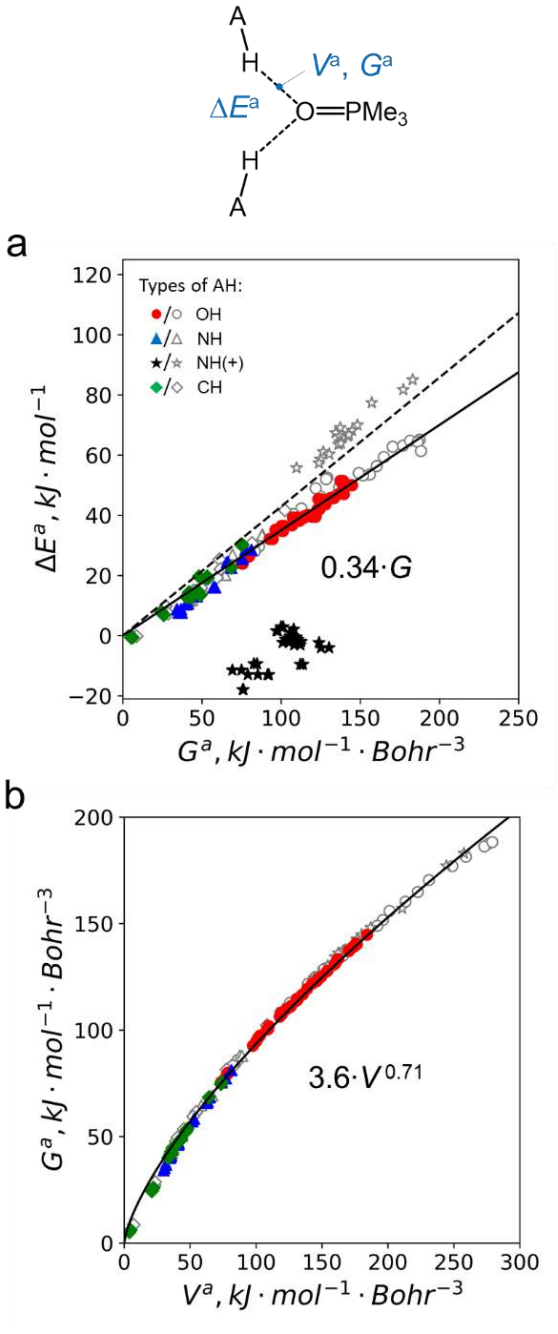

Figure 2.21. (a) Correlation between the hydrogen bond energy ΔE^a and local electron kinetic energy density G^a calculated at BCP. (b) Correlation between G^a and local electron potential energy density V^a calculated at BCP. Open gray symbols correspond to 1:1 complexes; filled red, blue and green symbols correspond to 1:2 complexes. Solid curves correspond to correlational function obtained by least squared fitting and shown next to the curves. The dashed line corresponds to the correlation proposed in [44,45].

of the hydrogen bond strength. The correlation $\Delta E^a(G^a)$ is general within the set of electroneutral complexes for both complexes with one and two proton donors, whereas the data points correspond to cationic complexes significantly deviate from this correlation and lie slightly above (in case of 1:1 complexes) or significantly below (in case of 1:2 complexes). Solid line correspond correlation coefficient $k = 0.34$ Bohr obtained for all electroneutral complexes (dashed line correspond coefficient $k = 0.43$ Bohr reported in [44,45]).

The strength of single hydrogen bond in cationic complexes vary in the range from *ca.* 55 kJ·mol^{-1} to *ca.* 85 kJ·mol^{-1} and higher than them in almost all electroneutral complexes. On the contrary, the strength of second hydrogen bond is negative for the most cationic complexes with two hydrogen bonds (see the values of ΔE^a for cationic complexes in Table 2.3). This can be explained by considering the profile of a total electron energy shown schematically in Figure 2.22 for isolated Me_3PO, isolated NH^+ proton donors and their 1:1 and 1:2 cationic complexes. The formation of 1:1 cationic complex lead to significant decrease in the total electron energy: strong hydrogen bond is formed. The total electron energy of 1:2 cationic complex is slightly more than them for 1:1 cationic complex for the most of cationic complexes considered here: the formation of two hydrogen bonds between Me_3PO and cationic proton donors is less energetically unfavorable than the formation of one hydrogen bond due to Coulomb repulsion of two positive charges on proton donors. Note that the strength of one hydrogen bond is also negative for only one electroneutral Me_3PO complex with methane **60** (complex 1:2), which may be associated with taking into account the relaxation energies of AH monomers when calculating energy ΔE: AH relaxation energy may contribute more to the calculated value of complexation energy and slightly underestimate it. It may have a particularly strong effect on the weakest complexes (including complex with methane – the weakest within the set of 1:2 complexes) and leads to negative strength of complexes, while the strength estimated by the G^a, V^a corresponds the positive strength. In the following sections we excluded cationic complexes (**38**)–(**56**) and complex with methane (**60**) from discussion.

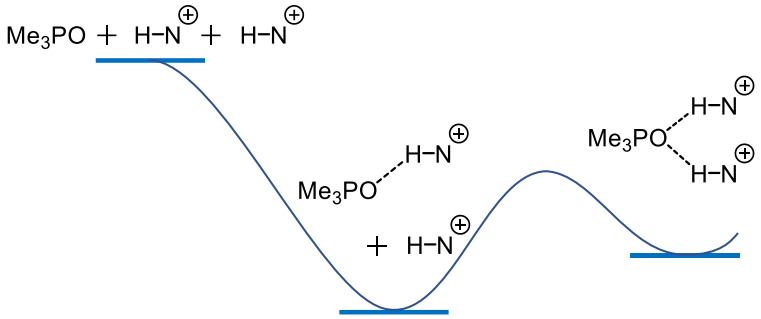

Figure 2.22. Schematic energy profile for the formation of most complexes formed by Me_3PO and cationic proton donors (HN^+).

Hydrogen bond energy: correlations with IR, NMR spectral parameters

Note that one of the goals of this part of work is to expand IR, NMR spectrum-energy correlations for the case of more complicated complexes than 1:1 complexes.

In this section we discussed the correlations between hydrogen bond strength, ΔE^t or ΔE^a, and three spectral parameters: $\Delta\nu^t_{P=O}$, $\Delta\delta H^a$ and $\Delta\delta P^t$ for both 1:2 and 1:1 complexes of Me_3PO. The correlations $\Delta E^t(\Delta\nu^t_{P=O})$, $\Delta E^a(\Delta\delta H^a)$ and $\Delta E^t(\Delta\delta P^t)$ shown in Figure 2.23a,b,c respectively. All these correlations are general for both complexes with one and two hydrogen bonds as well as for all type of proton donors. It seems that spectral characteristics of P=O group, $\Delta\nu^t_{P=O}$ and $\Delta\delta P$, sensitive to the strength of both hydrogen bonds ΔE^t, while the spectral characteristic of bridging proton, $\Delta\delta H$, sensitive to the strength of only one hydrogen bond ΔE^a. The correlations $\Delta E^t(\Delta\nu^t_{P=O})$ and $\Delta E^t(\Delta\delta P^t)$ seems slightly nonlinear. Solid curves in the Figure 2.23a,c also correspond to power functions $\Delta E^t = 2.7\cdot(\Delta\nu^t_{P=O})^{0.79}$ and $\Delta E^t = 6.6\cdot(\Delta\delta P^t)^{0.83}$, which described correlations and were obtained by the least squares fitting. In opposite, the correlation between ΔE^a and $\Delta\delta H^a$ is seems linear with coefficient $k = 6.0$ kJ·mol^{-1}·ppm^{-1} (solid line in Figure 2.23b correspond these coefficient). The scattering of data points from all correlations is less than 10%.

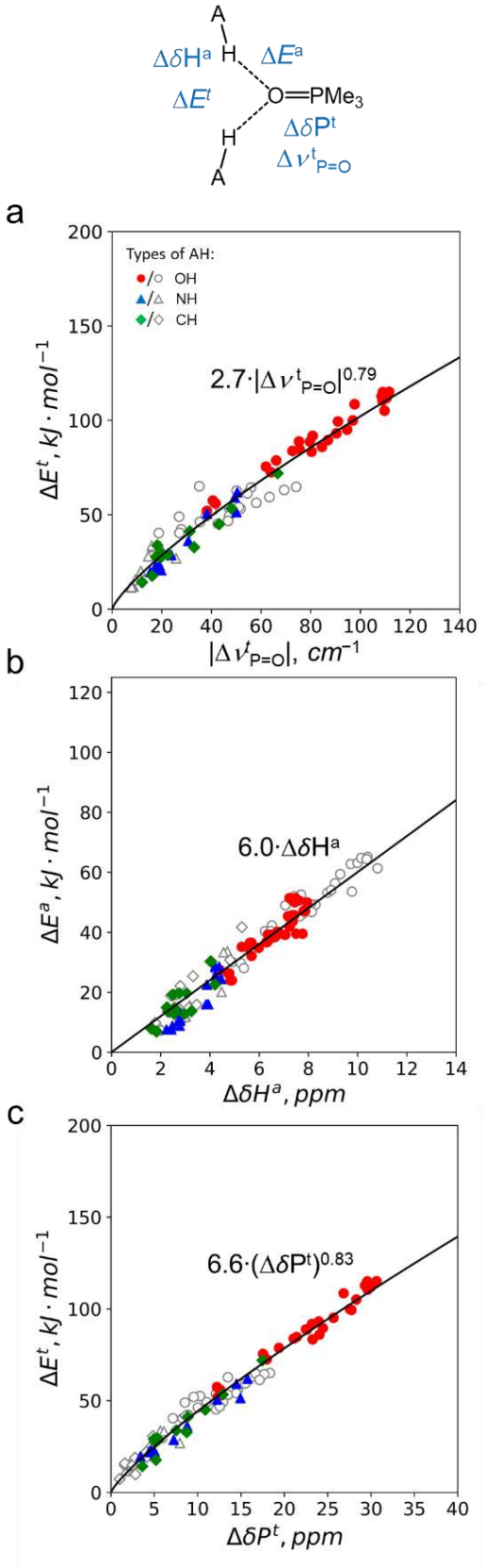

Figure 2.23. Correlations between (a) total complexation energy ΔE^t and $|\Delta\nu^t_{P=O}|$, (b) hydrogen bond energy ΔE^a and $\Delta\delta H^a$, (c) ΔE^t and $\Delta\delta P^t$. Solid lines correspond to the results of least squares fitting for both 1:1 and 1:2 complexes.

In general terms, IR and NMR spectral parameters considered here given similar estimations of hydrogen bonds strength for all electroneutral complexes of Me_3PO with one or two proton donors. In the case of 1:2 complexes and, probably, more complicated complexes, together spectral parameters $\Delta\nu^{t}_{P=O}$, $\Delta\delta H^{a}$ as well as $\Delta\delta P^{t}$, $\Delta\delta H^{a}$ complement each other and may be applied for the estimation of total complexation energy or the strength of each hydrogen bond separately. In this case the using of together NMR parameters seems more convenient in experimental investigation since only one sample preparation is required and NMR spectra are recorded using the same equipment. The correlations between the spectral parameters $|\Delta\nu^{t}_{P=O}|$, $\Delta\delta H^{a}$, $\Delta\delta P^{t}$ and local electron kinetic and potential energy densities, G^{a}, V^{a}, $G^{t} = G^{a} + G$ and $V^{t} = V^{a} + V$ are given in Appendix A, Figures A4–A6.

Cooperativity effects on hydrogen bonds strength

The mutual influence of two hydrogen bonds in 1:2 complexes to each other leads to decrease in the strength of each of them in comparison with the strength of one hydrogen bond in 1:1 complex, *i.e.* anticooperativity effects on the hydrogen bond strength manifest as demonstrated in Figure 2.24a by correlations between the strength of hydrogen bonds in 1:1 complex, ΔE, and the strength of one hydrogen bond in 1:2 complex, ΔE^{a}. The dashed line corresponds the equal values of ΔE and ΔE^{a} for Me_3PO complexes with same proton donors, *i.e.* this line indicates the boundary between cooperative and anticooperative hydrogen bonds. All points lie blow this line, which especially noticeable for stronger complexes. The correlation between $\Delta\Delta E/\Delta E$ and ΔE shown in Figure 2.24b conveys the same information more clearly: the data points lie below horizontal dashed line correspond to anticooperativity effects on the strength in these complexes. Both correlations are general for complexes with different types of proton donors. The value of anticooperativity effects on the strength of two hydrogen

bonds in 1:2 complex varies from 0% up to ~40% depending on the energy of single hydrogen-bonded in 1:1 complex with the same proton donor: anticooperativity effect is greater for the complexes with stronger hydrogen bond. The same patterns hold for correlations $G^a(G)$ and $\Delta G/G(G)$ shown in Appendix A, Figure A7, for which the scattering of data points less than for correlation $\Delta E^a(\Delta E)$ and $\Delta\Delta E/\Delta E(\Delta E)$. The

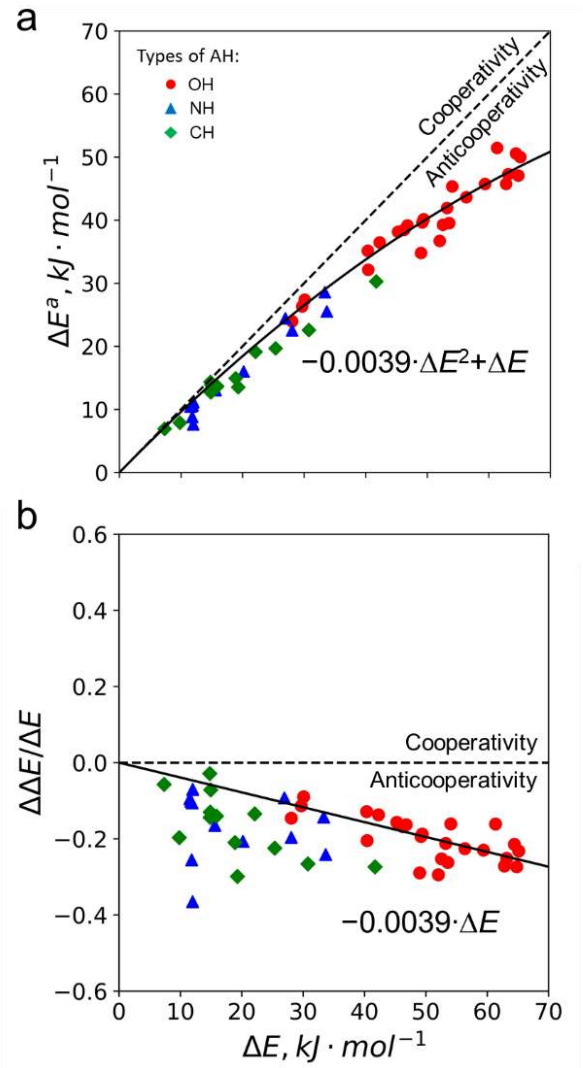

Figure 2.24 (a) Correlation between hydrogen bond energy in 1:2 complexes ΔE^a and the hydrogen bond energy in 1:1 complexes ΔE. (b) Correlation between relative cooperativity on hydrogen bond energy $\Delta\Delta E/\Delta E$ ($\Delta\Delta E = \Delta E^a - \Delta E$) and ΔE. Solid lines correspond to correlational curves obtained from correlation functions for $\Delta\Delta G/G(G)$ (see Appendix A, Figure A7b) and $\Delta E^a(G^a)$ (see Figure 2.21). Dashed lines indicate the boundary between regions of cooperativity and anticooperativity effects.

correlation between $\Delta G/G$ and G (see Appendix A, Figure A7b) well described by the linear function $\Delta G/G = -0.0013 \cdot G$ with coefficient obtained by the least squared fitting. Using last equation and linear correlation between $\Delta E^a(G^a)$ (see Figure 2.21a) the function $\Delta\Delta E/\Delta E = -0.0039 \cdot \Delta E$ was derived and shown by the solid curve in Figure 2.24b. The spread of data points for weak complexes may be explained by the greater relative errors in $\Delta\Delta E/\Delta E$ for them. The correlation $\Delta E^a(\Delta E)$ is slightly nonlinear and could be described by the following function derived from the last equation: $\Delta E^a = -0.0039 \cdot \Delta E^2 + \Delta E$.

Cooperativity effects on IR and NMR spectral parameters

The sensitivity of IR and NMR spectral characteristics to formation of 1:2 complexes various strength is discussed in this section.

Figure 2.25a–c shows the correlations between the strength of hydrogen bond ΔE in complexes with one proton donor and cooperativity effects on IR and NMR spectral parameters: the changes of stretching vibrations, $|\Delta\Delta\nu_{P=O}|$, ^{1}H and ^{31}P NMR chemical shifts, $\Delta\Delta\delta$H and $\Delta\Delta\delta$P. The strength of hydrogen bond in 1:1 complexes, ΔE, is plotted on the abscissa axis to demonstrate the change in sensitivity of spectral characteristics upon formation of the second hydrogen bond depending on the strength of one hydrogen bond. The absolute values of these spectral parameters increase with strengthening of hydrogen bond in 1:1 complexes and correlations seem the general for all types of hydrogen bond. The correlations $\Delta\Delta\delta$P(ΔE) and $|\Delta\Delta\nu_{P=O}|(\Delta E)$ demonstrate the similar trend: the changes of spectral characteristics monotonously and almost linearly increase with increasing of ΔE in all range of complexation energies. In contrast, the correlation $\Delta\Delta\delta$H(ΔE) seems significantly nonlinear: the values of $\Delta\Delta\delta$H increase more for stronger

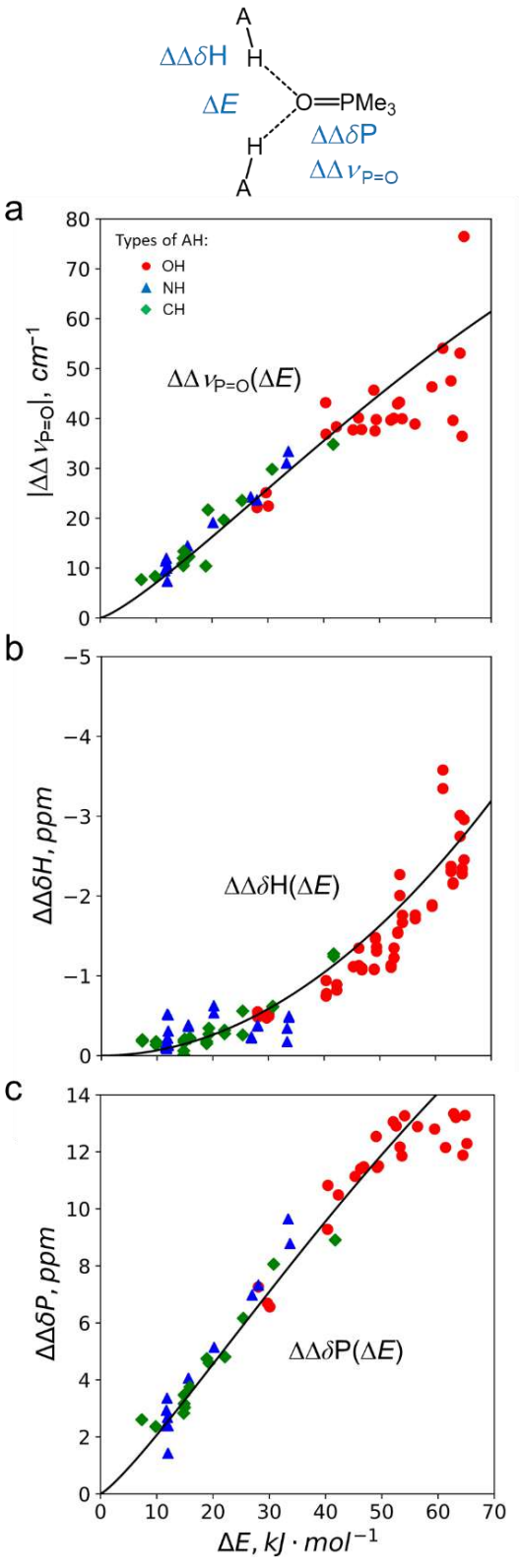

Figure 2.25. Correlations between energy of hydrogen bond in 1:1 complexes, ΔE, and cooperativity effects on IR and NMR spectral parameters: (a) $\Delta\Delta\nu_{P=O} = \Delta\nu^{t}_{P=O} - \Delta\nu_{P=O}$, (b) $\Delta\Delta\delta H = \Delta\delta H^{a} - \Delta\delta H$ and (c) $\Delta\Delta\delta P = \Delta\delta P^{t} - \Delta\delta P$. Solid lines correspond to correlation functions $\Delta\Delta\nu_{P=O}(\Delta E)$, $\Delta\Delta\delta H(\Delta E)$ and $\Delta\Delta\delta P(\Delta E)$ and explicitly given in Appendix A, Table A3.

complexes. The functions described these correlations $\Delta\Delta\nu_{P=O}(\Delta E)$, $\Delta\Delta\delta H(\Delta E)$ and $\Delta\Delta\delta P(\Delta E)$ were derived from fitting functions for correlations shown earlier in Figures 2.23 and 2.24 and they explicit equations are given in Appendix A, Table A3. The correlation curves corresponded by these functions are shown in Figure 2.25a–c by the solid lines. Each of them curves are well describe corresponding data points. Notice that all three functions, strictly speaking, indicate nonlinearity of considered correlations. The scattering of data points from correlation curves is slightly less for $\Delta\Delta\nu_{P=O}(\Delta E)$ and $\Delta\Delta\delta P(\Delta E)$ than for $\Delta\Delta\delta H(\Delta E)$, and especially significant for strongest complexes (with hydrogen bond strength more than ~50 kJ·mol^{-1}).

Hydrogen bonds geometry: interatomic distances

The interdependence of q_1 and q_2 was reported for 1:1 complexes of Me_3PO and proton donors **1**–**70** (see Figure 2.9). In this section we test the same interdependence for complexes of Me_3PO with two proton donors. The correlation between hydrogen bond coordinates $q_1^a = \frac{1}{2}(r_1^a - r_2^a)$ and $q_2^a = r_1^a + r_2^a$ is shown in Figure 2.26 for 1:2 complexes (red, green and blue symbols; the data points refer to 1:1 complexes also shown in the Figure 2.26 by the gray symbols). The interdependence $q_2^a(q_1^a)$ also may described by the same set of parametric equations (1.1)–(1.3) as for 1:1 complexes. Curves built according these equations are shown in Figure 2.26 by the solid lines and marked in red for $Me_3PO\cdots HO$, blue for $Me_3PO\cdots HN$ (and $Me_3PO\cdots HN^+$) and green for $Me_3PO\cdots HC$ types of hydrogen bonds in complexes. These curves perfect describe the data points correspond the hydrogen bond distances in both 1:1 and 1:2 complexes. Notice that the data points refer to 1:2 complexes generally shift upper along of curves in comparison with the data points for 1:1 complexes, that indicates the hydrogen bond becomes longer upon formation of two hydrogen bonds.

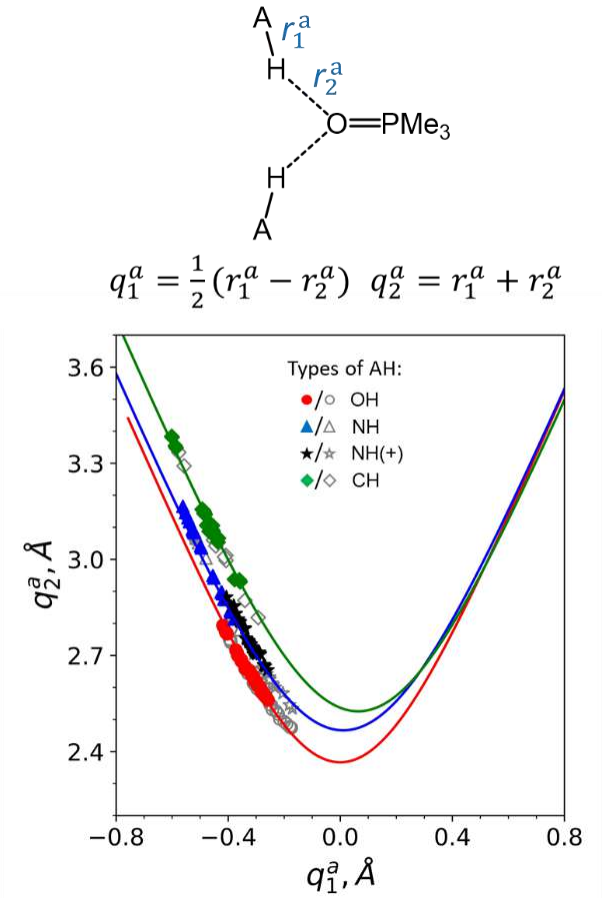

Figure 2.26 Correlation between hydrogen bond coordinates q_2^a and q_1^a. Open gray symbols correspond to 1:1 complexes; filled red, blue and green symbols correspond to 1:2 complexes. The solid lines correspond to correlation curves obtained from equations (1.1)–(1.3) with numerical values of parameters taken from ref. [28,29] and collected in Table 2.2.

The relation between hydrogen bond strength and distances applies as the rule: the stronger hydrogen bonds are shorter it is, the opposite also holds. The correlation between the hydrogen bond strength and one of hydrogen bond distances r_2^a is shown in Figure 2.27 for 1:2 complexes (red, blue and green symbols) and 1:1 complexes (gray symbols). The correlation seems general for both 1:1 and 1:2 complexes and also for all types of hydrogen bond. Besides, this correlation significantly nonlinear, especially for weakest (longest) hydrogen bonds. For all Me_3PO complexes with proton donors **1**–**70**, in which hydrogen bonds stronger than *ca.* 10 kJ·mol^{-1}, roughly rule is performed: the strengthening of hydrogen bonds up to 10 kJ·mol^{-1} leads to lengthening up to ~0.1 Å.

Similar correlation $G^{a}(r_2^a)$ shown in Appendix A, Figure A8 and also nonlinear, characterized by a small scattering of data points and well described by the exponent function $G^{a} = 561.4 \cdot \exp\left(-\frac{r_2^a - 0.96}{0.426}\right)$ for both 1:1 and 1:2 complexes. Taking into account last equation and linearity of correlation $\Delta E^{a}(G^{a})$ the fitting of data point shown in Figure 2.27 was performed by the exponential function $\Delta E = 197.1 \cdot \exp\left(-\frac{r_2^a - 0.96}{0.426}\right)$, where coefficients 0.96 Å, 0.426 Å were fixed, while the coefficient 197.1 kJ·mol^{-1} was obtained as the fitting results. The curve corresponded this function shown in Figure 2.27 by the solid line and well describe the general trends (slightly better for strongest complexes than for weakest).

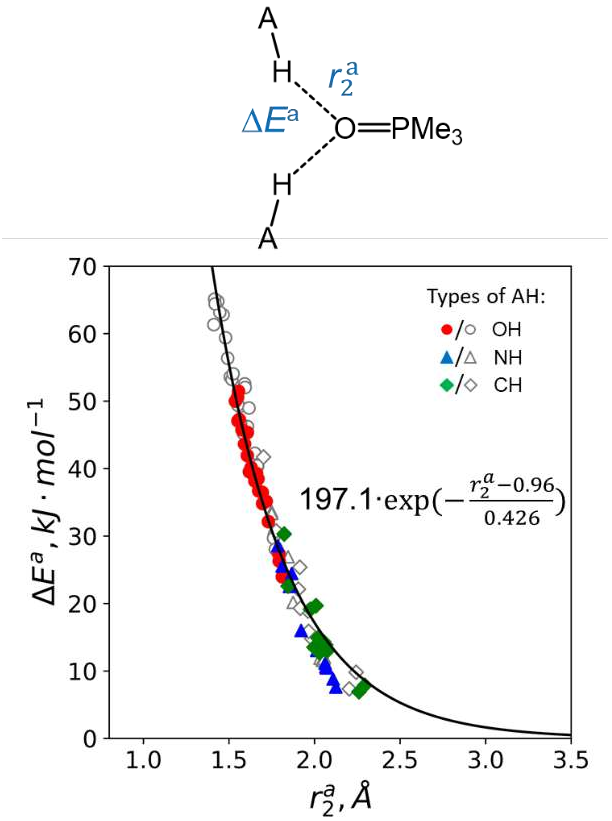

Figure 2.27. Correlation between ΔE^{a} and hydrogen bond length r_2^a. Open gray symbols correspond to 1:1 complexes; filled red, blue and green symbols correspond to 1:2 complexes. The solid line correspond least squares fitting by the exponential function, for which coefficients 0.96 Å and 0.426 Å were fixed due to well correlations $G^{a}(r_2^a)$ shown in Appendix A, Figure A8, and $\Delta E^{a}(G^{a})$ shown in Figure 2.21.

Hydrogen bonds geometry: correlation with IR, NMR spectral parameters

In this section we discuss the correlation between geometry and spectral parameters of 1:1 and 1:2 complexes with Me_3PO.

The changes of ^1H and ^{31}P NMR chemical shifts, $\Delta\delta H^a$ and $\Delta\delta P^t$, as well as the changes of the P=O stretching vibrations, $\Delta\nu^t_{P=O}$, correlate with hydrogen bond distance r_2^a as can be seen in Figure 2.28a–c (which means that the same spectral characteristic also correlate with another hydrogen bond distance, r_1^a, due to the interdependence of two hydrogen bond distances as shown in Figure 2.26). The spectral characteristics $\Delta\delta H^a$, $\Delta\delta P^t$ and $\Delta\nu^t_{P=O}$ respond to the changes in the wide range of hydrogen bond distances: from ~2.5 Å up to ~1.4 Å. The correlations $\Delta\delta P^t(r_2^a)$ and $\Delta\nu^t_{P=O}(r_2^a)$ are differ for Me_3PO complexes with one and two proton donors. In opposite, the correlation $\Delta\delta H^a(r_2^a)$ is general for both types of complexes. It seems natural science the both r_2^a and $\Delta\delta H^a$ reflect individual characteristic of each hydrogen bond independent of type of complexes (1:1 or 1:2 complexes), whereas $\Delta\delta P^t$ and $\Delta\nu^t_{P=O}$ respond to characteristics of both hydrogen bonds in complexes as a whole. At once all these geometry-spectra correlations seem independent from the type of proton donors: the correlations hold for OH, NH and CH proton donors simultaneously.

The functions described correlations $\Delta\delta P^t(r_2^a)$ and $\Delta\delta P(r_2)$ were obtained as the fitting result performed by exponential functions: $\Delta\delta P^t = a \cdot \exp\left(-\frac{r_2^a - r_2^0}{b_2}\right)$ for 1:2 complexes and $\Delta\delta P = a \cdot \exp\left(-\frac{r_2 - r_2^0}{b_2}\right)$ for 1:1 complexes, correlations of this type were previously reported in refs. [29,162]. Correlation coefficients b_2 and r_2^0 in this function were fixed at 0.322 Å and 0.96 Å respectively, while the values of coefficient a was obtained by the least square fitting: a = 73.8 ppm for 1:1 complexes and a = 188.3 ppm for 1:2 complexes (see solid lines in Figure 2.28: black for 1:2 complexes, gray for 1:1 complexes). The value of coefficient a meaning the greatest change of chemical shift $\Delta\delta P^t$ ($\Delta\delta P$) corresponded by the ^{31}P NMR chemical shift in isolated doubly (or once)

protonated trimethylphosphine oxide and is reproduced by quantum chemical calculations (70.2 ppm). The correlations $|\Delta\nu^{t}_{P=O}|(r_2^a)$ for 1:2 complexes and $|\Delta\nu_{P=O}|(r_2)$ for 1:1 complexes well described by the similar exponential functions derived from correlations $\Delta E^{t}(|\Delta\nu^{t}_{P=O}|)$ and $\Delta E^{a}(r_2^a)$ (or $\Delta E(|\Delta\nu_{P=O}|)$ and $\Delta E(r_2)$ in the case of 1:1 complexes). The correlation functions for both $\Delta\delta H^{a}(r_2^a)$ and $\Delta\delta H(r_2)$ were received automatically as the results of approximation of correlations $\Delta E^{a}(r_2^a)$, $\Delta E(r_2)$ shown in Figure 2.27 and $\Delta E^{a}(\Delta\delta H^{a})$, $\Delta E(\Delta\delta H)$ shown in Figure 2.23. The set of solid curves in Figure 2.28 correspond the function obtained in this section and well describe corresponding sets of data points.

Strong correlations shown in Figure 2.28 indicate the availability of hydrogen bond geometry estimation by the shifts of signal in ^{1}H and ^{31}P NMR spectra or by the shift of P=O band in IR spectra upon complexation. In the case of complexes with two hydrogen bonds using $\Delta\delta H$ values, it is possible to determine the characteristics of each hydrogen bond, the characteristics of both hydrogen bonds may be determined by using $\Delta\delta P$ and $\Delta\nu_{P=O}$ values.

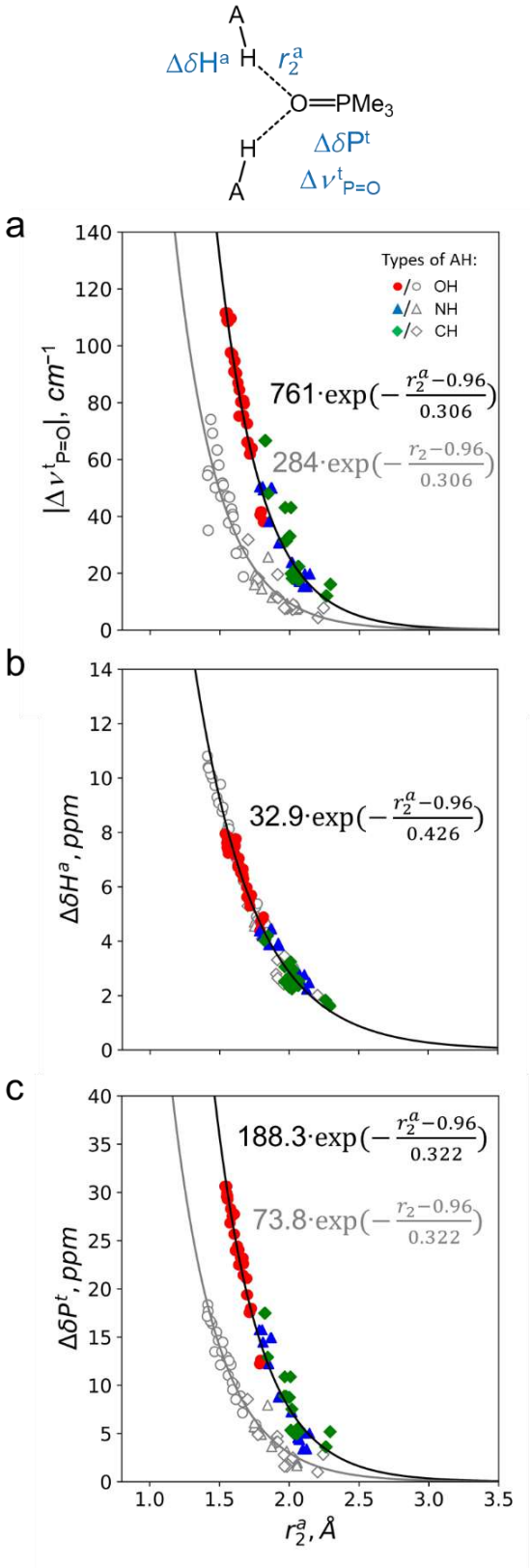

Figure 2.28. Correlation between interatomic distance r_2^a and IR, NMR spectral parameters: (a) $|\Delta\nu^{t}_{P=O}|$, (b) $\Delta\delta H^{a}$ and (c) $\Delta\delta P^{t}$. Solid lines correspond to fitting curves (see text) obtained for 1:1 complexes (gray lines) and 1:2 complexes (black lines).

Cooperativity effects on hydrogen bonds lengths

The mutual influence of two hydrogen bonds on interatomic distances is shown in Figure 2.29 for (a) absolute values of distances, r_2^a, and (b) the relative values of r_2^a changes, $\Delta r_2/r_2$, similar to the same for the strength as shown in section above. Here dashed lines also indicate the boundary between the cooperativity and anticooperativity effects. The anticooperativity of two hydrogen bonds on their distances seems less evident than once on their strength (Figure 2.24): the deviations of data points from dashed lines are noticeable mostly for the stronger complexes as shown in Figure 2.29a. In contrast, anticooperativity effects are well visible on the correlation between $\Delta r_2/r_2$ and r_2, in Figure 2.29b, which more especially manifest on the example of complexes with $Me_3PO\cdots HO$ hydrogen bonds (red circles). The functions $r_2^a(r_2)$ and $\Delta r_2/r_2(r_2)$ describe correlations corresponded in Figure 2.29a,b and were derived from the correlation function for $\Delta E^a(\Delta E)$ and $\Delta E^a(r_2^a)$ (see Figure 2.24 and Figure 2.27). The explicit equations of correlation function for $r_2^a(r_2)$ and $\Delta r_2/r_2(r_2)$ are listed in Appendix A, Table A3. Note that the data points in Figure 2.29a,b fit well by the correlation curves (solid lines) built in accordance with these functions with the slightly larger spread of points for complexes with $Me_3PO\cdots HC$ hydrogen bonds. Similar correlation between anticooperativity effects on the set of spectral parameters ($\Delta\delta$H, $\Delta\delta$P and $\Delta\nu_{P=O}$) and hydrogen bond distances, r_2, given in Appendix A, Figure A9.

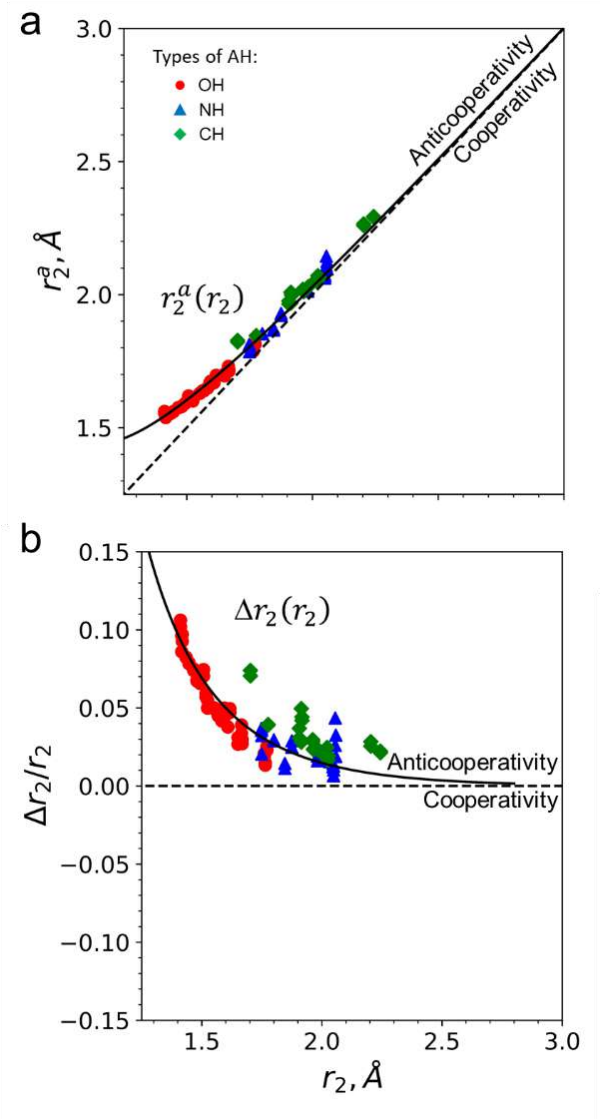

Figure 2.29. (a) Correlation between hydrogen bond distances r_2 and r_2^a, (b) correlation between r_2 and relative cooperativity effect on hydrogen bond distance $\Delta r_2/r_2$ ($\Delta r_2 = r_2^a - r_2$). Solid lines correspond to correlation functions $r_2^a(r_2)$ and $\Delta r_2/r_2(r_2)$ given explicitly in Appendix A, Table A3 (derived from fitting functions for correlations shown in Figure 2.24 and Figure 2.27). Dashed lines indicate the boundary between regions of cooperativity and anticooperativity effects.

Conclusions

Using quantum chemistry methods we studied 140 hydrogen-bonded 1:1 and 1:2 complexes formed by trimethylphosphine oxide and various OH, CH, NH and NH^+ proton donors in a polar medium in the wide range of hydrogen bonds energies and geometries. The set of following NMR and IR spectral characteristics of Me_3PO complexes was calculated: ^1H and ^{31}P NMR chemical shifts, P=O stretching vibration frequencies. It is shown that these parameters are sensitive to the formation of hydrogen bonds: δP and δH change up to 11 ppm and 30 ppm, respectively, and $\nu_{P=O}$ changes up to 110 cm^{-1} upon complexation. We have demonstrated power correlations between the changes of ^1H, ^{31}P NMR chemical shits, P=O stretching vibrational frequencies and hydrogen bond energies; exponential correlation between hydrogen bond energies, the changes of NMR, IR spectral parameters and hydrogen bond distances r_2 and r_2^a for both 1:1 and 1:2 complexes. The spectral characteristics of proton donor group P=O, $\Delta\delta P$ ($\Delta\delta P^t$) and $\nu_{P=O}$ ($\nu^t_{P=O}$), are sensitive to common changes in the strength and distances of hydrogen bonds in both 1:1 and 1:2 complexes, while $\Delta\delta H$ ($\Delta\delta H^a$) most sensitive to the characteristics of individual hydrogen bonds. We concluded that both parameters $\Delta\delta H^a$ and $\Delta\delta P^t$ (or $\Delta\delta H^a$ and $\Delta\nu^t_{P=O}$) may complement each other in application for estimation of hydrogen bond energy and distances. We demonstrate significant anticooperativity effects of hydrogen bonds in 1:2 complexes manifest on the main spectral parameters, hydrogen bonds energies and distances. The obtained correlation functions for the mentioned parameters are proposed to assess the strength (lengths) of hydrogen bonds and the values of anticooperativity effects on them based on the spectral characteristics of phosphine oxide as the probe molecule.

Chapter 3. Experimental investigation of Ph_3PO complexes with substituted phenols in CDF_3/CDF_2Cl freons mixture by low temperature NMR spectroscopy

3.1. Introduction and problem statement

The correlation between the strength of $R_3PO\cdots HA$ hydrogen bond and the change of chemical shift of phosphorus atom $\Delta\delta P$ in complexes discussed in Chapter 2. It is theoretical prediction on model systems, which requires confirmation. In this chapter, we experimentally establish the presence of such correlation for complexes of triphenylphosphine oxide (Ph_3PO) and different proton donors in solution by low temperature NMR spectroscopy.

In this chapter, we choice of triphenylphosphine oxide as a proton acceptor for practical reasons: Ph_3PO is strong proton acceptor; sufficient soluble in many organic solvents (including CDF_3/CDF_2Cl freons mixture used in this chapter), which is necessary for recording spectra; Ph_3PO signals do not make it difficult to assign other signals in IR and NMR spectra. We chose 18 different substituted phenols as proton donors, the structures of phenols shown in Figure 3.1. The proton-donating ability of substituted phenols (**1**–**18**) is determined by the type of substituents: halides (fluorine, chlorine, bromine, iodine), nitro group, cyano group; the position of the substituent: *ortho*-, *meta*, *para*-; the number of substitutions: unsubstituted phenol, mono-, di-, penta- substituted phenols.

We used the mixture of liquid deuterated freons CDF_3/CDF_2Cl to obtain non-averaged NMR parameters of the complexes, *i.e.* to slow down the processes of molecular exchange; the mixture of freons freezes at ~90 K and characterized by spectral transparency in the studied range of chemical shifts in NMR spectra (see Section 3.2 of this chapter).

The complexation enthalpy ΔH was estimated by the change of chemical shift of bridging proton upon complexation, $\Delta\delta$H, using the correlation previously proposed in the literature for OHO hydrogen bonds [163]. As will be shown below, the hydrogen bond strength varies in the range from ~18 kJ·mol^{-1} to ~77 kJ·mol^{-1} within the set of studied complexes formed by Ph_3PO and various substituted phenols (**1**–**18**). The chemical shifts of bridging protons range from ~10 ppm. up to ~14 ppm in ^{1}H NMR spectra, the chemical shift of phosphorus atom of triphenylphosphine oxide changes upon complexation up to 10 ppm in ^{31}P NMR spectra.

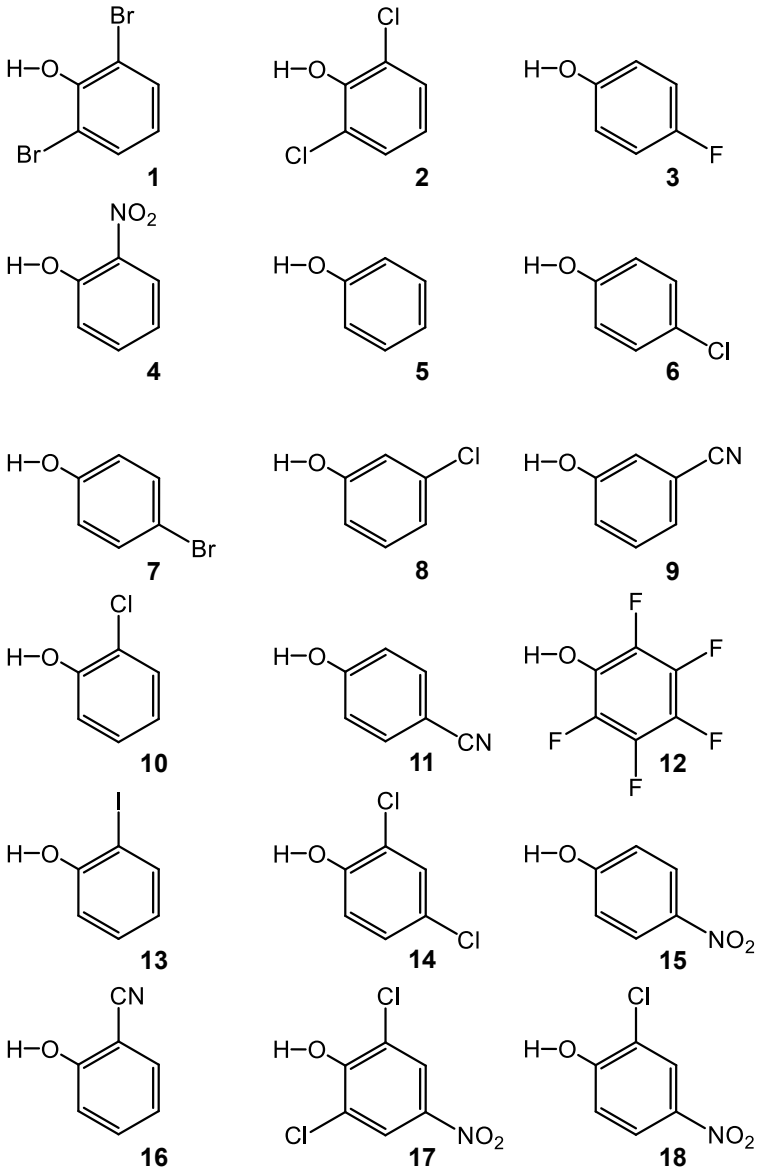

Figure 3.1. The set of substituted phenols (**1**–**18**) considered as proton donors in this chapter.

3.2. Main characteristics of CDF_3/CDF_2Cl freons mixture

Complexes of small molecules with an intermolecular hydrogen bond are characterized by relatively short lifetime in solutions. The processes of molecular exchange occur rapidly at room temperature in NMR time scale. The observed chemical shift is weighted average for all forms of complexes in solution. The chemical shifts of free molecules may be observed in the spectra at high dilution with solvent. Chemical shifts of individual complexes become observable when lifetime of complexes increases and (or) the equilibrium shifts to complexation. One of the most accessible ways to increase the lifetime of complexes is to lower temperature of the solution. The chemical shifts of various complexes with medium strength hydrogen bonds are observed separately at significant decrease in temperature, which significantly reduces the set of suitable solvents. The most commonly used in NMR deuterated solvents usually have a melting (freezing) point above 160 K, which is usually not sufficient to observe individual forms of hydrogen-bonded complexes. Moreover, the additional difficulties appear due to the viscosity of solution increases with decreasing temperature (and becomes especially large near the freezing point), which influences the spin-spin relaxation times and leads to signals broadening in NMR spectra. Finally, the solubility of organic compounds generally decreases with decreasing temperature. These processes make it difficult to study hydrogen bonds in complexes at low temperatures in standard solvents. In this work, the mixture of liquefied gases CDF_3/CDF_2Cl was used as a solvent and characterized by a set of following unique physicochemical properties that provide an advantage for studying hydrogen bonds (in comparison with other solvents):

1. The mixture of gases CDF_3/CDF_2Cl freezes at ~90 K, which makes it possible to record NMR spectra in solution in the wide temperature range: from room temperature to 100 K.
2. Many organic compounds have sufficient solubility in the mixture of liquefied gases CDF_3/CDF_2Cl to recording low-temperature NMR spectra.

3. The mixture of freons is characterized by spectral transparency within the range of observed chemical shifts of bridging proton signals in ^{1}H NMR spectra.
4. The water impurities in solution freeze at ~160 K and therefore do not compete with the studied molecules for the formation of hydrogen bonds.

The mixture of gases CDF_3/CDF_2Cl was previously used to obtain non-averaged signals of neutral [20,164] and anionic [164,165] hydrogen-bonded self-associates, to study heteronuclear acid-base interactions, including those with proton transition [61,166,167], to model the interactions side chains of amino acid with cofactors [56], to study H/D isotope effects on spectral parameters [164,167] and *etc.* NMR spectra of liquefied gases CDF_3/CDF_2Cl used as the solvent in this part of the work are shown in Figure 3.2 for ^{1}H, in Figure 3.3a,b for ^{13}C and ^{19}F respectively. The set of signals are observed in ^{1}H NMR spectra: the triplet at 7.21 ppm ($^{2}J_{HF}$=63.3 Hz) related to the signal of CHF_2Cl component of freon mixture, quartet at a 6.50 ppm ($^{2}J_{HF}$=79.6 Hz) related to the CHF_3 component, and doublet at 7.54 ppm ($^{2}J_{HF}$=53.7 Hz) related to $CHFCl_2$ component. The signal intensities correspond the relative ratio of non-deuterated components in the mixture. The main components are CHF_2Cl and CHF_3, while $CHFCl_2$ is contained in much smaller amounts and often the signals of this component are not detected in NMR spectra.

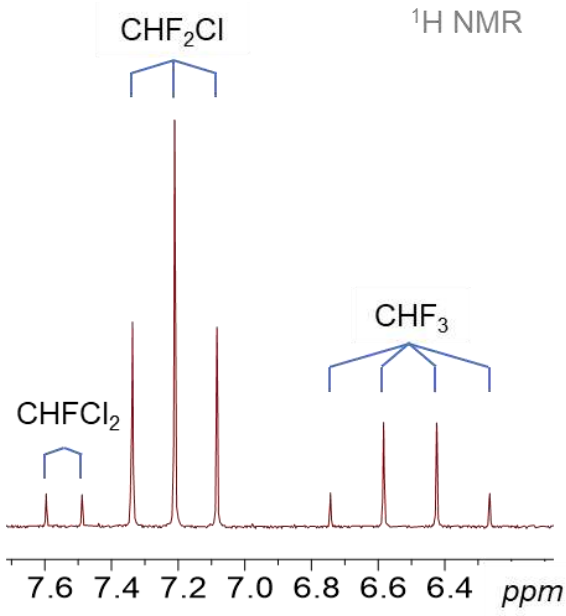

Figure 3.2. The part of ^{1}H NMR spectra in the range of observed signals corresponded by the mixture of gases CDF_3/CDF_2Cl.

Two sets of signals are observed in the ^{13}C NMR spectra recorded for freons mixture: the triplet assigned to CDF_2Cl, the quartet assigned to CDF_3 as shown in Figure 3.3a, the signals of $CDFCl_2$ in this spectrum are not observed in the spectra due to low concentration of this component in the mixture. The signal of each component is also observed in the ^{19}F NMR spectra. Note that relative ratio of deuterated components in the mixture can be determined by relative integral intensities in the ^{19}F NMR spectra. In this case, the ratio of relative integral intensities of CDF_3 and CDF_2Cl components is 0.30 to 0.70, which corresponds to the content of mixture components in ratio of approximately 1:3. This ratio varies from synthesis to synthesis and depends on many factors, from examples, the amount of added catalyst, the presence of impurities in the reagents, local reaction conditions and *etc*. Nevertheless, the method of freon synthesis developed over many years allows us quite predictable to obtain the mixture of gases CDF_3/CDF_2Cl with ratio of approximately 1:3. The synthesis procedure is described in detail in the next section.

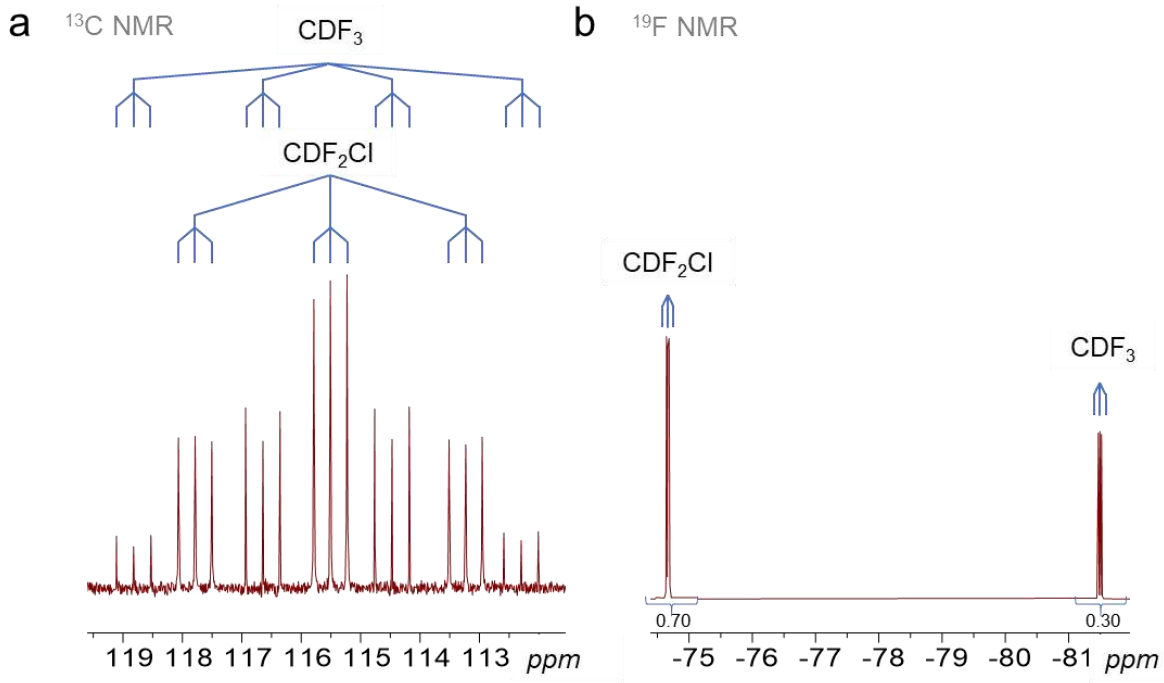

Figure 3.3. The part of (a) ^{13}C and (b) ^{19}F NMR spectra recorded for the mixture of gases CDF_3/CDF_2Cl. Relative integral intensities of signals assigned to CDF_2Cl and CDF_3 in this sample are 0.70 and 0.30 respectively.

3.3. Synthesis of the mixture of deuterated freons CDF_3/CDF_2Cl

The mixture CDF_3/CDF_2Cl was synthesized from SbF_3 and $CDCl_3$ using $SbCl_5$ as the catalyst. Reagents SbF_3 and $SbCl_5$ were purchased from *Sigma Aldrich*, while $CDCl_3$ was provided by *Carl Roth GmbH+Co*. All reagents were stored in sealed packages in a place inaccessible to light. Additionally, SbF_3 powder was dried in vacuum desiccator for 12–15 hours over P_2O_5 immediately before the start of synthesis. Reagents $CDCl_3$ and $SbCl_5$ were used without additional purification. The freons mixture was synthesized in steel sealed autoclave HR100 (provided by *Berghof–Maasen*, internal volume of the autoclave 100 ml, operating pressure: up to 150 atm., operating temperature: up to 500 K), equipped with PTFE cup, according to following reaction equation:

$$CDCl_3 + SbF_3 \xrightarrow{SbCl_5} CDF_3 + CDF_2Cl + CDFCl_2$$

The reagents, 30 g of $SbF3_3$ and 13.5 ml of $CDCl_3$, were placed in a PTFE cup and 1–2 ml of $SbCl_5$ were added in the cup using a Pasteur Pipette. The resulting reagent mixture was thoroughly mixed with a steel spatula. The autoclave was hermetically sealed and immersed in water bath with temperature of water close to 98 °C. After 3.5 hours, the autoclave was removed and cooled in cold bath (the mixture of water and ice) for about 30 minutes. And then the autoclave was connected to vacuum system.

The high-vacuum system is used for subsequent purification of freons mixture and includes KOH tube, Schlenk line, taps, two vacuum traps and high vacuum pump TPS-Compact. KOH tube is used for additional purification of freons mixture from synthesis byproducts and water. TPS-Compact system is manufactured by Agilent Technology and consists of pre-vacuum pump, Agilent IDP-3, and turbomolecular pump, Twis Torr 74 FS. The pressure in system is measured by Pirani gauge integrated in TPS-Compact system. The operating pressure in the system is approximately $6 \cdot 10^{-6}$ mbar. Following set of equipment was attached to Schlenk line: flask with dry Al_2O_3, sampling

cylinder (for long-term storage of freons mixture) and barometer (used for rough estimation of pressure in isolated Schlenk line). The high vacuum line is shown in Figure 3.4 (the nitrogen traps and high vacuum pump are outside the figure). Sampling cylinder Hoke 4HS75 with the volume of 75 ml is able to withstand pressures up to 120 atm., which is sufficient for safe and reliable storage of freons mixture for a long time.

The contents of the autoclave were passed through KOH tube and condensed on Al_2O_2 using liquid nitrogen bath. Then the bath with liquid nitrogen was replaced with a cold bath made from a mixture of ethanol and liquid nitrogen (bath temperature close to 140 K). At this temperature, used freons mixture holds in liquid state and water molecules are effectively adsorbed on Al_2O_3. After drying, freons mixture was condensed from the flask into sampling cylinder, where the mixture was kept until required.

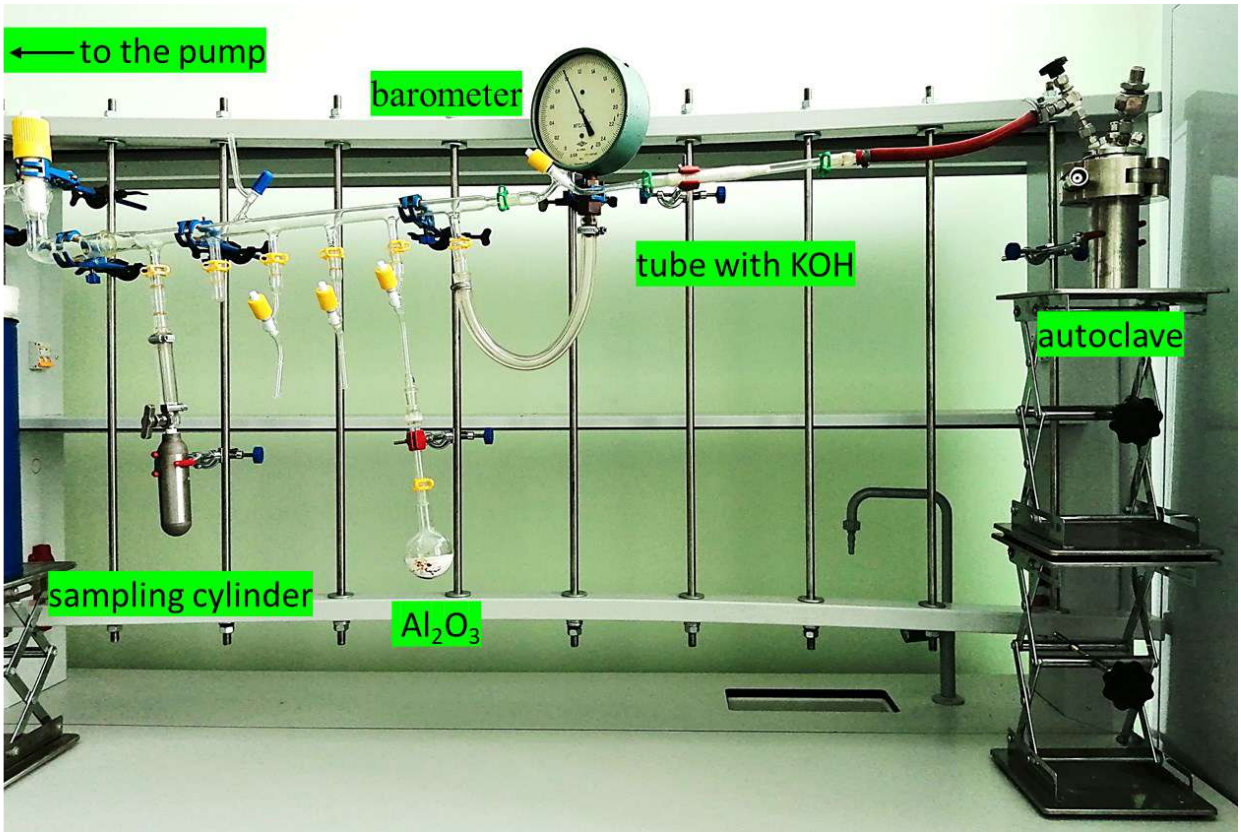

Figure 3.4. Photo of the high-vacuum line used to purify the freons mixture after synthesis.

3.4. Preparation of samples in CDF_3/CDF_2Cl mixture

We prepared the series of samples containing solutions of Ph_3PO and substituted phenols (**1**–**18**) with 1:1 or 1:2 relative molar concentrations in the solution of liquefied gases CDF_3/CDF_2Cl. Each sample contained approximately $1.93 \cdot 10^{-6}$ mol of triphenylphosphine oxide. Low concentration of the studied compounds (0.005–0.010 $mol \cdot l^{-1}$) in the solution is sufficient for recording ^{1}H and ^{31}P NMR spectra and does not lead to noticeable changes in the main physicochemical properties of the solvent: low viscosity, low freezing point.

Primary solutions of Ph_3PO and substituted phenols in chloroform ($CHCl_3$) were prepared for each sample. The primary solution was prepared according to following procedure: 5.37 mg of Ph_3PO ($19.3 \cdot 10^{-6}$ mol) and calculated amount of substituted phenol (in the ratio of 1:1 or 1:2 in mol respectively) was diluted with 1 ml of chloroform ($CHCl_3$). Using an Eppendorf Pipettes, 0.1 ml of primary solution was transferred to vacuum NMR tube (manufactured by *Wilmad*, outer diameter: 5 mm; wall thickness: 1.4 mm; inner diameter: 2.2 mm), which was hermetically sealed with J. Young valve. NMR tube containing primary solution was attached to vacuum system.

Chloroform from primary solutions was slowly pumped out of NMR tubes, slightly open J. Young valves: Ph_3PO and substituted phenol settled on the walls of NMR tube. Freons mixture was added into the system from sampling cylinder, controlling the pressure in Schlenk line using barometer scale. The entire volume of freons in the system was condensed into round-bottomed flask with Al_2O_3 and additionally dried in the same way as during synthesis (see Section 3.3). After that, freons mixture was condensed on the walls of NMR tubes cooled with liquid nitrogen. The height of liquid column obtained by condensation of freons in NMR tube varied from 7 cm (approximately 0.28 ml of the solvent) to 10 cm (approximately 0.4 ml of the solvent). The volume of liquid in NMR tube was controlled by pressure change in the line during freons mixture condensation. Having condensed required volume of the solvent, NMR tubes were hermetically closed,

disconnected from the line and submitted for recording of NMR spectra. Total compounds concentrations in the solution varied from 0.005 mol·l^{-1} to 0.010 mol·l^{-1}.

3.5. Recording ^{1}H and ^{31}P NMR spectra for solutions in CDF_3/CDF_2Cl mixture

The set of ^{1}H and $^{31}P\{^{1}H\}$ NMR spectra of studied compounds in solutions in CDF_3/CDF_2Cl were recorded using Bruker 500 MHz Avance III spectrometer (11.74 T) equipped with low-temperature two-channel broadband probe. The preparation of samples was carried out jointly with Omar Alkhuder, a master's student in Chemistry. The spectra were recorded at room temperature and 100 K without sample rotation.

The spectra were recorded at frequency 499.92 MHz for ^{1}H nuclei and 202.36 MHz for ^{31}P nuclei. The number of accumulations was 128 scans (for ^{1}H NMR spectra) and 256 scans (for ^{31}P NMR spectra). All ^{31}P NMR spectra were recorded with proton decoupling. The following parameters were used: 30° pulses, 1 s (for ^{1}H nuclei) and 2 s (for ^{31}P nuclei) delay between pulses. The total registration time for the spectra of one sample was 8–10 minutes for ^{1}H NMR spectra and 13–15 minutes for ^{31}P NMR spectra. Chemical shift scales were calibrated relative to TMS signals (for ^{1}H NMR spectra) and H_3PO_4 (for ^{31}P NMR spectra) using a single scale according to IUPAC recommendations [168]. The spectra were processed using MestReNova 14.2.1 program [169].

3.6. Main results and discussion

Complexes of Ph_3PO and substituted phenols in solution in CDF_3/CDF_2Cl

Low-field parts of ^1H and $^{31}P\{H\}$ NMR spectra recorded for two solutions of Ph_3PO and phenol **18** with different concentrations of phenol **18** are in solution in liquefied deuterated freons CDF_3/CDF_2Cl at 100 K shown in Figure 3.5 as an example. The NMR spectra of solutions with other phenols studied in this chapter are shown below. The ratio of phenol **18** concentration to Ph_3PO concentration in solutions was about 1:1.17 (Figure 3.5a,b) and 1:0.39 (Figure 3.5c,d). Single signal is observed at 13.4 ppm in low-field part of ^1H NMR spectrum (Figure 3.5a) and located in the range of bridging protons chemical shifts in hydrogen-bonded complexes. In the ^{31}P NMR spectra of the same solution (Figure 3.5b), two signals are observed at 33.2 ppm and 36.3 ppm, their relative integral intensities are in the ratio of 1 and 7.5 respectively. Signal located at 33.2 ppm corresponded to "free" Ph_3PO (see Appendix B, Figure B1). The signal located at 36.3 ppm was assigned to hydrogen-bonded complex of Ph_3PO with phenol **18**. Based on relative concentration of phenol **18** and Ph_3PO in solution (2.3:1) we assign the signals at 13.4 ppm in ^1H NMR spectra and 36.3 ppm in ^{31}P NMR spectra to complex of Ph_3PO and phenol **18** with a single hydrogen bond (1:1 complex).

The number of signals in the ^1H NMR spectra (Figure 3.5c) increases after increasing the concentration of phenol **18**, signals are observed at 13.4 ppm, 12.5 ppm, and 11.8 ppm with relative intensities equal to 1.0, 3.1 and 11.3 respectively. The number of signals in the ^{31}P NMR spectra also increases (Figure 3.5d). The signals are observed at 36.3 ppm, 39.3 ppm and 42.8 ppm, their relative intensities are 1.0, 1.2 and 3.9 respectively.

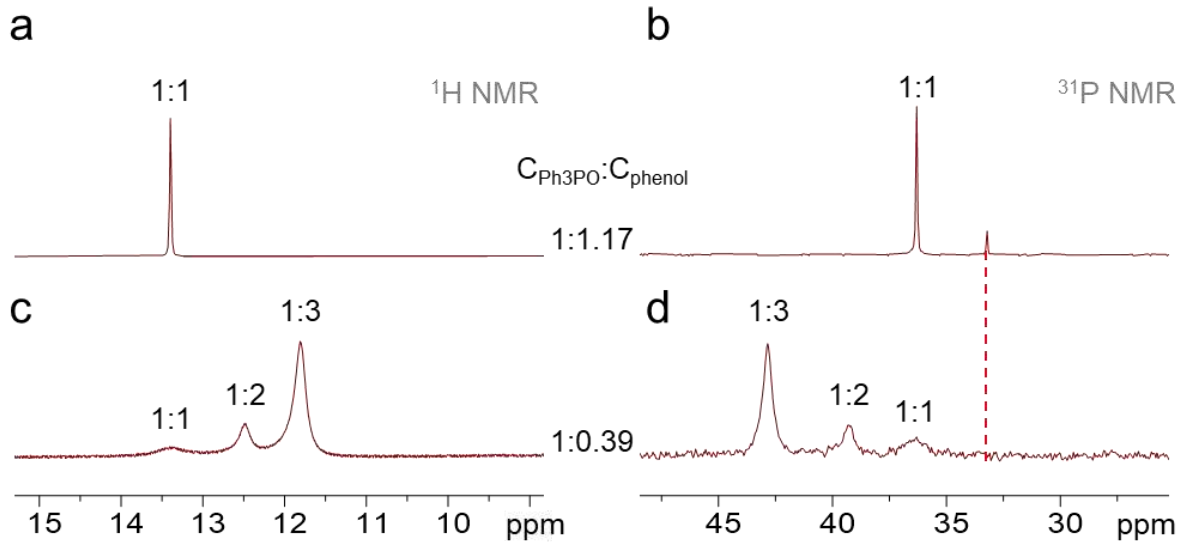

Figure 3.5. Low-field parts of the NMR spectra recorded for solution of Ph_3PO and phenol **18** in CDF_3/CDF_2Cl at 100 K: (a) ^{1}H NMR and (b) ^{31}P NMR spectra of solutions with concentration ratio phenol **18** to Ph_3PO of approximately 1:1.17 (in mol), (c) ^{1}H NMR and (d) ^{31}P NMR spectra of solutions with concentration ratio phenol **18** to Ph_3PO of approximately 1:0.39 (in mol). The dashed line indicates the location of the ^{31}P NMR signal corresponded to "free" Ph_3PO.

The total number of signals in the low-field part of ^{1}H NMR spectra indicates the number of protons in OH groups of phenol **18** that differ in shielding, while the number of signals in ^{31}P NMR spectra indicates the number of nonequivalent ^{31}P nuclei of Ph_3PO in solution. Consequently, several types of complexes with hydrogen bonds between Ph_3PO and phenol **18** are formed in the solution. An increase in phenol **18** concentration in solution leads to the redistribution of equilibrium between different types of complexes. Based on the number of observed signals and their relative integral intensities, the stoichiometry of complexes may be determined. By analyzing the signals and their intensities in the ^{1}H and ^{31}P NMR spectra for samples with different concentration ratios of phenol **18** and Ph_3PO (Figure 3.5c,d), we established that in solution one Ph_3PO molecule may be involved in the formation of the hydrogen bond with one (1:1 complexes), two (1:2 complexes) and even three (1:3 complexes) molecules of phenol **18**. Signals at 13.4 ppm. in the ^{1}H NMR spectra and at 36.3 ppm. in the ^{31}P NMR spectra were assigned to complexes with one hydrogen bond between Ph_3PO and phenol **18**, *i.e.*

to 1:1 complexes. Signals located at 12.5 ppm in ^{1}H NMR spectra and 39.3 ppm in ^{31}P NMR spectra were assigned to 1:2 complexes, while signals located at 11.8 ppm in ^{1}H NMR spectra and 42.8 ppm in ^{31}P NMR spectra were assigned to 1:3 complexes. The proposed structures of all three types of hydrogen-bonded complexes formed by Ph_3PO and substituted phenol **18** in solution in CDF_3/CDF_2Cl are schematically shown in Figure 3.6.

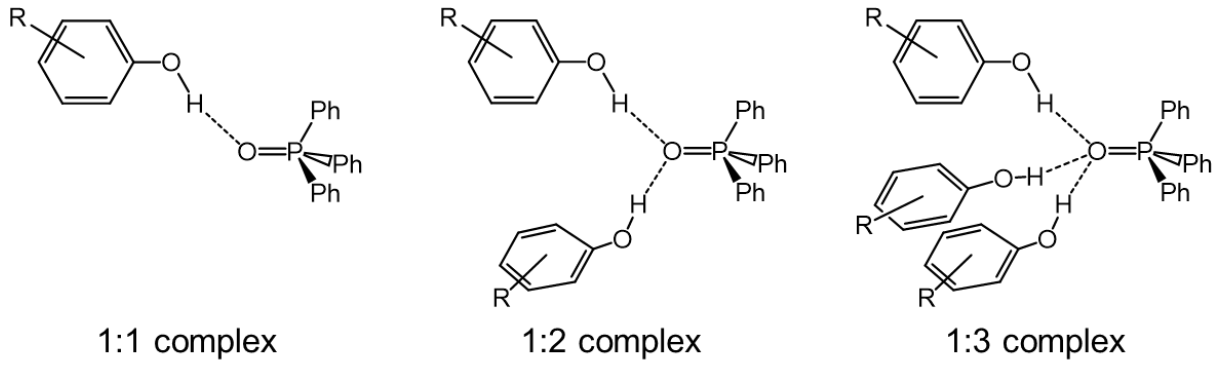

Figure 3.6. Structures of Ph_3PO complexes with one (1:1 complex), two (1:2 complex) and three (1:3 complex) molecules of substituted phenol.

Spectra of complexes formed by Ph_3PO and substituted phenols

Low-field parts of ^{1}H NMR (a) and ^{31}P NMR (b) spectra of Ph_3PO solutions with substituted phenols **1–18** in solution in mixture of CDF_3/CDF_2Cl at 100 K are shown in Figure 3.7. Since the concentrations of Ph_3PO and substituted phenols in the solution were comparable, equilibrium in the solution shifted mainly to 1:1 complexes. However, the signals assigned to 1:2 complexes are observed for solutions with substituted phenols **3**, **5**–**9**, **11**, **12**, **15** and **16**. The signals assigned to 1:3 complexes were observed only in the case of substituted phenol **18** as shown in Figures 3.5c,d and only in the case of a significant excess of phenol in solution. The assignment of signals in NMR spectra of solutions with substituted phenols **1**–**17** to 1:1 and 1:2 complexes carried out based on the

number of signals and their relative integral intensities, as described above on the example of Ph_3PO solutions and substituted phenol **18**. In some cases, the intensity of signals of 1:2 complexes in the ^1H and ^{31}P NMR spectra is very low and one of the signals is poorly visible among the noise. Interesting that we did not find a signals in ^1H NMR spectra of studied solutions assigned to protons in OH groups of "free" substituted phenols or their self-associates, *i.e.*, apparently, all substituted phenol molecules in solution in CDF_3/CDF_2Cl at 100 K either participate in formation of complexes with Ph_3PO or freeze out of the solution. The latter is confirmed by the change in relative concentrations of Ph_3PO and substituted phenol upon temperature decrease. At once, we observe the signal of "free" Ph_3PO in some ^{31}P NMR spectra, the position of this signal indicated by dashed line in Figure 3.7. Chemical shifts of bridging protons, $\delta H_{1:1}$, $\delta H_{1:2}$ and $\delta H_{1:3}$, and nuclei of phosphorus atom of triphenylphosphine oxide, $\delta P_{1:1}$, $\delta P_{1:2}$ and $\delta P_{1:3}$, in 1:1, 1:2, 1:3 complexes detected in ^1H and ^{31}P NMR spectra of Ph_3PO and substituted phenols **1**–**18** solutions are collected in Table 3.1.

The general pattern is observed for all complexes: the formation of each hydrogen bond between Ph_3PO and substituted phenol leads to decrease in the strength of each bond and associated with the shift of bridging protons signals to stronger field in ^1H NMR spectra [163] relative to the signal of 1:1 complex, *i.e.* anticooperativity of hydrogen bonds on chemical shifts of bridging protons is observed. On the contrary, the ^{31}P signals of complexes shift to weaker field in spectra relative to the signal of 1:1 complex with increasing of hydrogen bonds number. Therefore, we conclude that chemical shifts of ^1H are markers of the strength of each hydrogen bond separately, while the chemical shift of ^{31}P of phosphine oxide is marker of total strength of all hydrogen bonds bonded with P=O group. The results of quantum chemical calculations of 1:2 complexes formed Me_3PO and proton donors also indicate sensitivity of δP to the total strength of hydrogen bonds, while δH is sensitive to the strength of single bond (see Chapter 2).

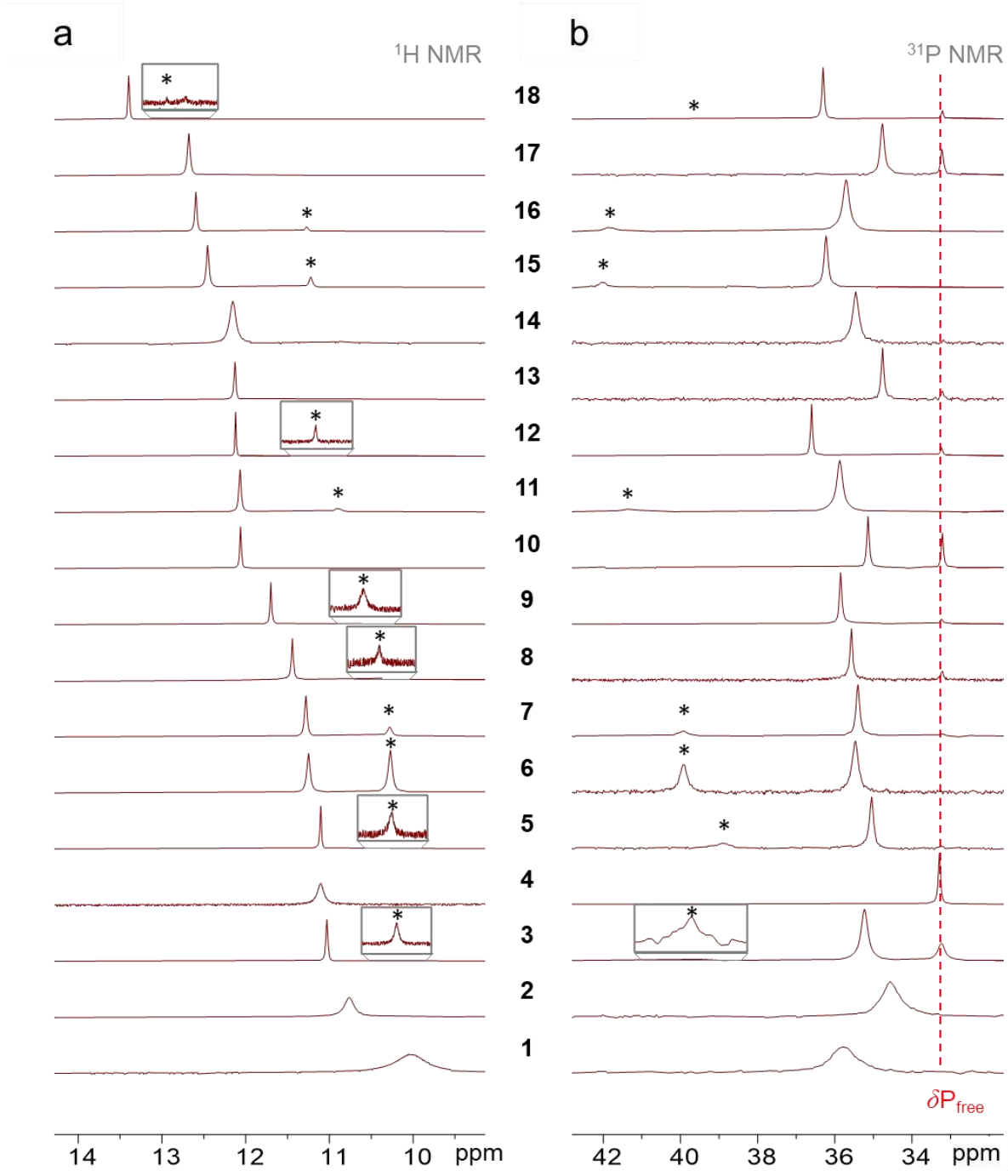

Figure 3.7. Low-field parts of (a) ^{1}H NMR and (b) ^{31}P NMR spectra of Ph_3PO and substituted phenols **1**–**18** in solutions in mixture of deuterated freons CDF_3/CDF_2Cl at 100 K. The dotted line indicates the position of ^{31}P NMR signal, δP_{free}, corresponded by "free" Ph_3PO. The signals assigned to 1:2 complexes are marked by (*). Signals with low intensity are shown in the spectra insets, for which the vertical scale is increased by approximately 10 times for clarity.

Table 3.1. Main spectral characteristics (chemical shifts $\delta H_{1:1}$, $\delta H_{1:2}$, $\delta H_{1:3}$ and $\delta P_{1:1}$, $\delta P_{1:2,}$ $\delta P_{1:3}$ in ppm) and energetic characteristics (enthalpies $\Delta H_{1:1}$, $\Delta H_{1:2}$, $\Delta H_{1:3}$ in kJ·mol^{-1}) of various stoichiometry with hydrogen bonds between Ph_3PO and substituted phenols **1**–**18**. The enthalpies of complex formation were calculated using linear correlation given in ref. [163] (see also Equation 3.1).

No.	Proton donor	$\delta H_{1:1}$	$\delta H_{1:2}$	$\delta H_{1:3}$	$\delta P_{1:1}$	$\delta P_{1:2}$	$\delta P_{1:3}$	$\Delta H_{1:1}$	$\Delta H_{1:2}$	$\Delta H_{1:3}$
1	2,6-dibromophenol	10.03	–	–	35.78	–	–	18.52	–	–
2	2,6-dichlorophenol	10.76	–	–	34.57	–	–	21.57	–	–
3	4-fluorophenol	11.03	10.11	–	35.23	39.48	–	22.70	37.70	–
4	2-nitrophenol	11.1	–	–	33.28	–	–	22.99	–	–
5	phenol	11.1	10.23	–	35.04	38.84	–	22.99	38.70	–
6	4-chlorophenol	11.25	10.27	–	35.47	39.92	–	23.62	39.04	–
7	4-bromophenol	11.28	10.28	–	35.4	39.91	–	23.74	39.12	–
8	3-chlorophenol	11.44	10.39	–	35.57	–	–	24.41	40.04	–
9	3-cyanophenol	11.7	10.56	–	35.85	–	–	25.50	41.46	–
10	2-chlorophenol	12.06	–	–	35.14	–	–	27.00	–	–
11	4-cyanophenol	12.07	10.91	–	35.87	41.31	–	27.04	44.39	–
12	2,3,4,5,6-fluorophenol	12.12	11.06	–	36.6	–	–	27.25	45.64	–
13	2-iodophenol	12.13	–	–	34.76	–	–	27.29	–	–
14	2,4-dichlorophenol	12.15	–	–	35.46	–	–	27.38	–	–
15	4-nitrophenol	12.45	11.22	–	36.23	42.03	–	28.63	46.98	–
16	2-cyanophenol	12.6	11.27	–	35.7	41.83	–	29.26	47.40	–
17	2,6-dichloro-4-nitrophenol	12.68	–	–	34.77	–	–	29.59	–	–
18	2-chloro-4-nitrophenol	13.4	12.5	11.8	36.3	39.3	42.84	32.60	57.68	77.74

The strength of hydrogen bonds in complexes: correlation with ΔδP

Recall that experimental examination of possibility of using observed change of ^{31}P chemical shift, ΔδP, for estimation of hydrogen bond strength is the main goal of this part of work. The chemical shift δP is sensitive to hydrogen bond formation in complexes differ stoichiometry and formed Ph_3PO and substituted phenols **1**–**18** as shown above. The total range of δP change is approximately 10 ppm (see Figure 3.7b and Table 3.1).

The general pattern is observed in ^{1}H NMR spectra of Ph_3PO and substituted phenols **1**–**18** in solutions: the signals of bridging protons shift to weaker field, to 10–13.5 ppm, with increasing of proton-donating ability of substituted phenols, that indicates the formation of medium strength hydrogen bonds in complexes. The change of proton chemical shift upon complexation, ΔδH, correlates with hydrogen bond strength defined as the enthalpy of complexation ΔH in this chapter. The correlation ΔH(δH) for O–H···O hydrogen bonds in various phenols and carboxylic acids is well described by the linear function (3.1) reported in ref. [163].

$$\Delta H \text{ (in kJ·mol}^{-1}) = 4.18 \cdot \Delta\text{H (in ppm)} + 1.67 \qquad (3.1)$$

The signals assigned to proton in hydroxyl groups of "free" phenols **1**–**18** were not detected in ^{1}H NMR spectra at 100 K, so the change of chemical shift upon complexation, $\Delta\delta H = \delta H - \delta H_{free}$, was calculated using average value of chemical shifts corresponded by "free" phenols in chloroform, δH_{free} = 6 ppm. This value was obtained from ^{1}H NMR spectra of "free" substituted phenols in solutions in chloroform at room temperature [170]. The strength of hydrogen bond in 1:1 complexes, $\Delta H_{1:1}$, was calculated from Eq. (3.1) and vary in the range from ~19 kJ·mol^{-1} to ~33 kJ·mol^{-1}, which is slightly less than the same for Me_3PO complexes with some substituted phenols (see Chapter 2). The strengths of hydrogen bonds in 1:2 complexes, $\Delta H_{1:2}$, and 1:3 complex, $\Delta H_{1:3}$, were calculated as algebraic sum of the strengths of all hydrogen bonds in complex, each of these hydrogen bonds was calculated using Eq. (3.1). The strength of hydrogen bonds in 1:2 complexes varies in the range from ~38 kJ·mol to ~58 kJ·mol, significantly higher

than the strength of hydrogen bonds in 1:1 complex with the same substituted phenols and less than the strength of hydrogen bonds in Me_3PO complexes with two proton donors (see Chapter 2). The obtained values of $\Delta H_{1:1}$, $\Delta H_{1:2}$ and $\Delta H_{1:3}$ are listed in Table 3.1.

The correlation between the total strength of hydrogen bonds and observed change of ^{31}P chemical shift, $\Delta\delta P$, in 1:1, 1:2, and 1:3 complexes is shown in Figure 3.8. There is tendency: $\Delta\delta P$ increases with increasing in total strength of hydrogen bonds in complexes. Well correlation $\Delta H(\Delta\delta P)$ is observed for all complexes with *meta*- and *para*-substituted phenols (filled symbols in Figure 3.8). The correlation $\Delta H(\Delta\delta P)$ seems to be general for complexes of different stoichiometry, the correlation seems nonlinear and well described by the power function $\Delta H = 16.6 \cdot \Delta\delta P^{0.47}$. The curve corresponded to this function is shown by the solid line in Figure 3.8. Data points corresponded to complexes with *meta*- and *para*- substituted phenols deviate from $\Delta H(\Delta\delta P)$ correlation by less than 3 $kJ \cdot mol^{-1}$.

Almost all points corresponded to complexes with *ortho*-substituted phenols (open symbols in Figure 3.8) deviate from correlation curve. This effect may be associated with the presence of additional interactions in complexes, that are schematically shown in Figure 3.9. Additional interactions may be found between P=O group of phosphine oxide and the substituent in *ortho* position: F, Cl, Br, I, as shown in Figure 3.9a,b. In the case when the substituent in *ortho* position is nitro group, for example in phenol **15**, strong intramolecular OHO hydrogen bond [171] may be formed, which is apparently remains after formation of complexes with Ph_3PO, *i.e.* bifurcate hydrogen bonds are formed in complexes, as shown in Figure 3.9. The last statement is confirmed in our experiments by the slight change in chemical shift δP upon complexation, 0.07 ppm, while chemical shift of the bridging proton (~11 ppm) indicates formation of medium strength hydrogen bond.

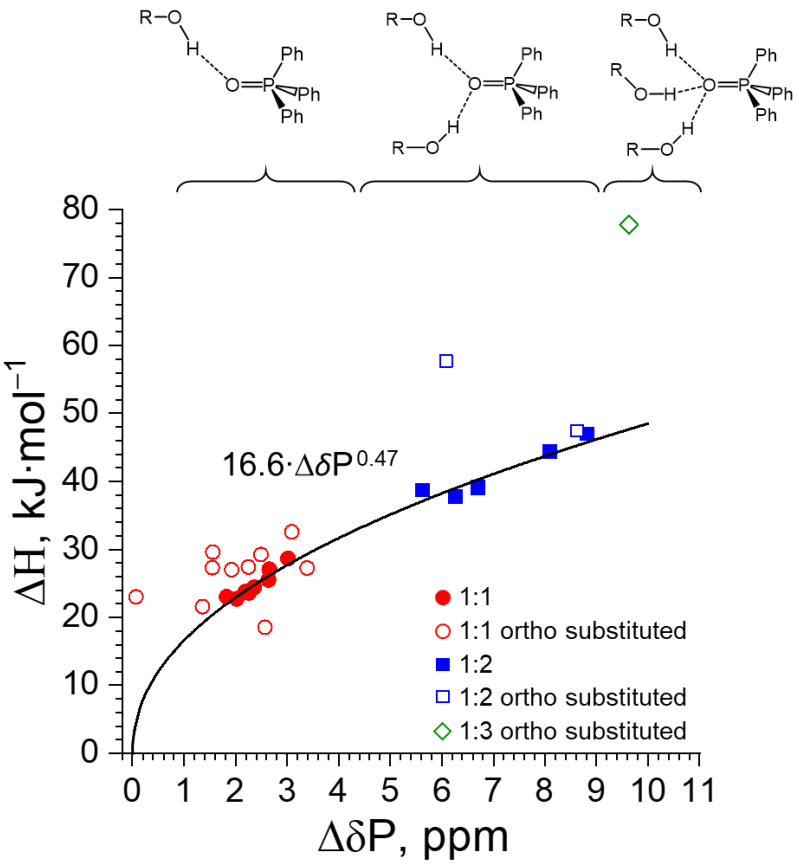

Figure 3.8. Correlation between ΔH and $\Delta\delta$P for 1:1 complexes (red circles), 1:2 complexes (blue squares) and 1:3 complexes (green diamonds) with hydrogen bonds between Ph_3PO and substituted phenols **1**–**18**. Open symbols corresponded to complexes with *ortho*-substituted phenols. The solid line corresponds to correlation curve obtained as the result of least squares fitting excluding data points for *ortho*-substituted phenols.

Note that correlation $\Delta H(\Delta\delta P)$ shown in Figure 3.8 is well described by the power function as well as correlation $\Delta E^t(\Delta\delta P^t)$ shown in Figure 2.23c (see Chapter 2). The coefficients and values of power in functions obtained for mentioned correlations differ, which was quite expected since: the characteristic of medium changed (the solvent was modeled implicitly in calculations (chloroform), while mixture of CDF_3/CDF_2Cl was used in the experiment), phosphine oxides with different substituents were chosen (Me_3PO in calculations, Ph_3PO in this study), and also the influence of additional weak hydrogen bonds between P=O group of phosphine oxide and solvent molecules calculations do not take into account.

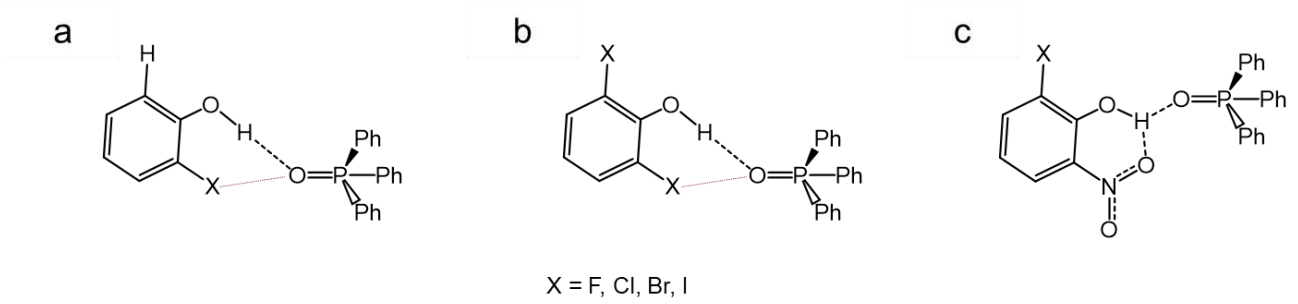

Figure 3.9. Suggested additional interactions in complexes formed by Ph_3PO and substituted phenols: interactions between P=O group of phosphine oxide and (a) X substituent (X = F, Cl, Br, I) of phenol in the *ortho* position (b) any of two X substituents of 2,6-substituted phenol and also (c) formation of bifurcate hydrogen bond with participation of nitro group in *ortho* position of phenol in complex with phenol **15**.

3.7. Conclusions

We experimentally studied hydrogen bonds in complexes formed by triphenylphosphine oxide and 18 different substituted phenols in solution in mixture of liquefied deuterated freons CDF_3/CDF_2Cl at 100 K. It was found that triphenylphosphine oxide may form one, two, or even three hydrogen bonds with substituted phenols. We showed that ^{31}P NMR chemical shift is sensitive to formation of hydrogen bonds and varies up to 10 ppm. We demonstrate the correlation between δP and total strength of hydrogen bonds, ΔH, formed with P=O group of phosphine oxide. The correlation $\Delta H(\Delta\delta P)$ is general for complexes with different stoichiometry formed by triphenylphosphine oxide and *meta*-substituted or *para*-substituted phenols, this correlation described by simple power function $\Delta H = 16.6 \cdot \Delta\delta P^{0.47}$. We assume that the deviation of data points corresponded to complexes with *ortho*-substituted phenols from general correlation may be explained by the presence of additional interactions between the substituent in *ortho* position and P=O group of phosphine oxide, and in some cases by the formation of bifurcate hydrogen bonds. We conclude that it is possible to accurately estimate the strength of hydrogen bonds in complexes with *meta*-substituted and *para*-substituted phenols using δP with the accuracy of 3 $kJ \cdot mol^{-1}$.

Chapter 4. Experimental IR spectroscopy investigation of complexes formed by phosphine oxides and substituted phenols in solution in CCl_4

4.1. Introduction and problem statement

The results of quantum chemical calculations of 1:1 and 1:2 trimethylphosphine oxide complexes with proton donors (see Chapter 2) indicate the presence of correlation between the strength of hydrogen bond and stretching vibrations frequency of P=O group in phosphine oxide, $\nu_{P=O}$, (see Figure 2.23a). Few experimental studies establishing the presence of such correlations in solutions have been found in the literature [144]. Therefore, in this part of work, we focused on experimental verification of correlation of $\Delta H(\Delta\nu_{P=O})$ for the set of 1:1 complexes with intermolecular hydrogen bonds formed by phosphine oxides and substituted phenols in solution in CCl_4 at room temperature by IR spectroscopy. We used carbon tetrachloride, CCl_4, as a solvent, because CCl_4 absorption bands do not fall in the spectral region in which OH and P=O groups vibrations are observed, and studied compounds well soluble in this solvent (in quantum chemical studies, Chapter 2, parameters of solvent corresponded to $CHCl_3$, however, $CHCl_3$ absorption bands may overlap the absorption bands of studied compounds in the spectra). Triphenylphosphine oxide (Ph_3PO), tri-*n*-butylphosphine oxide (Bu_3PO) and hexamethylphosphoramide ($(Me_2N)_3PO$) were chosen as proton acceptors (see structures in Figure 4.1).

As proton donors, we chose nine substituted phenols that noticeably differ in their proton-donating ability, see Figure 4.2 (the numbers of substituted phenols entered earlier in Chapter 3 are saved for consistency), the alcohol molecule CF_3CH_2OH was also added to the set. Note that the set of substituted phenols contains phenols with one (**18**, **19**) and two (**1**, **17**) ortho-substituents. In Chapter 2, we showed that data points corresponding to Ph_3PO complexes with such phenols deviate from $\Delta H(\delta P)$ correlation, so in this chapter,

we additionally investigate the influence of substituents in the *ortho*- position of substituted phenols on $\Delta H(\Delta\nu_{P=O})$ correlation for complexes with phosphine oxides.

For each 1:1 complex, which has the general structure as shown in Figure 4.3, we were focusing on estimating complexation enthalpies, ΔH, using OH groups vibrational frequencies, ν_{OH}. The primary goal was to assess experimentally the possibility of using the change of P=O stretching frequency upon complexation, $\Delta\nu_{P=O}$, for prediction of the strength of the complexes.

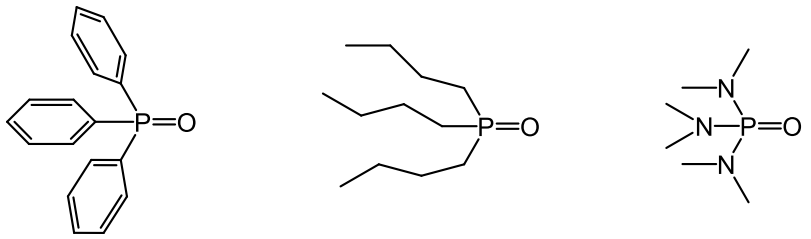

Ph_3PO **Bu_3PO** **$(Me_2N)_3PO$**

Figure 4.1. The set of P=O proton acceptors considered in this chapter: triphenylphosphine oxide (Ph_3PO), tri-*n*-butylphosphine oxide (Bu_3PO) and hexamethylphosphoramide ($(Me_2N)_3PO$).

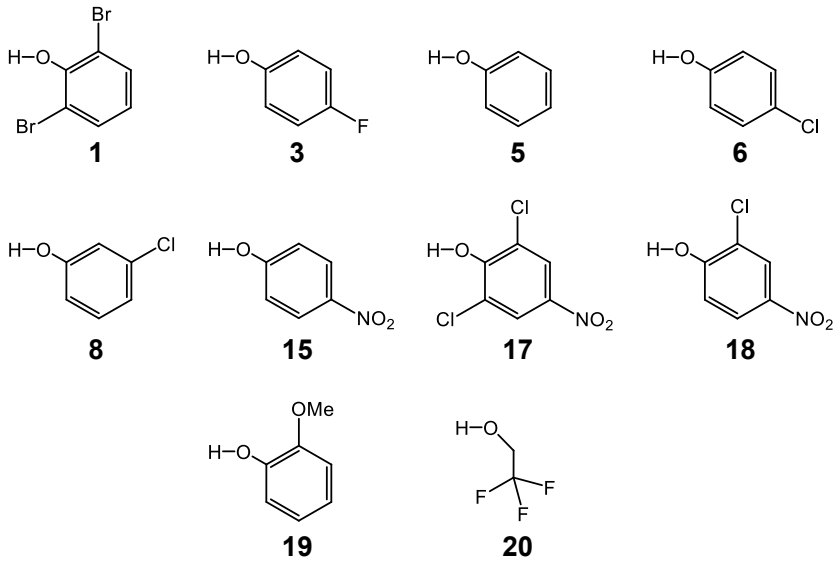

Figure 4.2. The set of OH proton donors considered in this chapter as partners in complexes with phosphine oxides.

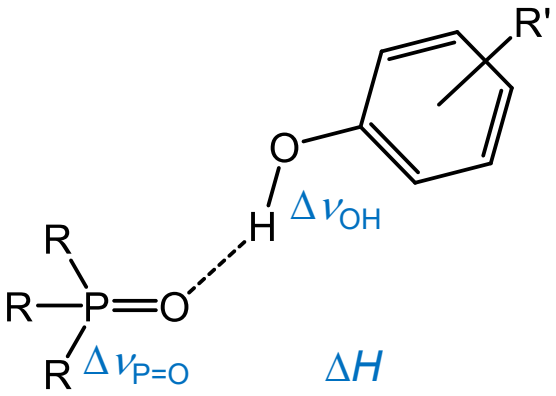

Figure 4.3. The general structure of complexes formed by phosphine oxides and substituted phenols (here, the similar structure of R_3PO complex with alcohol **20** is omitted for brevity). The following set of the main energetic and IR spectral parameters is considered in this work: the complexation enthalpy, ΔH; the changes of stretching vibrational frequency of P=O group, $\Delta\nu_{P=O}$, and OH group, $\Delta\nu_{OH}$.

4.2. Sample preparation

Phosphine oxides (Ph_3PO, Bu_3PO and $(Me_2N)_3PO$) and proton donors (substituted phenols and the alcohol) were purchased from *Sigma-Aldrich* and used without further purification. Firstly, the 2–10 mmol·L^{-1} stock solution of R_3PO in CCl_4 were prepared. For each phosphine oxide, approximately 2 mL of the stock solution were transferred to a flask to which the chosen proton donor was subsequently added until a saturated solution was formed or the concentration of proton donor in solution became approximately eight times the concentration of phosphine oxide. One half of the resulting solution was then used for the measurement of IR spectra, while to the remaining solution the stock solution of R_3PO was added, giving a solution with the same concentration of R_3PO as before and halved concentration of the proton donor. Then the procedure was repeated several times, resulting in a series of solutions with the concentration of proton donor equal to 1/2, 1/4, 1/8, 1/16 and 1/32 of the initial one for each pair of phosphine oxide and phenol.

4.3. IR spectra measurement for solutions in CCl_4

The infrared spectra were recorded with a Nikolet 6700 Fourier spectrometer. The instrument was equipped with a Ge/KBr beam splitter, a DTGS TEC detector, and a globar as a light source. The spectra were recorded by Ph.D., Assoc. Prof. R.E. Asfin. The spectra were recorded with a resolution of 1 cm^{-1} at room temperature near 22 °C. 50 co-added interferograms were recorded to obtain each spectrum. The standard liquid cells with a path length of 1.03 mm or 0.544 mm were used. The spectra of complexes were obtained by consequent subtraction of spectra of monomers from the spectra of their mixtures as described in ref. [172]. The spectra of monomers of investigated phenols and the alcohol (see Figure 4.2) were subtracted based mostly on the intensity of the ν_{OH} band. This band in the spectra of monomers differs essentially by wavenumber and shape from the analogous band in the spectra of complexes. However, it seems that in some cases the wavenumber of maximum of this band slightly depends on concentration of phenol and other components of the mixture. It leads to some dispersion-like features in the resulting spectrum of the complex in the region of the ν_{OH} band of monomer. The spectra of monomers of phosphine oxides were subtracted based on the intensity of the $\nu_{P=O}$ band of R_3PO monomer. In the following, from the concentration series obtained for each combination of phosphine oxide and proton donor we chose spectra of samples for which concentration dependence of band location and shapes was no longer detectable upon further dilution.

4.4. Main results and discussions

Spectra of individual compounds

IR spectra of Ph_3PO, Bu_3PO and $(Me_2N)_3PO$ solutions in CCl_4 (4–6 mmol·L^{-1}) at room temperature in the regions 3700–2000 cm^{-1} and 1100–1250 cm^{-1} are shown in Appendix C, Figures C1–C3. The 3700–2000 cm^{-1} region contains the CH stretching bands, present for all three studied phosphine oxides. The 1100–1250 cm^{-1} region contains the P=O stretching band, among others. For Ph_3PO, the strong $\nu_{P=O}$ band is located near 1202 cm^{-1}; the medium strong bands for C–P stretching and doubly/triply degenerate C–H bendings are visible as well. For Bu_3PO, the $\nu_{P=O}$ band near 1169 cm^{-1} is the strongest band in the region. For $(Me_2N)_3PO$, the $\nu_{P=O}$ band is located at 1212 cm^{-1}; previously, a slightly different value of 1207 cm^{-1} was reported in ref. [173]. The wavenumbers of P=O stretching vibrations are collected in Appendix C, Table C1.

For future reference and comparison with spectra of hydrogen-bonded complexes with phosphine oxides, we have also recorded spectra of 8–60 mmol·L^{-1} solutions of proton donors in CCl_4. For clarity, in the next section these spectra are shown together with the spectra of complexes. The wavenumbers of OH stretching vibrations are also collected in Appendix C, Table C1.

Spectra of complexes of phosphine oxides and substituted phenols

Upon addition of proton donors to the solutions of phosphine oxides several spectral changes occurred. As we focus on the study of 1:1 complexes, some precautions were taken in order to suppress the formation of various complexes of different stoichiometry, such as 1:2, 1:3, and *etc*. In order to achieve this, we were diluting the samples as described in Sample preparation, until the concentration dependence of shapes of absorption bands related to complex became insignificant. All further analysis is based on the spectra of these diluted samples. Below we consider the changes occurring in the OH stretching region and P=O stretching spectral region separately.

For clarity, let us consider the appearance of IR spectra and describe the procedure of the analysis on the example of one particular complex, namely, Ph_3PO complex with 4-fluorophenol **3**. The IR spectra of free Ph_3PO, free phenol **3** and their complex are shown in Figure 4.4a in the region 3700–2000 cm^{-1}.

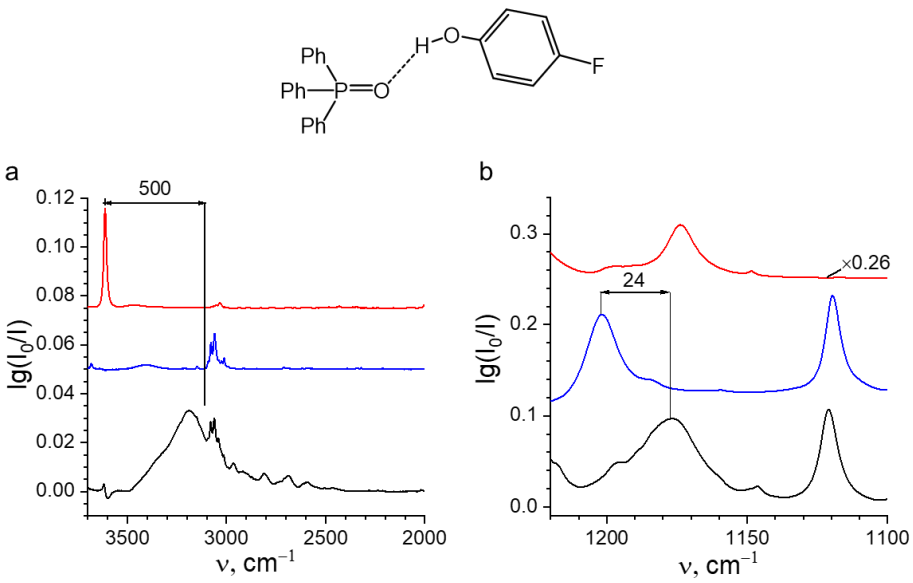

Figure 4.4. IR spectra of free 4-fluorophenol **3** (marked in red), free Ph_3PO (marked in blue) and their complex (marked in black) in solution in CCl_4 at room temperature. (a) The region of stretching vibrations of OH group; (b) the region of stretching vibrations of P=O group. Shifts of ν_{OH} and $\nu_{P=O}$ bands upon complexation are indicated. The spectra have been shifted vertically for clarity.

The narrow ν_{OH} band of monomeric **3** is located at 3613 cm^{-1}. Upon complexation the strong broad asymmetric ν_{OH} band appears in the region 3500–2500 cm^{-1}. The width and the shift of this band point out the formation of moderately strong hydrogen bond in the complex. As a marker for the hydrogen bond strength the shift of the first moment of the ν_{OH} band, M_1, with respect to that of the monomer, is often used [83]. The value of M_1, also referred to as "the center of gravity", is defined as $M_1 = 1/M_0 \int A(\nu)\nu d\nu$, where $A(\nu)$ is absorbance and M_0 is the integrated intensity of the band $M_0 = \int A(\nu)d\nu$. Integration is carried out over the band. The locations of M_1 and the ν_{OH} band of monomer are indicated in Figure 4.4a as black vertical bars, denoting the shift of the ν_{OH} band upon complexation, $\Delta\nu_{OH}$.

Broadness of OH bands in hydrogen-bonded complexes often can be explained by Fermi resonances of the ν_{OH} mode with combination transitions and overtones of fingerprint modes, which intensity essentially increased by interaction with the ν_{OH} mode [174–177]. The first moment of the resulting band should then coincide with a frequency of the ν_{OH} transition in the zeroth approximation, *i.e.* if the intensity of combination bands and overtone bands is zero. It allows one to compare the experimental first moment of the band of a complex with the calculated frequency of the ν_{OH} vibration or its shift upon complexation. As a side note, it should be mentioned, that the ν_{CH} bands of phenol rings of both Ph_3PO and **3** overlap with the broad ν_{OH} band. We subtracted the ν_{CH} bands using the spectra of monomers, as described in Section 4.3, assuming that their frequencies and intensities do not change significantly upon complexation. Such subtraction procedure slightly influences the accuracy of determination of M_1 (i.e. the location of ν_{OH} band), but it does not affect significantly the results of this study.

The set of IR spectra for all other combinations of phosphine oxides and proton donors is presented in Appendix C, Figures C4–C6, while the numerical values of $\Delta\nu_{OH}$ are collected in Table 4.1.

When considering the spectral region of P=O stretching (ca. 1100–1250 cm^{-1}), one should keep in mind that in the same region bands for several other vibrations appear, which complicates the assignment. Namely, it is the $\nu_{C–P}$ band and doubly/triply

degenerate C–H bendings of Ph_3PO, $\nu_{C–N}$ band for $(Me_2N)_3PO$ (1199 ± 2 cm^{-1}), δ(OH) band of phenols, CF vibrations for trifluoroethanol **20** and possibly some other bands.

Again, for brevity let us consider the example of TPPO complex with 4-fluorophenol **3**. In Figure 4.4b the spectra of free Ph_3PO, free phenol **3** and their complex are shown. In this case, as well as in all the other cases, the $\nu_{P=O}$ band shifts to low frequencies and becomes slightly broader upon complexation. We define the location of the $\nu_{P=O}$ band as the position of its maximum (measured with the precision of ±1 cm^{-1}). For all other complexes the IR spectra in the region of P=O stretching are shown in Appendix C, Figures C4–C6, and the $\Delta\nu_{P=O}$ values are collected in Table 4.1.

Table 4.1. The experimental band wavenumbers and shifts (in cm^{-1}) in IR spectra of Ph_3PO, Bu_3PO, $(Me_2N)_3PO$, proton donors **1**, **3**, **5**, **6**, **8**, **15**, **17**, **18**, **19**, **20** and their 1:1 complexes in solution in CCl_4 recorded at room temperature: the center of gravity of ν_{OH} band, M_1; the shifts of OH stretching band, $\Delta\nu_{OH} = M_1 - \nu_{OH}^{free}$; the P=O stretching band, $\nu_{P=O}$; the shifts of P=O stretching band, $\Delta\nu_{P=O} = \nu_{P=O} - \nu_{P=O}^{free}$; and also the values of complexation enthalpy, ΔH (in $kJ \cdot mol^{-1}$), estimated from the shifts of ν_{OH} band upon complexation (more details are given in text). The numeric values of $\nu_{P=O}^{free}$ and ν_{OH}^{free} are given in Appendix C, Table C1.

Proton donor	**Complexes with Ph_3PO**					**Complexes with Bu_3PO**					**Complexes with $(Me_2N)_3PO$**				
No.	M_1[a]	$\Delta\nu_{OH}$[a]	$\nu_{P=O}$	$\Delta\nu_{P=O}$[b]	ΔH	M_1[a]	$\Delta\nu_{OH}$[a]	$\nu_{P=O}$	$\Delta\nu_{P=O}$[b]	ΔH	M_1[a]	$\Delta\nu_{OH}$[a]	$\nu_{P=O}$	$\Delta\nu_{P=O}$[b]	ΔH
1	3160	–400	1184	–18	25.9	3060	–500	1148	–21	29.0	3020	–540	1171	–41	30.2
3	3120	–490	1179	–23	28.8	3060	–550	1148	–21	30.5	3030	–580	1174	–38	31.3[c]
5	3110	–500	1178	–24	29.2	3070	–540	1149	–20	30.3	3055	–560	1173	–39	30.7[d]
6	3090	–520	1177	–25	29.6	3020	–590	1146	–23	31.6	3020	–590	1172	–40	31.6[e]
8	3070	–540	1176	–26	30.1	3005	–600	1146	–23	31.9	3000	–610	1172	–40	32.0
15	2985	–610	1171	–31	32.1	2875	–720	1141	–28	34.9	2890	–700	1164	–48	34.5
17	2890	–640	1167	–35	32.9	2765	–760	1135	–34	35.9	2805	–720	1160	–52	35.0
18	3005	–510	1159	–43	29.4	2850	–670	1143	–26	33.5	2875	–640	1164	–48	32.9
19	2815	–700	1149	–53	34.5	2660	–860	1118	–51	38.1	2720	–800	1137	–75	36.7
20	3225	–390	1185	–17	25.8	3150	–470	1148	–21	28.2	3170	–450	1178	–34	27.6[f]

[a] *The measurement accuracy is ±30 cm^{-1}*

[b] *The measurement accuracy is ±3 cm^{-1}*

[c] 29.9 *in Ref.* [178]

[d] 32.3 *in Ref.* [178]

[e] 33.5 *in Ref.* [178]

[f] 34.2 *in Ref.* [179]

Correlations between $\Delta\nu_{OH}$ and $\Delta\nu_{P=O}$

In Table 4.1 the shifts of $\nu_{P=O}$ bands, $\Delta\nu_{P=O}$, and ν_{OH} bands, $\Delta\nu_{OH}$, for studied complexes were given. Here, the correlations between $|\Delta\nu_{P=O}|$ and $|\Delta\nu_{OH}|$ are shown in Figure 4.5 for complexes of proton donors with Ph_3PO (black circles), Bu_3PO (blue circles), $(Me_2N)_3PO$ (red circles). Within the set of studied complexes $|\Delta\nu_{P=O}|$ vary in the wide range from 17 cm^{-1} to 75 cm^{-1}, whereas $|\Delta\nu_{OH}|$ vary in the range from 390 cm^{-1} to 860 cm^{-1}. It seems that the correlations between $|\Delta\nu_{OH}|$ and $|\Delta\nu_{P=O}|$ are individual within each set of complexes with different phosphine oxides and monotonic over the entire range: $|\Delta\nu_{P=O}|$ increase with increasing of $|\Delta\nu_{OH}|$. The scattering of data points for Ph_3PO complexes with weaker proton donors **19**, **3**, **5**, **6**, **8** is smaller than that for complexes of Bu_3PO or $(Me_2N)_3PO$ with the same proton donors. In contrast, in case of stronger proton donors **1**, **15**, **17**, **18** the scattering of data points is smaller for Bu_3PO complexes. Note that the data point corresponding to Ph_3PO complex with 2,6-dibromophenol **1** deviates significantly from the general trend. It is likely to be associated with the proximity of the P=O oxygen and one of the *ortho*-halogens as was discussed in Chapter 3 (see Figure 3.8).

The correlation between $\Delta\nu_{P=O}$ and $\Delta\nu_{OH}$ could be described reasonably well by the power function $|\Delta\nu_{OH}| = a\cdot(|\Delta\nu_{P=O}|)^b$, where coefficients a and b are individual for each phosphine oxide. These coefficients were obtained by the least square fitting and the resulting equations are collected in Table 4.2 (in case of Ph_3PO the outlying data point for its complex with 2,6-dibromophenol **1** was excluded from the fitting).

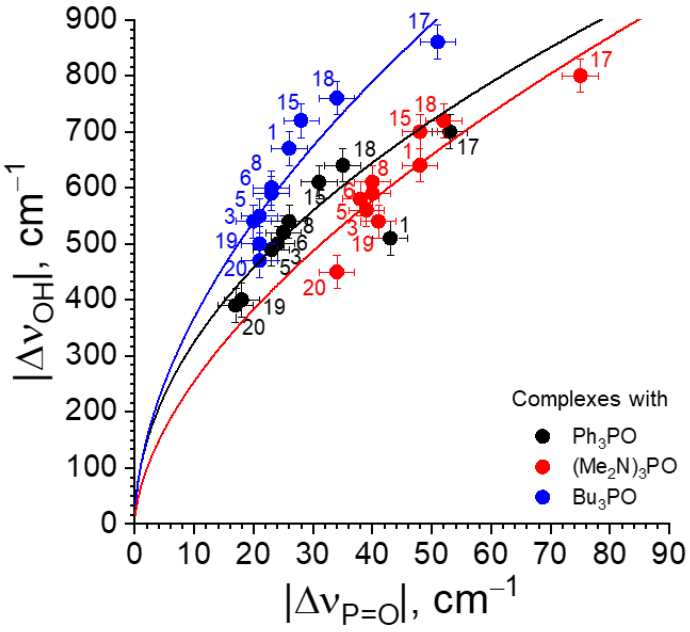

Figure 4.5. Correlations between $|\Delta\nu_{OH}|$ and $|\Delta\nu_{P=O}|$ based on IR experimental data set listed in Table 4.1. The solid curves correspond to the correlation functions explicitly given in Table 4.2.

Table 4.2. The fitting functions obtained for $\Delta\nu_{OH}(\Delta\nu_{P=O})$ and $\Delta H(\Delta\nu_{P=O})$ correlations ($\Delta\nu_{OH}$, $\Delta\nu_{P=O}$ в см$^{-1}$, ΔH в кДж·моль$^{-1}$; solid curves built using these functions are shown in Figure 4.5 and Figure 4.6).

Complexes with	Functions for $\Delta\nu_{OH}(\Delta\nu_{P=O})$ correlation	Function for $\Delta H(\Delta\nu_{P=O})$ correlation
Ph_3PO	$\lvert\Delta\nu_{OH}\rvert = 104\cdot(\lvert\Delta\nu_{P=O}\rvert)^{0.49}$	$\Delta H = 13.3\cdot(\lvert\Delta\nu_{P=O}\rvert)^{0.25}$
Bu_3PO	$\lvert\Delta\nu_{OH}\rvert = 104\cdot(\lvert\Delta\nu_{P=O}\rvert)^{0.55}$	$\Delta H = 13.3\cdot(\lvert\Delta\nu_{P=O}\rvert)^{0.28}$
$(Me_2N)_3PO$	$\lvert\Delta\nu_{OH}\rvert = 65\cdot(\lvert\Delta\nu_{P=O}\rvert)^{0.59}$	$\Delta H = 10.5\cdot(\lvert\Delta\nu_{P=O}\rvert)^{0.30}$

The strength of hydrogen bonds in complexes: correlation with $\Delta\nu_{P=O}$

Now we are turning to the main goal of this part of work, an estimation of the complexation enthalpy, ΔH, using the shift of $\nu_{P=O}$ band upon complexation. For non-covalent complexes, when the direct measurements are not available, the ΔH values are usually estimated using their correlations with certain spectral parameters. There are several literature examples of such ΔH estimations for complexes with phosphine oxides via measurements the complexation equilibrium constants. For instance, the equilibrium constants were obtained from the changes in intensity of the ν_{OH} band of monomers in IR spectra recorded for CCl_4 solutions of alcohols [179] or substituted phenols [178] upon addition of $(Me_2N)_3PO$ (see Table 4.1).

Here, we start by estimating the complexation enthalpies for the set of studied complexes using the shifts of ν_{OH} band upon complexation, $\Delta\nu_{OH}$, according to equation previously mentioned by Rozenberg in ref. [180] $\Delta H = 1.3\cdot(|\Delta\nu_{OH}|)^{0.5}$, where ΔH in $kJ\cdot mol^{-1}$, $\Delta\nu_{OH}$ in cm^{-1}. The values of ΔH estimated using this equation are listed in Table 4.1 for all complexes studied in this chapter. Within the set of 30 complexes ΔH vary in the range from ~25 $kJ\cdot mol^{-1}$ to ~40 $kJ\cdot mol^{-1}$. The ΔH values for $(Me_2N)_3PO$ complexes with phenols **3**, **5** and **6** match very well – within 2 $kJ\cdot mol^{-1}$ – those reported in refs. [178,179] , while for $(Me_2N)_3PO$ complex with the alcohol **20** the deviation is somewhat larger, *ca.* 7 $kJ\cdot mol^{-1}$. The latter could be explained by the tendency for alcohols to self-dimerize, which makes the approach for enthalpy measurement used in refs. [178,179] works probably less applicable.

The correlations between $\Delta\nu_{P=O}$ and the estimated values of ΔH are shown in Figure 4.6. Visually, the $\Delta H(|\Delta\nu_{P=O}|)$ plot is quite similar to the one shown in Figure 4.5, since the ΔH values were calculated from $|\Delta\nu_{OH}|$ using the power function. Therefore, the fitting functions obtained for data points shown in Figure 4.6 are also power functions and are given in Table 4.2. It seems that the exponents of the fitted power functions depend slightly on the type of phosphine oxide and vary in the range from 0.25 to 0.35.

In summary, there is a strong correlation between ΔH and $|\Delta\nu_{P=O}|$ for complexes of phosphine oxides R_3PO, though the numerical parameters of the correlation depend on the substituents R.

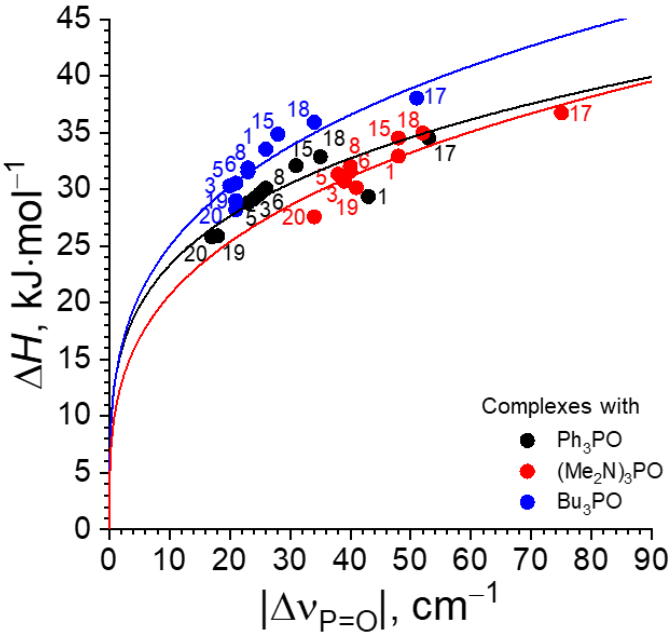

Figure 4.6. Correlations between complexation enthalpy, ΔH, estimated from shifts of ν_{OH} bands in IR spectra, and $|\Delta\nu_{P=O}|$ for complexes formed by studied proton donors with Ph_3PO (black circles), Bu_3PO (blue circles) and $(Me_2N)_3PO$ (red circles). Solid curves correspond to the correlation functions explicitly given in Table 4.2.

4.5. Conclusions

In this chapter we have experimentally investigated 30 hydrogen-bonded complexes formed by three phosphine oxides, Ph_3PO, Bu_3PO, $(Me_2N)_3PO$ with nine different substituted phenols and one alcohol. By the analysis of IR spectra recorded for the solutions of the studied complexes in CCl_4 we demonstrate confident non-linear correlations between complexation enthalpies and the shifts of $\nu_{P=O}$ bands within the range of considered hydrogen bond strengths (25–40 kJ·mol^{-1}).

The obtained correlation functions seem to be limited by the range of application, as their numerical parameters differ for differently substituted phosphine oxides. Nevertheless, there is enough similarity between all reported correlation functions, so that a rough estimation rule could be proposed: a shift of the $\nu_{P=O}$ bands by 5 cm^{-1} corresponds to the change in the strength of a hydrogen bond by approximately 1 kJ·mol^{-1}. It can also be argued that the accuracy of ΔH values estimated from the shifts of ν_{OH} and $\nu_{P=O}$ bands is approximately equal to 3 kJ·mol^{-1} and thus both $\Delta\nu_{OH}$ and $\Delta\nu_{P=O}$ may be used for predicting the hydrogen bond strength.

Conclusion

In this work, the energetic, geometric and spectral characteristics of hydrogen bonds in complexes formed by phosphine oxides and proton donors were studied theoretically, using quantum chemistry methods, and experimentally using IR and low-temperature NMR spectroscopy. For each data set the correlations were established between changes in the spectral characteristics of P=O group of phosphine oxides, $\Delta\delta$P and $\Delta\nu_{P=O}$, and the strength of hydrogen bonds in the complexes.

Quantum chemical calculations of 140 complexes with one and two hydrogen bonds between trimethylphosphine oxide and OH, NH, NH^+, CH proton donors in a polar aprotic medium (chloroform) demonstrate the presence of correlations between the strength of hydrogen bond, interatomic distances in hydrogen bridge and the change in ^{31}P chemical shift in NMR spectra, $\Delta\delta$P, and also the change in the frequency of P=O stretching vibration in IR spectra, $\Delta\nu_{P=O}$, upon complexation. We demonstrate the presence of correlations between hydrogen bond strength, hydrogen bond distances, $\Delta\delta$P and $\Delta\nu_{P=O}$. It was established that hydrogen bonds in complexes with two proton donors interact anticooperatively. Significant anticooperativity effects of hydrogen bonds in 1:2 complexes manifest on the main spectral parameters, energies and distances of hydrogen bonds. The set of correlations was proposed to evaluate the anticooperativity effects on the strength and distances of hydrogen bonds in complexes using the changes of spectral parameters $\Delta\nu_{P=O}$ and $\Delta\delta$P upon complex formation.

Complexes of triphenylphosphine oxide with 18 substituted phenols were studied experimentally in solution in the mixture of liquefied deuterated freons CDF_3/CDF_2Cl at 100 K using low-temperature NMR spectroscopy. It was found that in solutions, complexes of phosphine oxide with one and two proton donor molecules are usually formed. It was first shown that P=O group of triphenylphosphine oxide may participate in the formation of three hydrogen bonds with proton donors. We demonstrate the correlation between $\Delta\delta$P and the total strength of hydrogen bonds formed with P=O group

of phosphine oxide. The correlation is common for complexes of different stoichiometries and described by simple power equation.

Experimentally, IR spectroscopy was used to study 30 hydrogen bonded complexes formed by three phosphine oxides, Ph_3PO, Bu_3PO, $(Me_2N)_3PO$ with nine different substituted phenols and one alcohol in CCl_4 solution at room temperature. Nonlinear correlations were demonstrated between the shift of $\nu_{P=O}$ band in IR spectra and complexation enthalpy. The correlations are general for all proton donors with each phosphine oxide.

Theoretical and experimental correlations obtained in these studies are proposed for estimating the strength of hydrogen bonds in complexes using IR and NMR spectral characteristics of P=O group of phosphine oxides in cases where direct measurement of the strength by other methods is unavailable or difficult.

Acknowledgments

This work contains the main results of research carried out over the past few years under the direction, support and direct participation of many people. I am grateful to each of them for their valuable comments, help, support and interesting discussions.

I would like to express special gratitude to my scientific supervisor Dr. Peter Tolstoy for his mentorship, responsiveness and continued support over so many years.

I express my gratitude to Assistant Professor Ruslan Asfin, the Department of Molecular Spectroscopy of Faculty of Physics of St. Petersburg State University, for organizing, recording IR spectra and support in analyzing the results.

I am especially grateful to Omar Alkhuder for his assistance in preparing samples, important comments and fruitful cooperation.

I thank the staff of the Non-covalent Interactions Laboratory for the friendly atmosphere, discussions, and assistance in conducting research. I am also grateful to the staff of the Department of Molecular Spectroscopy, the Faculty of Physics of St. Petersburg State University, for the knowledge and experience that I received during my studies.

I especially thank my family for their support, understanding and care.

I thank Mikhail Vovk, employee of the “Magnetic Resonance Research Centre”, for recording NMR spectra at low temperatures.

Quantum chemical calculations and recording of IR and NMR spectra were performed using equipment and resources of the Scientific Park of St. Petersburg State University. The research was supported by Russian Science Foundation, grants No. 18-13-00050 and 23-13-00095, and Megagrant No. 075-15-2022-1112.

References

1. Kostin M.A. Phosphine oxides as NMR and IR spectroscopic probes for the estimation of the geometry and energy of PO···H–A hydrogen bonds // Phys. Chem. Chem. Phys. – 2022. – Vol. 24, № 11. – Pp. 7121–7133.
2. Kostin M.A. Complexes of phosphine oxides with substituted phenols: hydrogen bond characterization based on shifts of P=O stretching bands // Phys. Chem. Chem. Phys. – 2024. – Vol. 26, № 13. – Pp. 10234–10242.
3. Goymer P. 100 years of the hydrogen bond // Nat Chem. – 2012. – Vol. 4, № 11. – Pp. 863–864.
4. Werner A. Ueber Haupt- und Nebenvalenzen und die Constitution der Ammoniumverbindungen // Justus Liebig's Annalen der Chemie. – 1902. – Vol. 322, № 3. – Pp. 261–296.
5. Moore T.S., Winmill T.F. CLXXVII. – The state of amines in aqueous solution // J. Chem. Soc. Faraday Trans. – 1912. – Vol. 101. – Pp. 1635–1676.
6. Pfeiffer P. Zur Theorie der Farblacke, II // Justus Liebig's Annalen der Chemie. – 1913. – Vol. 398, № 2. – Pp. 137–196.
7. Langmuir I. Types of valence // Science. – 1921. – Vol. 54, № 1386. – Pp. 59–67.
8. Latimer W.M., Polarity and ionization from the standpoint of the lewis theory of valence // J. Am. Chem. Soc. – 1920. – Vol. 42, № 7. – Pp. 1419–1433.
9. Coulson C.A. THE HYDROGEN BOND: A review of the present interpretations and an introduction to the theoretical papers presented at the Congress // Hydrogen Bonding. Pergamon – 1959. – Pp. 339–360.
10. Morokuma K. Why Do Molecules Interact? The Origin of Electron Donor-Acceptor Complexes, Hydrogen Bonding, and Proton Affinity // Acc. Chem. Res. – 1977. – Vol. 10, № 8. – Pp. 294–300.
11. Kitaura K., A new energy decomposition scheme for molecular interactions within the Hartree-Fock approximation // Int. J. Quantum Chem. – 1976. – Vol. 10, № 2. – Pp. 325–340.

12. Morokuma K. Molecular orbital studies of hydrogen bonds. III. C=O ···H–O hydrogen bond in $H_2CO\cdots H_2O$ and $H_2CO\cdots 2H_2O$ // J. Chem. Phys. – 1971. – Vol. 55, № 3. – Pp. 1236–1244.
13. Arunan E. Definition of the hydrogen bond (IUPAC Recommendations 2011) // Pure App. Chem. – 2011. – Vol. 83, № 8. – Pp. 1637–1641.
14. Jeffrey G.A. Hydrogen-Bond Structure in Carbohydrate Crystals // Acc. Chem. Res. – 1978. – Vol. 11, № 7. – Pp. 264–270.
15. Jeffrey G.A. Hydrogen-bonding: An update // Crystallogr. Rev. – 1995. – Vol. 4, № 3. – Pp. 213–254.
16. Salbego P.R.S. [2]Rotaxanes Bearing a Tetralactam Macrocycle: The Role of a Trifurcated Hydrogen Bond in the Crystalline State // Eur. J. Org. Chem. – 2019. Vol. 2019, № 21. – Pp. 3464–3471.
17. Panigrahi S.K., Strong and weak hydrogen bonds in drug-DNA complexes: A statistical analysis // J. Biosci. – 2007. – Vol. 32, № 4. – Pp. 677–691.
18. Kurzydłowski D. Hydrogen-bonded cyclic dimers at large compression: The case of 1h-pyrrolo[3,2-h]quinoline and 2-(2′-pyridyl)pyrrole // Molecules. – 2021. – Vol. 26, № 13. – P. 3802.
19. Mulloyarova V. V. Cyclic trimers of phosphinic acids in polar aprotic solvent: Symmetry, chirality and H/D isotope effects on NMR chemical shifts // Phys. Chem. Chem. Phys. – 2018. – Vol. 20, № 7. – Pp. 4901–4910.
20. Giba I.S., Self-assembly of hydrogen-bonded cage tetramers of phosphonic acid // Symmetry – 2021. – Vol. 13, № 2. – P. 258.
21. Gilli G., The Nature of the Hydrogen Bond: Outline of a Comprehensive Hydrogen Bond Theory // New York: Oxford University Press. – 2009. – P. 251.
22. Woińska M. Hirshfeld atom refinement for modelling strong hydrogen bonds // Acta Crystallogr. A – 2014. – Vol. 70, № 5. – Pp. 483–498.
23. Woińska M. Hydrogen atoms can be located accurately and precisely by x-ray crystallography // Sci. Adv. – 2016. – Vol. 2, № 5. – P. e1600192.
24. Fugel M. Probing the accuracy and precision of Hirshfeld atom refinement with HARt interfaced with Olex2 // IUCrJ. – 2018. – Vol. 5, №1. – P. 32–44.

25. Sheldrick G.M. Crystal structure refinement with SHELXL // Acta Crystallogr. C – 2015. – Vol. 71, № 1. – Pp. 3–8.
26. Steiner T. Lenthening of the covalent O–H bond in O–H···O hydrogen bonds re-examined from low-temperature neutron diffraction data of organic compounds // Acta Crystallogr. B. – 1994. – Vol. 50, № 3. – Pp. 348–357.
27. Bertolasi V. Resonance-assisted O-H···O hydrogen bonding: Its role in the crystalline self-recognition of β-diketone enols and its structural and IR characterization // Chem. Eur. J. – 1996. – Vol. 2, № 8. – Pp. 925–934.
28. Steiner T. Lengthening of the covalent X–H bond in heteronuclear hydrogen bonds quantified from organic and organometallic neutron crystal structures // J. Phys. Chem. A. – 1998. – Vol. 102, № 35. – Pp. 7041–7052.
29. Limbach H.-H. OHO Hydrogen Bond Geometries and NMR Chemical Shifts: From Equilibrium Structures to Geometric H/D Isotope Effects, with Applications for Water, Protonated Water, and Compressed Ice // Isr. J. Chem. – 2009. – Vol. 49, № 2. – Pp. 199–216.
30. Larson J.W. Gas-phase bifluoride ion. An ion cyclotron resonance determination of the hydrogen bond energy in fluoride ion (FHF-) from gas-phase fluoride transfer equilibrium measurements // J. Am. Chem. Soc. – 1982. – Vol. 104, № 21. – Pp. 5848–5849.
31. Asfin R.E. The infrared spectra and enthalpies of strongly bound dimers of phosphinic acids in the gas phase. $(CH_2Cl)_2POOH$ and $(C_6H_5)_2POOH$ // J. Mol. Struct. – 2002. – Vol. 608, № 2–3. – Pp. 161–168.
32. Larson J.W. Gas-phase bihalide and pseudobihalide ions. An ion cyclotron resonance determination of hydrogen bond energies in XHY- species (X, Y = F, Cl, Br, CN) // Inorg. Chem. – 1984. – Vol. 23, № 14. – Pp. 2029–2033.
33. Wenthold P.G. Bond dissociation energies of F_2^- and HF_2^-. A gas-phase experimental and G2 theoretical study // J. Phys. Chem. – 1995. – Vol. 99, № 7. – Pp. 2002–2005.
34. Stein C. Accurate bond dissociation energies (D_0) for FHF^- isotopologues // Mol. Phys. – 2013. – Vol. 111, № 16–17. – Pp. 2647–2652.

35. Feyereisen M.W. Hydrogen bond energy of the water dimer // J. Phys. Chem. – 1996. – Vol. 100, № 8. – Pp. 2993–2997.
36. Anithaa V.S. Theoretical investigation on hydrogen bond interaction of diketo/keto-enol form uracil and thymine tautomers with intercalators // J. Mol. Model. – 2017. – Vol. 23, № 12. – P. 333.
37. Grabowski S.J. What is Common for Dihydrogen Bond and H…σ Interaction– Theoretical Analysis and Experimental Evidences // Challenges and Advances in Computational Chemistry and Physics. – 2015. – Vol. 19. – Pp. 159–187.
38. Hori Y. Local structure and hydrogen bond characteristics of imidazole molecules for proton conduction in acid and base proton-conducting composite materials // Phys. Chem. Chem. Phys. – 2018. – Vol. 20, № 15. – Pp. 10311–10318.
39. Kumar M. Quantum chemistry study of proton transport in imidazole chains // J. Phys. Chem. B. – 2015. – Vol. 119, № 7. – Pp. 3213–3222.
40. Lippincott E.R. One-dimensional model of the hydrogen bond // J. Chem. Phys. – 1955. – Vol. 23, № 6. – Pp. 1099–1106.
41. Schroeder R. Potential function model of hydrogen bonds. II // J. Phys. Chem. – 1957. – Vol. 61, № 7. – Pp. 921–928.
42. Tupikina E.Y. Correlations of NHN hydrogen bond energy with geometry and ^{1}H NMR chemical shift difference of NH protons for aniline complexes // J. Chem. Phys. – 2019. – Vol. 150, № 11. – P. 114305.
43. Grabowski S.J. Hydrogen bonding strength – measures based on geometric and topological parameters // J. Phys. Org. Chem. – 2004. – Vol. 17, № 1. – Pp. 18–31.
44. Vener M. V. Intermolecular hydrogen bond energies in crystals evaluated using electron density properties: DFT computations with periodic boundary conditions // J. Comput. Chem. – 2012. – Vol. 33, № 29. – Pp. 2303–2309.
45. Mata I. Relationships between interaction energy, intermolecular distance and electron density properties in hydrogen bonded complexes under external electric fields // Chem. Phys. Lett. – 2011. – Vol. 507, № 1–3. – Pp. 185–189.

46. Espinosa E. Hydrogen bond strengths revealed by topological analyses of experimentally observed electron densities // Chem. Phys. Lett. – 1998. – Vol. 285, № 3–4. – Pp. 170–173.
47. Tsirelson V. Determination of the electron localization function from electron density // Chem. Phys. Lett. – 2002. – Vol. 351, № 1–2. – Pp. 142–148.
48. Abramov Y.A. On the Possibility of Kinetic Energy Density Evaluation from the Experimental Electron-Density Distribution // Acta Crystallogr. A. – 1997. – Vol. 53, № 3. – Pp. 264–272.
49. Jeffrey G.A. The correlation between hydrogen-bond lengths and proton chemical shifts in crystals // Acta Crystallogr. B. – 1986. – Vol. 42, № 4. – Pp. 410–413.
50. Berglund B. Correlations between proton chemical shift tensors, deuterium quadrupole couplings, and bond distances for hydrogen bonds in solids // J. Chem. Phys. – 1980. – Vol. 73, № 5. – Pp. 2037–2043.
51. Sternberg U. The Influence of Short-Range Geometry on the Chemical Shift of Protons in Hydrogen Bonds // J. Magn. Reson. A. – 1994. – Vol. 108, № 2. – Pp. 142–150.
52. Harris T.K. NMR studies of strong hydrogen bonds in enzymes and in a model compound // J. Mol. Struct. – 2000. – Vol. 552, № 1–3. – Pp. 97–109.
53. Eyman D.P. Nuclear Magnetic Resonance Studies of Hydrogen Bonding // J. Am. Chem. Soc. – 1966. – Vol. 88, № 8. – Pp. 1617–1620.
54. Purcell K.F. Linear Enthalpy-Spectral Shift Correlations for 1,1,1,3,3,3-Hexafluoro-2-propanol // J. Am. Chem. Soc. – 1969. – Vol. 91, № 15. – Pp. 4019–4027.
55. Baran E. Mean Amplitudes of Vibration for Some Linear Gold(I) Complexes // Spectrosc. Lett. – 1975. – Vol. 8, № 2–3. – Pp. 151–155.
56. Tolstoy P.M. Characterization of Fluxional Hydrogen-Bonded Complexes of Acetic Acid and Acetate by NMR: Geometries and Isotope and Solvent Effects // J. Am. Chem. Soc. – 2004. – Vol. 126, № 17. – Pp. 5621–5634.
57. Shenderovich I.G. Low-temperature NMR studies of the structure and dynamics of a novel series of acid-base complexes of HF with collidine exhibiting scalar

couplings across hydrogen bonds // J. Am. Chem. Soc. – 2003. – Vol. 125, № 38. – Pp. 11710–11720.

58. Tolstoy P.M. NMR studies of solid state – Solvent and H/D isotope effects on hydrogen bond geometries of 1:1 complexes of collidine with carboxylic acids // J. Mol. Struct. – 2004. – Vol. 700, № 1. – Pp. 19–27.
59. Marek R. ^{15}N NMR Spectroscopy in Structural Analysis: An Update (2001–2005) // Curr. Org. Chem. – 2007. – Vol. 11, № 13. – Pp. 1154–1205.
60. Silva A.M.N. Determination of the pKa value of the hydroxyl group in the α-hydroxycarboxylates citrate, malate and lactate by 13C NMR: Implications for metal coordination in biological systems // BioMetals. – 2009. – Vol. 22, № 5. – Pp. 771–778.
61. Giba I.S. Sensitivity of ^{31}P NMR chemical shifts to hydrogen bond geometry and molecular conformation for complexes of phosphinic acids with pyridines // Magn. Reson. Chem. – 2021. – Vol. 59, № 4. – Pp. 465–477.
62. Koeppe B. Reaction pathways of proton transfer in hydrogen-bonded phenol-carboxylate complexes explored by combined UV-Vis and NMR spectroscopy // J. Am. Chem. Soc. – 2011. – Vol. 133, № 20. – Pp. 7897–7908.
63. Alkorta I. Do coupling constants and chemical shifts provide evidence for the existence of resonance-assisted hydrogen bonds? // Mol. Phys. – 2004. – Vol. 102, № 23–24. – Pp. 2563–2574.
64. Del Bene J.E., Interpreting ^{2h}J(F,N), ^{1h}J(H,N) and ^{1}J(F,H) in the hydrogen-bonded FH-collidine complex // Magn. Reson. Chem. – 2002. – Vol. 40, № 12. – Pp. 767–771.
65. Bagno A. Complete prediction of the ^{1}H NMR spectrum of organic molecules by DFT calculations of chemical shifts and spin-spin coupling constants // Chem. Eur. J. – 2001. – Vol. 7, № 8. – Pp. 1652–1661.
66. Benedict H. Nuclear scalar spin-spin couplings and geometries of hydrogen bonds // J. Am. Chem. Soc. – 2000. – Vol. 122, № 9. – Pp. 1979–1988.
67. Szafran M. A critical review of the isotope effect in IR spectra // J. Mol. Struct. – 1994. – Vol. 321, № 1–2. – Pp. 57–77.

68. Ichikawa M. Hydrogen-bond geometry and its isotope effect in crystals with OHO bonds - Revisited // J. Mol. Struct. – 2000. – Vol. 552, № 1–3. – Pp. 63–70.
69. Sokolov N.D. Tentative study of strong hydrogen bond dynamics. Part II. Vibrational frequency considerations // J. Mol. Struct. –1990. – Vol. 222, № 3–4. – Pp. 365–386.
70. Manikandan K. The occurrence of C–H···O hydrogen bonds in α-helices and helix termini in globular proteins // Proteins. – 2004. – Vol. 56, № 4. – Pp. 768–781.
71. Grech E. Isotopic effects in NH···N hydrogen bonds // Chem. Phys. Lett. – 1986. – Vol. 128, № 3. – Pp. 259–263.
72. Dziembowska T. NMR study of proton transfer equilibrium in Schiff bases derived from 2-hydroxy-1-naphthaldehyde and 1-hydroxy-2-acetonaphthone. Deuterium isotope effects on ^{13}C and ^{15}N chemical shifts // Magn. Reson. Chem. – 2001. – Vol. 39, № S1. – Pp. S67–S80.
73. Dohnal V. A simple relation between ^{1}H NMR data and mixing enthalpy for systems with complex formation by hydrogen bonding // J. Phys. Chem. B. – 2002. – Vol. 106, № 47. – Pp. 12307–12310.
74. Ishikawa R. Developing model systems for the NMR study of substituent effects on the N–H···N hydrogen bond in duplex DNA // Magn. Reson. Chem. – 2001. – Vol. 39. – Pp. S159–S165.
75. Denisov G.S. Stretching Vibrations of Amino Group and Inter/Intramolecular Hydrogen Bond in Anilines // Croat. Chem. Acta. – 1992. – Vol. 65, № 1. – Pp. 89–100.
76. Iogansen A. V. Direct proportionality of the hydrogen bonding energy and the intensification of the stretching ν(XH) vibration in infrared spectra // Spectrochim. Acta A. – 1999. – Vol. 55, № 7–8. – Pp. 1585–1612.
77. Hippler M. Quantum-chemical study and FTIR jet spectroscopy of $CHCl_3$-NH_3 association in the gas phase // Phys. Chem. Chem. Phys. – 2010. – Vol. 12, № 41. – Pp. 13555–13565.

78. Mikenda W. Stretching frequency versus bond distance correlation of O–D(H)···Y (Y = N, O, S, Se, Cl, Br, I) hydrogen bonds in solid hydrates // J. Mol. Struct. – 1986. – Vol. 147, № 1–2. – Pp. 1–15.
79. Rozenberg M. Variable temperature FTIR spectra of polycrystalline purine nucleobases and estimating strengths of individual hydrogen bonds // Spectrochim. Acta A. – 2021. – Vol. 251. – P. 119323.
80. Rozenberg M. An empirical correlation between stretching vibration redshift and hydrogen bond length // Phys. Chem. Chem. Phys. – 2000. – Vol. 2, № 12. – Pp. 2699–2702.
81. Osipova E.S. Dihydrogen Bonding and Proton Transfer from MH and OH Acids to Group 10 Metal Hydrides [($^{t\mathrm{Bu}}$PCP)MH] [$^{t\mathrm{Bu}}$PCP = κ^3-2,6-(tBu$_2$PCH$_2$)$_2$C$_6$H$_3$; M = Ni, Pd] // Eur. J. Inorg. Chem. – 2016. – Vol. 2016, № 9. – Pp. 1415–1424.
82. Voronova E.D. Comprehensive Insight into the Hydrogen Bonding of Silanes // Chem.: Asian J. – 2018. – Vol. 13, № 20. – Pp. 3084–3089.
83. Novak A. Hydrogen bonding in solids correlation of spectroscopic and crystallographic data // Large Molecules. – 1974. – Pp. 177–216.
84. Badger R.M. Spectroscopic studies of the hydrogen bond. II. The shift of the O–H vibrational frequency in the formation of the hydrogen bond // J. Chem. Phys. – 1937. – Vol. 5, № 11. – Pp. 839–851.
85. Tupikina E.Y. New look at the Badger-Bauer rule: Correlations of spectroscopic IR and NMR parameters with hydrogen bond energy and geometry. FHF complexes // J. Mol. Struct. – 2018. – Vol. 1164. – Pp. 129–136.
86. Denisov G.S. Correlation relationships between the energy and spectroscopic parameters of complexes with F···HF hydrogen bond // Doklady Phys. Chem. – 2017. – Vol. 475, № 1. – Pp. 49–52.
87. Koeppe B. Polar solvent fluctuations drive proton transfer in hydrogen bonded complexes of carboxylic acid with pyridines: NMR, IR and ab initio MD study // Phys. Chem. Chem. – 2017. – Vol. 19, № 2. – Pp. 1010–1028.
88. Takei K. Correlation between the hydrogen-bond structures and the C=O stretching frequencies of carboxylic acids as studied by density functional theory calculations:

Theoretical basis for interpretation of infrared bands of carboxylic groups in proteins // J. Phys. Chem. B. – 2008. – Vol. 112, № 21. – Pp. 6725–6731.

89. Vaz P.D. C–H···O hydrogen bonds in liquid cyclohexanone revealed by the νC=O splitting and the νC–H blue shift // J. Raman Spectrosc. – 2003. – Vol. 34, № 11. – Pp. 863–867.
90. Candelaresi M. Chemical equilibrium probed by two-dimensional IR spectroscopy: Hydrogen bond dynamics of methyl acetate in water // J. Phys. Chem. A. – 2009. – Vol. 113, № 46. – Pp. 12783–12790.
91. Tupikina E.Y. Estimations of FH···X hydrogen bond energies from IR intensities: Iogansen's rule revisited // J. Comput. Chem. – 2021. – Vol. 42, № 8. – Pp. 564–571.
92. Iogansen A. V. The enhancement and displacement of the IR band of hydrogen chloride as a function of the energy of the hydrogen bond // J. Appl. Spectrosc. – 1973. – Vol. 18, № 4. – Pp. 499–503.
93. Iogansen A. V. Intensity of ν(A–H) infrared bands and N–H…B hydrogen bonds // J. Appl. Spectrosc. – 1969. – Vol. 11, № 6. – Pp. 1487–1492.
94. Iogansen A. V. The characteristic bands of the stretching vibrations of the nitro group in infrared absorption - II. Correlation of the frequencies and intensities with the structure of the molecules // J. Appl. Spectrosc. – 1965. – Vol. 3, № 6. – Pp. 404–411.
95. Becker E.D. Infrared studies of hydrogen bonding in alcohol-base systems // Spectrochim. Acta. – 1961. – Vol. 17, № 4. – Pp. 436–447.
96. Nibbering E.T.J. Vibrational dynamics of hydrogen bonds // Analysis and Control of Ultrafast Photoinduced Reactions. – 2007. – Vol. 87. – Pp. 619-687.
97. Falk M. The frequency of the HOH bending fundamental in solids and liquids // Spectrochim. Acta A. – 1984. – Vol. 40, № 1. – Pp. 43–48.
98. Seki T. The bending mode of water: A powerful probe for hydrogen bond structure of aqueous systems // J. Phys. Chem. Lett. – 2020. – Vol. 11, № 19. – Pp. 8459–8469.

99. Iliescu S. Polymers containing phosphorus groups and polyethers: From synthesis to application // Chem. Cent. J. – 2012. – Vol. 6 – 132.
100. Monge S. Phosphorus-containing polymers: A great opportunity for the biomedical field // Biomacromolecules. – 2011. – Vol. 12, № 6. – Pp. 1973–1982.
101. Petreus O. Synthesis and characterization of new polyesters with enhanced phosphorus content // Eur. Polym. J. – 2005. – Vol. 41, № 11. – Pp. 2663–2670.
102. Chang Y.L. A novel phosphorus-containing polymer as a highly effective flame retardant // Macromol. Mater. Eng. – 2004. – Vol. 289, № 8. – Pp. 703–707.
103. Allcock H.R. Phenylphosphonic acid functionalized poly[aryloxyphosphazenes] // Macromolecules. – 2002. – Vol. 35, № 9. – Pp. 3484–3489.
104. Lee Y.J. High-resolution solid-state NMR studies of poly(vinyl phosphonic acid) proton-conducting polymer: Molecular structure and proton dynamics // J. Phys. Chem. B. – 2007. – Vol. 111, № 33. – Pp. 9711–9721.
105. Jiangs F. Phase behavior and proton conduction in poly(vinylphosphonic acid)/ polyethylene oxide blends // Macromolecules. – 2010. – Vol. 43, № 8. – Pp. 3876–3881.
106. Van Leeuwen P.W.N.M. Secondary Phosphine Oxides: Bifunctional Ligands in Catalysis // ChemCatChem. – 2020. – Vol. 12, № 16. – Pp. 3982–3994.
107. Cano I. An iridium-SPO complex as bifunctional catalyst for the highly selective hydrogenation of aldehydes // Catal. Sci. Technol. – 2018. – Vol. 8, № 1. – Pp. 221–228.
108. Denmark S.E. Phosphine oxides as stabilizing ligands for the palladium-catalyzed cross-coupling of potassium aryldimethylsilanolates // Tetrahedron. – 2007. – Vol. 63, № 26. – Pp. 5730–5738.
109. Shaikh T.M. Secondary phosphine oxides: Versatile ligands in transition metal-catalyzed cross-coupling reactions // Coordination Chemistry Reviews. – 2012. – Vol. 256, № 9–10. – Pp. 771–803.
110. Iyer G. Tracking Single Proteins in Live Cells Using Single-Chain Antibody Fragment-Fluorescent Quantum Dot Affinity Pair // Methods in Enzymology. – 2010. – Vol. 475. – Pp. 61–79.

111. Pinaud F. Bioactivation and Cell Targeting of Semiconductor CdSe/ZnS Nanocrystals with Phytochelatin-Related Peptides // J. Am. Chem. Soc. – 2004. – Vol. 126, № 19. – Pp. 6115–6123.
112. Cuypers R. Hydrogen Bonding in Phosphine Oxide/Phosphate-Phenol Complexes // ChemPhysChem. – 2010. – Vol. 11, № 10. – Pp. 2230–2240.
113. Hilliard C.R. Structures and Unexpected Dynamic Properties of Phosphine Oxides Adsorbed on Silica Surfaces // Chem. Eur. J. – 2014. – Vol. 20, № 52. – Pp. 17292–17295.
114. Tupikina E.Y. P=O Moiety as an Ambidextrous Hydrogen Bond Acceptor // J. Phys. Chem. C. – 2018. – Vol. 122, № 3. – Pp. 1711–1720.
115. Shenderovich I.G. Effect of noncovalent interactions on the ^{31}P chemical shift tensor of phosphine oxides, phosphinic, phosphonic, and phosphoric acids, and their complexes with lead(II) // J. Phys. Chem. C. – 2013. – Vol. 117, № 50. – Pp. 26689–26702.
116. Alkorta I. Is it possible to use the ^{31}P chemical shifts of phosphines to measure hydrogen bond acidities (HBA)? A comparative study with the use of the ^{15}N chemical shifts of amines for measuring HBA // J. Phys. Org. Chem. – 2017. – Vol. 30, № 11. – P. e3690.
117. Giba I.S. Influence of Hydrogen Bonds in 1:1 Complexes of Phosphinic Acids with Substituted Pyridines on ^{1}H and ^{31}P NMR Chemical Shifts // J. Phys. Chem. A. – 2019. – Vol. 123, № 11. – Pp. 2252–2260.
118. Ostras' A.S. Phosphine Oxides as Spectroscopic Halogen Bond Descriptors: IR and NMR Correlations with Interatomic Distances and Complexation Energy // Molecules. – 2020. – Vol. 25, № 6. – P. 1406.
119. Mulloyarova V. V. H/D Isotope Effects on ^{1}H-NMR Chemical Shifts in Cyclic Heterodimers and Heterotrimers of Phosphinic and Phosphoric Acids // Molecules. – 2020. – Vol. 25, № 8. – P. 1907.
120. Shenderovich I.G. Electric field effect on ^{31}P NMR magnetic shielding // J. Chem. Phys. – 2020. – Vol. 153, № 18. – P. 184501.

121. Begimova G. Effect of Hydrogen Bonding to Water on the ^{31}P Chemical Shift Tensor of Phenyl- and Trialkylphosphine Oxides and α-Amino Phosphonates // J. Phys. Chem. C. – 2016. – Vol. 120, № 16. – Pp. 8717–8729.
122. Arp F.F. Hydrogen peroxide adducts of triarylphosphine oxides // Dalton Trans. – 2019. – Vol. 48, № 38. – Pp. 14312–14325.
123. Ahn S.H. Di(hydroperoxy)cycloalkanes Stabilized via Hydrogen Bonding by Phosphine Oxides: Safe and Efficient Baeyer-Villiger Oxidants // ACS Sustain. Chem. Eng. – 2018. – Vol. 6, № 5. – Pp. 6829–6840.
124. Pires E. Study of interactions between Brønsted acids and trimethylphosphine oxide in solution by ^{31}P NMR: Evidence for 2:1 species // Phys. Chem. Chem. Phys. – 2020. – Vol. 22, № 42. – Pp. 24351–24358.
125. Kühl O. Phosphorus-31 NMR spectroscopy: A concise introduction for the synthetic organic and organometallic chemist // Springer – 2008. – Pp. 1–131.
126. Latypov S.K. Quantum chemical calculations of ^{31}P NMR chemical shifts: scopes and limitations // Phys. Chem. Chem. Phys. – 2015. – Vol. 17, № 10. – Pp. 6976–6987.
127. Quinn L. Phosphorus-31 NMR Spectral Properties in Compound Characterization and Structural Analysis // Wiley. – 1994.
128. Zheng A. ^{31}P NMR Chemical Shifts of Phosphorus Probes as Reliable and Practical Acidity Scales for Solid and Liquid Catalysts // Chem. Rev. – 2017. – Vol. 117, № 19. – Pp. 12475–12531.
129. Mayer U. The acceptor number – a quantitative empirical parameter for the electrophilic properties of solvents // Monatsh. Chem. – 1975. – Vol. 106, № 6. – Pp. 1235–1257.
130. Pahl J. Highly Lewis acidic cationic alkaline earth metal complexes // Chem. Commun. – 2018. – Vol. 54, № 63. – Pp. 8685–8688.
131. Beckett M.A. Lewis acidity of tris(pentafluorophenyl) borane: crystal and molecular structure of $B(C_6F_5)_3 \cdot OPEt_3$ // Inorg. Chem. Commun. – 2000. – Vol. 3, № 10. – Pp. 530–533.

132. Beckett M.A. A convenient n.m.r. method for the measurement of Lewis acidity at boron centres: Correlation of reaction rates of Lewis acid initiated epoxide polymerizations with Lewis acidity // Polymer. – 1996. – Vol. 37, № 20. – Pp. 4629–4631.
133. McCune J.A. Brønsted acids in ionic liquids: How acidity depends on the liquid structure // Phys. Chem. Chem. Phys. – 2014. – Vol. 16, № 42. – Pp. 23233–23243.
134. Osegovic J.P. Measurement of the Global Acidity of Solid Acids by ^{31}P MAS NMR of Chemisorbed Triethylphosphine Oxide // J. Phys. Chem. B. – 2000. – Vol. 104, № 1. – Pp. 147–154.
135. Symons M.C.R. Triethylphosphine oxide as an infrared probe of solvent structure. The significance of acceptor numbers // J. Chem. Soc. Faraday Trans. – 1982. – Vol. 78, № 10. – Pp. 3033–3044.
136. Diemoz K. NMR Quantification of Hydrogen-Bond-Activating Effects for Organocatalysts including Boronic Acids // J. Org. Chem. – 2019. – Vol. 84, № 3. – Pp. 1126–1138.
137. Jennings J.J. NMR quantification of H-bond donating ability for bioactive functional groups and isosteres // Eur. J. Med. Chem. – 2020. – Vol. 207. – P. 112693.
138. Nödling A.R. ^{31}P NMR Spectroscopically Quantified Hydrogen-Bonding Strength of Thioureas and Their Catalytic Activity in Diels–Alder Reactions // Eur. J. Org. Chem. – 2014. – Vol. 2014, № 29. – Pp. 6394–6398.
139. Chakalov E.R. The Distance between Minima of Electron Density and Electrostatic Potential as a Measure of Halogen Bond Strength // Molecules. – 2022. – Vol. 27, № 15. – P. 4848.
140. Hilliard C.R. Synthesis, purification, and characterization of phosphine oxides and their hydrogen peroxide adducts // Dalton Trans. – 2012. – Vol. 41, № 6. – P. 1742–1754.
141. Cotton F.A. The effect of complex-formation by phosphine oxides on their P–O stretching frequencies // J. Chem. Soc. – 1960. – P. 2199–2203.

142. Jensen J.O. Vibrational frequencies and structural determination of trimethylphosphine oxide // J. Mol. Struct. (theochem). – 2005. – Vol. 723, № 1–3. – Pp. 1–8.
143. Reva I. Photoinduced oxidation of triphenylphosphine isolated in a low-temperature oxygen matrix // Chem. Phys. Lett. – 2008. – Vol. 467, № 1–3. – Pp. 97–100.
144. Bel'skii V.E. Study of the association of phosphoryl compounds with proton donors at the ν(P=O) frequency in IR spectra // Zhurnal Obshchei Khimii. – 1979. – Vol. 49, № 10. – Pp. 2241–2245.
145. Mayer U. IR-spectroscopic investigations on solute-solvent interactions Part 1: Solvation of triethylphosphine oxide in aprotic and CH-acidic solvents // Monatsh. Chem. – 1988. – Vol. 119, № 11. – Pp. 1207–1221.
146. Mayer U. IR-spectroscopic investigations on solute-solvent interactions Part 2: Solvation of triethylphosphine oxide in hydroxylic solvents // Monatsh. Chem. – 1988. – Vol. 119, № 11. – Pp. 1223–1239.
147. Symons M.C.R. Infrared and NMR studies of probes in binary solvent systems // Pure Appl. Chem. – 1986. – Vol. 58, № 8. – Pp. 1121–1132.
148. Bader R.F.W. A quantum theory of molecular structure and its applications // Chem. Rev. – 1991. – Vol. 91, № 5. – Pp. 893–928.
149. Frisch M.J. Gaussian 16, Revision C.01 // Gaussian, Inc. – Wallingford CT. – 2016.
150. Becke A.D. Density-functional thermochemistry. III. The role of exact exchange // J. Chem. Phys. – 1993. – Vol. 98, № 7. – Pp. 5648–5652.
151. Lee C. Development of the Colle-Salvetti correlation-energy formula into a functional of the electron density // Phys. Rev. B. – 1988. – Vol. 37, № 2. – P. 785–789.
152. Vosko S.H. Accurate spin-dependent electron liquid correlation energies for local spin density calculations: a critical analysis // Can. J. Phys. – 1980. – Vol. 58, № 8. – Pp. 1200–1211.

153. Stephens P. Ab Initio calculation of vibrational absorption and circular dichroism spectra using density functional force fields // J. Phys. Chem. – 1994. – Vol. 98, № 45. – Pp. 11623–11627.
154. Tomasi J. Quantum Mechanical Continuum Solvation Models // Chem. Rev. – 2005. – Vol. 105, № 8. – Pp. 2999–3093.
155. Multiwfn. URL: http://sobereva.com/multiwfn.
156. Lu T. Multiwfn: A multifunctional wavefunction analyzer // J. Comput. Chem. – 2012. – Vol. 33, № 5. – Pp. 580–592.
157. Dennington R. GaussView, Version 6.1 – Semichem, Inc. – 2009.
158. Bankiewicz B. Does electron density in bond critical point reflect the formal charge distribution in H-bridges? The case of charge-assisted hydrogen bonds (CAHBs) // Comput. Theor. Chem. – 2011. – Vol. 966, № 1–3. – Pp. 113–119.
159. Bhatta R.S. A brief review of Badger-Bauer rule and its validation from a first-principles approach // Mod. Phys. Lett. B. – 2014. – Vol. 28, № 29. – P. 1430014.
160. Golub I.E. Dimerization mechanism of bis(triphenylphosphine)copper(I) tetrahydroborate: Proton transfer via a dihydrogen bond // Inorg. Chem. – 2012. – Vol. 51, № 12. – Pp. 6486–6497.
161. Solomonov B.N. Calorimetric determination of hydrogen-bonding enthalpy for neat aliphatic alcohols // J. Phys. Org. Chem. – 2005. – Vol. 18, № 11. – Pp. 1132–1137.
162. Limbach H.-H. NMR parameters and geometries of OHN and ODN hydrogen bonds of pyridine-acid complexes // Chem. Eur. J. – 2004. – Vol. 10, № 20. – Pp. 5195–5204.
163. Reuben J. Intramolecular Hydrogen Bonding as Reflected in the Deuterium Isotope Effects on Carbon-13 Chemical Shifts. Correlation with Hydrogen Bond Energies // J. Am. Chem. Soc. – 1986. – Vol. 108, № 8. – Pp. 1735–1738.
164. Detering C. Vicinal H/D isotope effects in NMR spectra of complexes with coupled hydrogen bonds. Phosphoric acids // Proc. USSR Acad. Sci. – 2001. –Vol. 379, № 3. – Pp. 353–356.

165. Shenderovich I.G. Nuclear magnetic resonance of hydrogen bonded clusters B between F^- and $(HF)_n$: Experiment and Theory // Ber. Bunsenges. Phys. Chem. Chem. Phys. – 1998. – Vol. 102, № 3. – Pp. 422–428.
166. Giba I.S. Influence of Hydrogen Bonds in 1:1 Complexes of Phosphinic Acids with Substituted Pyridines on ^{1}H and ^{31}P NMR Chemical Shifts // J. Phys. Chem. A. – 2019. – Vol. 123, № 11. – Pp. 2252–2260.
167. Golubev N.S. Study of hydrogen bonds of hypophosphorous acid by ^{1}H, ^{2}H, ^{31}P, and ^{15}N NMR spectroscopy under slow exchange conditions // Russ. J. Gen. Chem. – 2006. – Vol. 76, № 6. – Pp. 915–924.
168. Harris R.K. NMR nomenclature: Nuclear spin properties and conventions for chemical shifts (IUPAC recommendations 2001) // Concepts Magn. Reson. – 2002. – Vol. 14, № 5. – Pp. 326–346.
169. Willcott M.R. MestRe Nova // J. Am. Chem. Soc. – 2009. – Vol. 131, № 36. – P. 13180
170. Abraham R.J., An NMR, IR and theoretical investigation of ^{1}H chemical shifts and hydrogen bonding in phenols // Magn. Reson. Chem. – 2007. – Vol. 45, № 10. – P. 865–877.
171. Boll P.M. Intra- and Intermolecular Hydrogen Bonds in Nitro- and Nitrosophenols. // Acta Chem. Scand. – 1958. – Vol. 12. – Pp. 1777–1781.
172. Asfin R.E. IR Spectra of Hydrogen-Bonded Complexes of Trifluoroacetic Acid with Acetone and Diethyl Ether in the Gas Phase. Interaction between CH and OH Stretching Vibrations // J. Phys. Chem. A. – 2019. – Vol. 123, № 15. – Pp. 3285–3292.
173. Blindheim U. Studies of hydrogen bonding–XX. Hydrogen bonding ability of phosphoryl compounds containing N–P and S–P bonds // Spectrochim. Acta A. – 1969. – Vol. 25, № 6. – Pp. 1105–1113.
174. Dreyer J. Hydrogen-bonded acetic acid dimers: Anharmonic coupling and linear infrared spectra studied with density-functional theory // J. Chem. Phys. – 2005. – Vol. 122, № 18. – P. 184306.

175. Rekik N. Explaining the Structure of the OH Stretching Band in the IR Spectra of Strongly Hydrogen-Bonded Dimers of Phosphinic Acid and Their Deuterated Analogs in the Gas Phase: A Computational Study // J. Phys. Chem. A. – 2012. – Vol. 116, № 18. – Pp. 4495–4509.
176. Van Hoozen B.L. Origin of the Hadži ABC structure: An ab initio study // J. Chem. Phys. – 2015. – Vol. 143, № 18. – P. 184305.
177. Asfin R.E. Particular features of the ν(OH) absorption band of strongly hydrogen-bonded complexes in the gas phase, low-temperature matrices, and crystalline films at 12–600 K // Opt. Spectrosc. – 2005. – Vol. 99, № 1. – Pp. 56–67.
178. Kuopio R. Hexamethylphosphoramide as a Proton Acceptor. Part 2. A Near-infrared Study of Its Heteroassociation with Substituted Phenols. // Acta Chem. Scand. – 1977. – Vol. 31. – Pp. 369–374.
179. Kuopio R. Hexamethylphosphoramide as Proton Acceptor. Part 1. A Near-infrared Study of Its Heteroassociation with Ordinary and Halogenated Alcohols. // Acta Chem. Scand. – 1976. – Vol. 30. – Pp. 1–7.
180. Rozenberg M. An empirical correlation between stretching vibration redshift and hydrogen bond length // Phys. Chem. Chem. Phys. – 2000. – Vol. 2, № 12. – Pp. 2699–2702.

Appendixes

Appendix A. Additional calculated parameters for Me_3PO complexes with proton donors 1–70 in an aprotic polar medium and correlations between some energetic, geometric and spectral parameters of complexes.

Table A1. Additional parameters for Me_3PO complexes with proton donors **1–70** in aprotic medium (chloroform): electron density ρ in atomic unit ($Bohr^{-3}$), laplacian of electron density $\Delta\rho$ ($Bohr^{-5}$). The last two columns contain pK_a values for proton donors in water at 25 °C and references to literature from which these values were taken.

No.	Proton donor	ρ	$\Delta\rho$	pK_a	*Refs.to* pK_a
OH proton donors					
1	Water	0.0360	0.1286	14.00	T. Silverstein and S. Heller, *J. Chem. Educ.*, **2017**, 94, 690–695.
2	Methanol	0.0365	0.1306	15.5	P. Ballinger and F. Long, *J. Am. Chem. Soc.*, **1960**, 82, 795–798.
3	Fluoromethanol	0.0481	0.1522	–	–
4	Difluoromethanol	0.0602	0.1617	–	–
5	Trifluoromethanol	0.0775	0.1672	–	–
6	Chloromethanol	0.0536	0.1595	–	–
7	Dichloromethanol	0.0694	0.1687	–	–
8	Ethanol	0.0353	0.1281	15.84	D. DeTar, *J. Am. Chem. Soc.*, **1982**, 104, 7205–7212.
9	2,2,2–Trifluoroethanol	0.0459	0.1493	12.4	J. Suh, D. Koh and C. Min, *J. Org. Chem.*, **1988**, 53, 1147–1153.
10	Formic acid	0.0629	0.1603	3.76	M. Kim, C. Kim, H. Lee and K. Kim, *J. Chem. Soc. Faraday Trans.*, **1996**, 92, 4951–4956.
11	Acetic acid	0.0579	0.1566	4.75	D. Barrón, S. Butí, M. Ruiz and J. Barbosa, *Phys. Chem. Chem. Phys.*, **1999**, 1, 295–298.
12	Chloroacetic acid	0.0687	0.1633	2.84	B. Chawla and S. Mehta, *J. Phys. Chem.*, **1984**, 88, 2650–2655.
13	Dichloroacetic acid	0.0759	0.1631	1.48	B. Chawla and S. Mehta, *J. Phys. Chem.*, **1984**, 88, 2650–2655.
14	Trichloroacetic acid	0.0830	0.1601	–	–
15	Trifluoroacetic acid	0.0856	0.1579	0.23	Z. Pawelka and M. Haulait-Pirson, *J. Phys. Chem.*, **1981**, 85, 1052–1057.
16	Benzoic acid	0.0602	0.1583	4.20	N. McHedlov-Petrossyan and R. Mayorga, *J. Chem. Soc. Faraday Trans.*, **1992**, 88, 3025–3032.
17	Pentafluorobenzoic acid	0.0734	0.1635	1.48	N. McHedlov-Petrossyan and R. Mayorga, *J. Chem. Soc. Faraday Trans.*, **1992**, 88, 3025–3032.
18	Methanesulfonic acid	0.0852	0.1555	–1.92	J. Guthrie, *Can. J. Chem.*, **1978**, 56, 2342–2354.
19	Benzenesulfonic acid	0.0896	0.1513	–2.7	J. Guthrie, *Can. J. Chem.*, **1978**, 56, 2342–2354.
20	p-Toluenesulfonic acid	0.0911	0.1484	–	–
21	Phenylphosphonic acid	0.0672	0.1616	1.83	H. Jaffé, L. Freedman and G. Doak, *J. Am. Chem. Soc.*, **1953**, 75, 2209–2211.
22	Phenol	0.0459	0.1483	9.99	G. Bouchard, P. Carrupt, B. Testa, V. Gobry and H. Girault, *Chem. Eur. J*, **2002**, 8, 3478–3484.
23	2–Nitrophenol	0.0560	0.1599	7.23	W. Mock and L. Morsch, *Tetrahedron*, **2001**, 57, 2957–2964.
24	3–Nitrophenol	0.0515	0.1588	8.38	J. Llor, *J. Solution Chem.*, **1999**, 28, 1–20.
25	4–Nitrophenol	0.0550	0.1612	7.15	W. Mock and L. Morsch, *Tetrahedron*, **2001**, 57, 2957–2964.
NH proton donors					
26	Ammonia	0.0195	0.0731	–	–
27	Dimethylamine	0.0202	0.0768	–	–
28	Aziridine	0.0229	0.0861	8.04	S. Searles, M. Tamres, F. Block and L. Quarterman, *J. Am. Chem. Soc.*, **1956**, 78, 4917–4920.
29	Azetidine	0.0199	0.0740	11.29	S. Searles, M. Tamres, F. Block and L. Quarterman, *J. Am. Chem. Soc.*, **1956**, 78, 4917–4920.
30	Pyrrolidine	0.0196	0.0719	11.27	S. Searles, M. Tamres, F. Block and L. Quarterman, *J. Am. Chem. Soc.*, **1956**, 78, 4917–4920.
31	Piperidine	0.0196	0.0734	11.22	S. Searles, M. Tamres, F. Block and L. Quarterman, *J. Am. Chem. Soc.*, **1956**, 78, 4917–4920.
32	Piperazine	0.0194	0.0723	9.82	C. Bernasconi, J. Moreira, L. Huang and K. Kittredge, *J. Am. Chem. Soc.*, **1999**, 121, 1674–1680.

33	2–Pyrrolidone	0.0312	0.1095	–	–
34	Pyrrole	0.0326	0.1232	16.50	A. Gervasini and A. Auroux, *J. Phys. Chem.*, **1993**, 97, 2628–2639.
35	Imidazole	0.0366	0.1349	7.18	B. Barszcz, M. Gabryszewski, J. Kulig and B. Lenarcik, *J. Chem. Soc. Dalt. Trans.*, **1986**, 2025–2028.
36	Pyrazole	0.0377	0.1315	2.66	B. Barszcz, M. Gabryszewski, J. Kulig and B. Lenarcik, *J. Chem. Soc. Dalt. Trans.*, **1986**, 2025–2028.
37	1,4–Dihydropyrazine	0.0277	0.1080	–	–
NH^+ proton donors					
38	Ammonium	0.0727	0.1577	9.20	Y. Yan, E. Zeitler, J. Gu, Y. Hu and A. Bocarsly, *J. Am. Chem. Soc.*, **2013**, 135, 14020–14023.
39	Dimethylammonium	0.0595	0.1649	–	–
40	Trimethylammonium	0.0575	0.1659	–	–
41	Imidazolium	0.0629	0.1621	7.09	S. Datta and A. Grzybowski, *J. Chem. Soc. B Phys. Org.*, **1966**, 136–140.
42	Pyridinium	0.0650	0.1668	5.31	A. Isao, U. Kikujiro and K. Hirondo, *Bull. Chem. Soc. Jpn.*, **1982**, 55, 713–716.
43	2–Picolinium	0.0589	0.1651	–	–
44	3–Picolinium	0.0630	0.1669	–	–
45	4–Picolinium	0.0621	0.1653	–	–
46	3,5–Lutidinium	0.0621	0.1659	–	–
47	2,6–Lutidinium	0.0540	0.1603	–	–
48	2,4,6–Collidinium	0.0528	0.1604	–	–
49	2–(Dimethylamino)pyridinium	0.0465	0.1510	–	–
50	3–(Dimethylamino)pyridinium	0.0594	0.1642	–	–
51	4–(Dimethylamino)pyridinium	0.0532	0.1580	9.73	C. Heo and J. Bunting, *J. Org. Chem.*, **1992**, 57, 3570–3578.
52	3,5–(Dimethylamino)pyridinium	0.0560	0.1620	–	–
53	3,4,5–(Trimethoxy)pyridinium	0.0576	0.1677	–	–
54	3,4,5–Trifluoropyridinium	0.0839	0.1653	–	–
55	3,4,5–Trichloropyridinium	0.0805	0.1675	–	–
56	3,5–Aminopyridinium	0.0598	0.1641	–	–
CH proton donors					
57	Trifluoroethylene	0.0202	0.0803	–	–
58	Trichloroethylene	0.0208	0.0814	–	–
59	Acetylene	0.0214	0.0862	–	–
60	Fluoroacetylene	0.0217	0.0896	–	–
61	Hydrogen cyanide	0.0344	0.1301	9.22	K. Ang, *J. Chem. Soc.*, **1959**, 3822–3825.
62	Trinitromethane	0.0440	0.1469	–	–
63	1,1–Dinitroethane	0.0271	0.1034	5.20	J. Belew and L. Hepler, *J. Am. Chem. Soc.*, **1956**, 78, 4005–4007.
64	2–Nitropropane	0.0145	0.0473	7.57	H. Gilbert, *J. Am. Chem. Soc.*, **1980**, 102, 7059–7065.
65	Trichloromethane	0.0269	0.1046	15.50	K. Klabunde and D. Burton, *J. Am. Chem. Soc.*, **1972**, 94, 5985–5990.
66	Dichloromethane	0.0210	0.0797	–	–
67	Chloromethane	0.0145	0.0517	–	–
68	Methane	0.0047	0.0154	–	–
69	Trifluoromethane	0.0233	0.0942	–	–
70	Tribromomethane	0.0262	0.1015	13.70	K. Klabunde and D. Burton, *J. Am. Chem. Soc.*, **1972**, 94, 5985–5990.

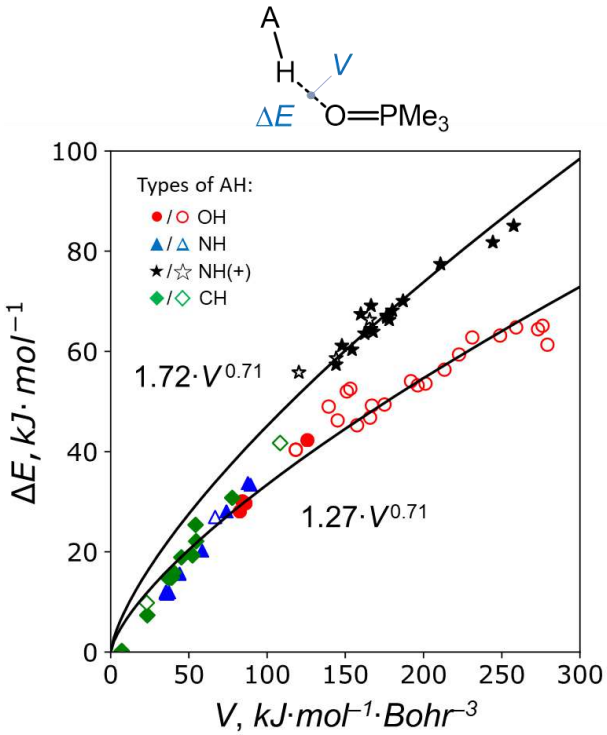

Figure A1. Correlation between ΔE and local electron potential energy density V. Solid lines correspond the result of least squares fitting of data points by the functions $\Delta E = k \cdot V^{0.71}$. The coefficient k is differ for complexes with cationic and neutral AH molecules. The power equal to 0.71 was fixed due to strong correlation $G(V)$ shown in Figure 2.11 and linear correlation $\Delta E(G)$ shown in Figure 2.10.

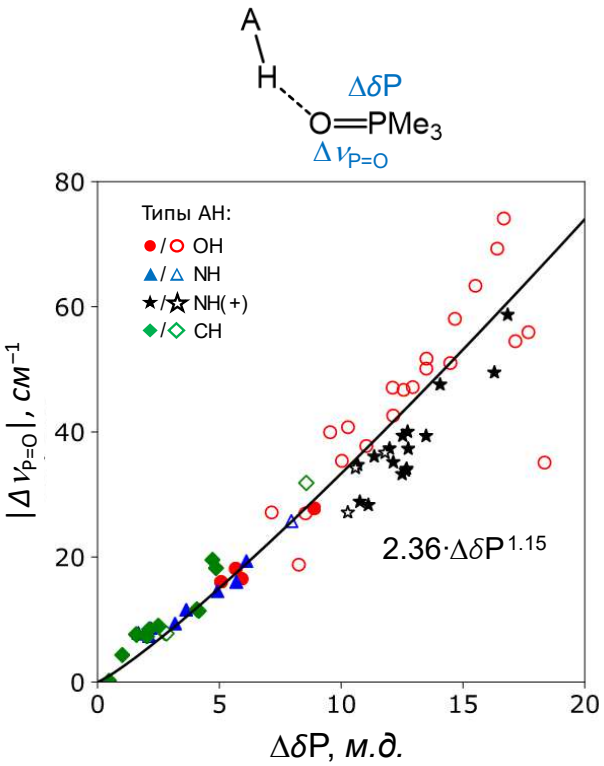

Figure A2. Correlation between $|\Delta\nu_{P=O}|$ and $\Delta\delta P$. Solid line corresponds the correlation function obtained as the result of least squares fitting of correlations $G(|\Delta\nu_{P=O}|)$ shown in Figure 2.12b and $G(\Delta\delta P)$ shown in Figure 2.14b.

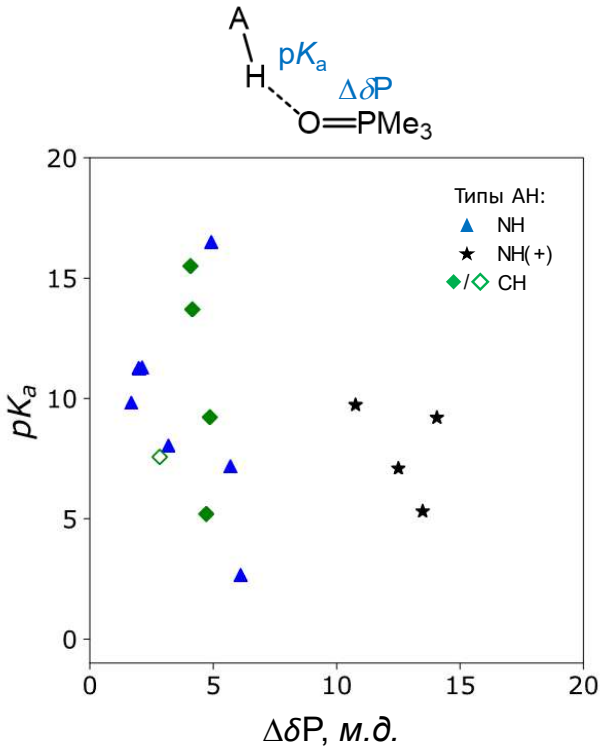

Figure A3. $\Delta\delta P$ and pK_a for NH, NH^+ and CH proton donors. The values of pK_a are taken from literature (see Appendix A, Table A1).

Table A2. Some energetic and geometric parameters of complexes formed by Me_3PO with two proton donors **1**–**70** in chloroform (PCM, ε = 4.7): local electron kinetic, G^a, and potential, V^a, energy densities in kJ·mol^{-1}·Bohr^{-3} (calculated at BCP); interatomic distance r_1^a in Å; hydrogen bond coordinates $q_1^a = 0.5 \cdot (r_1^a - r_2^a)$ and $q_2^a = r_1^a + r_2^a$ in Å, hydrogen bond angles α (P=O···H), β (O···H–A) (in degrees); dihedral angles γ (in degrees, defined as shown in Figure 2.20).

No.	Proton donor	G^a	V^a	r_1^a	q_1^a	q_2^a	α	β	γ
OH proton donors									
1	Water	79.7	78.4	0.980	–0.405	2.770	128.1	179.7	175.3
2	Methanol	79.7	78.4	0.978	–0.408	2.771	128.7	179.1	179.3
3	Fluoromethanol	101.9	109.7	0.988	–0.353	2.682	128.6	177.2	178.5
4	Difluoromethanol	114.6	130.8	1.002	–0.318	2.640	128.1	175.5	176.1
5	Trifluoromethanol	132.8	161.4	1.011	–0.283	2.587	128.0	176.8	175.4
6	Chloromethanol	108.3	119.8	0.992	–0.339	2.661	127.3	177.2	171.1
7	Dichloromethanol	119.4	138.7	1.004	–0.308	2.624	129.7	171.8	177.0
8	Ethanol	75.7	73.7	0.978	–0.417	2.790	126.5	176.5	179.6
9	2,2,2-Trifluoroethanol	96.4	101.6	0.984	–0.367	2.702	129.0	175.9	161.7
10	Formic acid	116.7	135.0	1.007	–0.311	2.636	126.3	173.8	150.5
11	Acetic acid	110.9	126.1	1.002	–0.324	2.654	124.5	173.8	144.1
12	Chloroacetic acid	122.9	145.7	1.010	–0.299	2.617	125.1	174.6	150.3
13	Dichloroacetic acid	131.4	160.1	1.015	–0.283	2.594	126.0	174.4	149.2
14	Trichloroacetic acid	137.1	170.3	1.018	–0.271	2.579	126.1	174.7	152.4
15	Trifluoroacetic acid	139.6	174.6	1.020	–0.266	2.573	126.9	174.7	159.2
16	Benzoic acid	113.7	130.6	1.003	–0.319	2.644	124.4	173.6	143.7
17	Pentafluorobenzoic acid	127.7	154.0	1.013	–0.289	2.604	125.5	174.8	152.8
18	Methanesulfonic acid	144.8	184.1	1.023	–0.258	2.561	126.8	174.1	162.6
19	Benzenesulfonic acid	140.3	176.4	1.021	–0.265	2.572	125.9	174.3	162.5
20	*p*-Toluenesulfonic acid	139.0	173.8	1.020	–0.268	2.575	125.5	174.8	163.8
21	Phenylphosphonic acid	123.5	146.6	1.006	–0.301	2.614	125.2	178.5	144.9
22	Phenol	92.7	97.6	0.986	–0.372	2.717	123.7	172.9	179.4
23	2-Nitrophenol	110.0	123.4	0.994	–0.334	2.655	125.5	174.2	176.3
24	3-Nitrophenol	100.4	109.1	0.990	–0.354	2.687	125.3	175.9	150.9
25	4-Nitrophenol	106.3	117.9	0.993	–0.341	2.667	125.8	175.6	179.7
NH proton donors									
26	Ammonia	40.8	35.1	1.022	–0.520	3.084	126.9	176.1	152.1
27	Dimethylamine	40.9	35.5	1.020	–0.523	3.086	126.9	177.6	173.8
28	Aziridine	46.8	41.5	1.023	–0.495	3.035	124.0	177.4	175.0
29	Azetidine	40.4	35.1	1.020	–0.526	3.091	125.3	178.9	173.0
30	Pyrrolidine	35.3	30.5	1.021	–0.552	3.146	122.7	171.9	156.9
31	Piperidine	40.3	34.8	1.019	–0.525	3.089	129.4	178.7	179.3
32	Piperazine	36.7	31.8	1.021	–0.544	3.130	123.8	170.7	158.0
33	2-Pyrrolidone	66.4	63.3	1.026	–0.420	2.893	123.6	179.5	149.2
34	Pyrrole	68.3	64.7	1.023	–0.415	2.877	129.7	178.5	178.1
35	Imidazole	75.7	74.1	1.027	–0.392	2.838	130.9	179.3	178.7
36	Pyrazole	81.2	81.4	1.029	–0.378	2.814	129.7	179.1	170.8
37	1,4-Dihydropyrazine	58.3	53.1	1.020	–0.451	2.942	128.8	176.3	176.9
NH^+ proton donors									
38	Ammonium	113.7	134.0	1.066	–0.286	2.704	127.5	177.0	179.3
39	Dimethylammonium	91.4	98.6	1.051	–0.341	2.786	126.5	178.9	177.1
40	Trimethylammonium	76.1	78.1	1.047	–0.379	2.853	123.8	177.9	179.3
41	Imidazolium	107.3	122.0	1.049	–0.308	2.715	127.0	176.8	174.5
42	Pyridinium	112.7	130.7	1.053	–0.299	2.704	125.4	176.0	173.5
43	2-Picolinium	112.1	129.1	1.051	–0.303	2.708	124.8	174.3	179.0
44	3-Picolinium	110.6	127.3	1.052	–0.303	2.711	125.1	177.9	174.4
45	4-Picolinium	105.3	118.8	1.049	–0.314	2.727	126.7	176.5	174.8

46	3,5-Lutidinium	109.7	125.7	1.051	–0.306	2.714	124.1	176.6	176.8
47	2,6-Lutidinium	85.3	90.3	1.044	–0.358	2.804	122.6	177.7	178.9
48	2,4,6-Collidinium	84.7	89.1	1.043	–0.360	2.806	124.9	176.4	179.2
49	2-(Dimethylamino)pyridinium	69.2	68.0	1.035	–0.406	2.882	126.0	158.8	178.4
50	3-(Dimethylamino)pyridinium	105.6	118.8	1.048	–0.315	2.727	126.3	178.8	178.8
51	4-(Dimethylamino)pyridinium	97.9	106.2	1.041	–0.335	2.751	128.1	176.2	173.6
52	3,5-(Dimethylamino)pyridinium	101.2	111.6	1.045	–0.326	2.741	128.8	177.5	176.4
53	3,4,5-(Trimethoxy)pyridinium	100.9	111.7	1.045	–0.325	2.740	126.4	178.5	175.5
54	3,4,5-Trifluoropyridinium	130.2	162.1	1.068	–0.259	2.655	122.7	177.9	169.5
55	3,4,5-Trichloropyridinium	123.9	150.8	1.063	–0.272	2.671	124.6	178.4	176.2
56	3,5-Diaminopyridinium	107.9	122.6	1.049	–0.311	2.720	123.6	179.3	166.6
CH proton donors									
57	Trifluoroethylene	40.0	33.4	1.085	–0.493	3.156	134.2	174.3	177.5
58	Trichloroethylene	42.0	35.3	1.087	–0.482	3.139	135.5	175.0	172.9
59	Acetylene	43.1	35.5	1.077	–0.476	3.106	133.0	179.6	179.2
60	Fluoroacetylene	44.9	37.3	1.076	–0.468	3.087	133.1	179.7	178.9
61	Hydrogen cyanide	68.4	64.1	1.092	–0.377	2.938	131.2	179.9	178.7
62	Trinitromethane	75.5	73.9	1.108	–0.357	2.930	132.1	176.2	166.9
63	1,1-Dinitroethane	48.1	42.4	1.097	–0.456	3.106	127.7	168.3	168.7
64	2-Nitropropane	24.3	20.9	1.090	–0.602	3.384	120.8	168.6	141.9
65	Trichloromethane	52.4	46.9	1.090	–0.443	3.066	129.0	175.3	177.4
66	Dichloromethane	41.8	35.9	1.088	–0.488	3.153	130.5	175.8	179.7
67	Chloromethane	26.0	22.2	1.088	–0.586	3.348	125.1	172.0	133.0
68	Methane	6.2	4.9	1.091	–0.935	4.053	128.4	175.5	178.2
69	Trifluoromethane	47.0	40.8	1.092	–0.464	3.112	133.8	176.0	178.0
70	Tribromomethane	49.1	43.4	1.090	–0.454	3.087	129.9	177.8	179.9

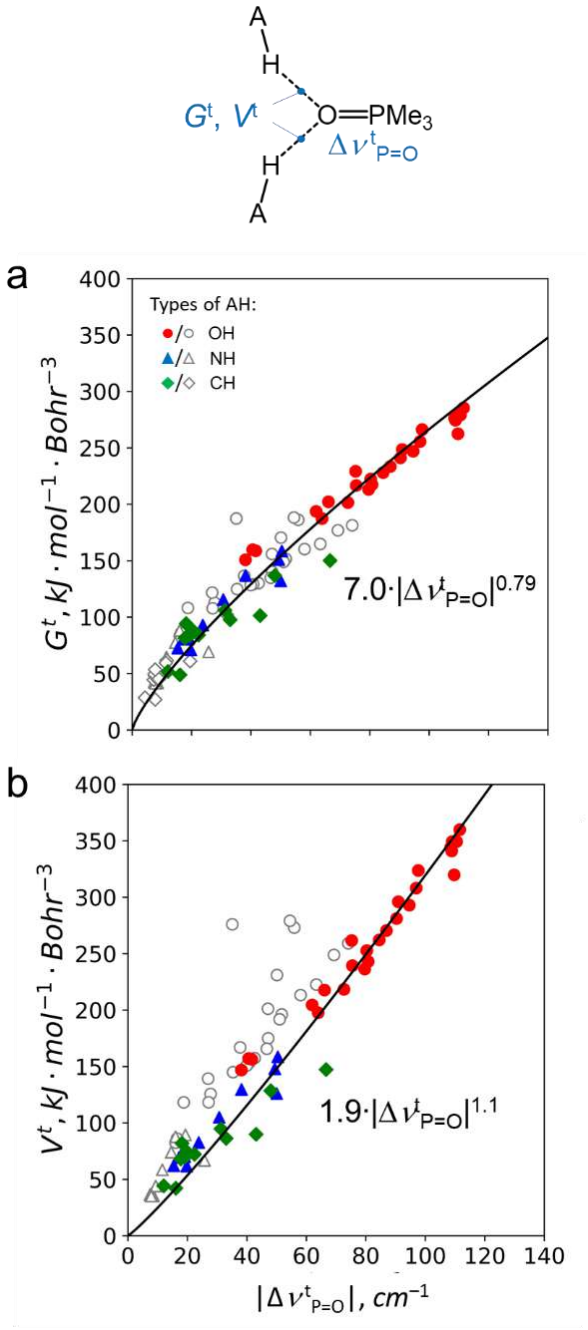

Figure A4. Correlations between $|\Delta\nu^t_{P=O}|$ and total local electron (a) kinetic energy density $G^t = G + G^a$ and (b) potential energy density $V^t = V + V^a$. As the correlation $\Delta E^a(G^a)$ is linear (Figure 2.21a) and the correlation $\Delta E^t(\Delta\nu^t_{P=O})$ is a power function (Figure 2.23a), the $G^t(|\Delta\nu^t_{P=O}|)$ and $V^t(|\Delta\nu^t_{P=O}|)$ should also be described by a power functions. Solid curves correspond to correlation power functions fitted for both 1:1 complexes (open gray symbols) and 1:2 complexes (filled red, blue and green symbols) by keeping the power value fixed at 0.79 for $G^t(|\Delta\nu^t_{P=O}|)$ and at 1.1 for $V^t(|\Delta\nu^t_{P=O}|)$.

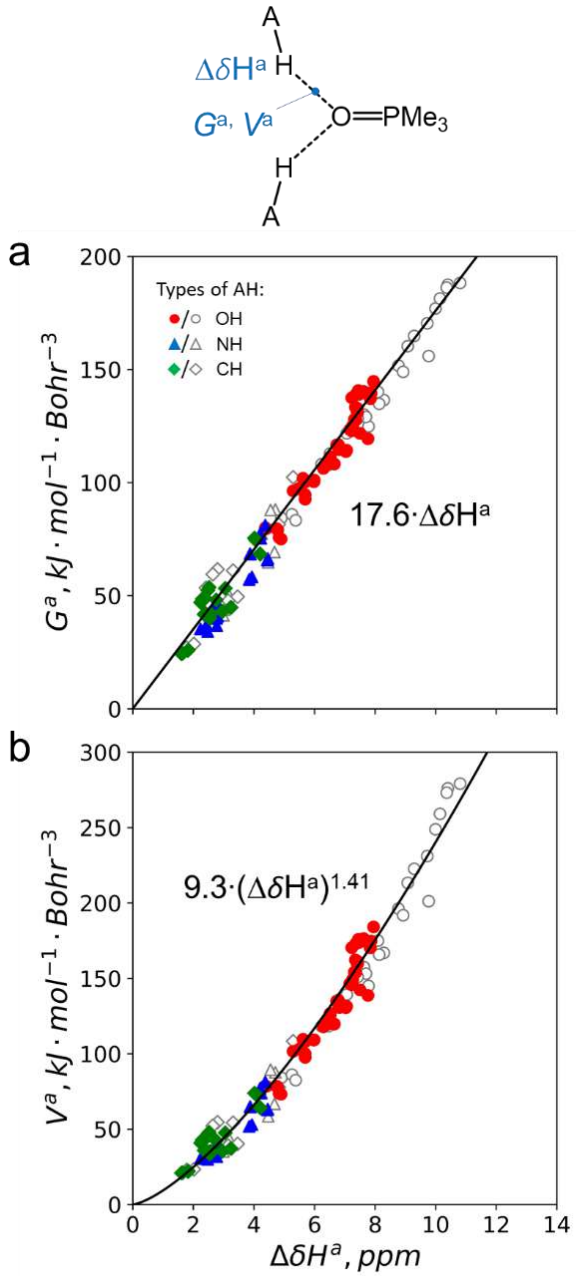

Figure A5. Correlations between $\Delta\delta H^a$ and (a) local electron kinetic energy density G^a and (b) local electron potential energy density V^a. As the correlations $\Delta E^a(G^a)$ and $\Delta E^a(\Delta\delta H^a)$ are linear (Figure 2.21a, Figure 2.23b), and the correlation $G^a(V^a)$ described by the power function (Figure 2.21b), the $G^a(\Delta\delta H^a)$ should be linear and $V^a(\Delta\delta H^a)$ should be described by a power function. Solid curves correspond to correlation functions fitted for both 1:1 (open gray symbols) and 1:2 complexes (filled red, blue and green symbols), the power value fixed at 1.41 for $V^a(\Delta\delta H^a)$.

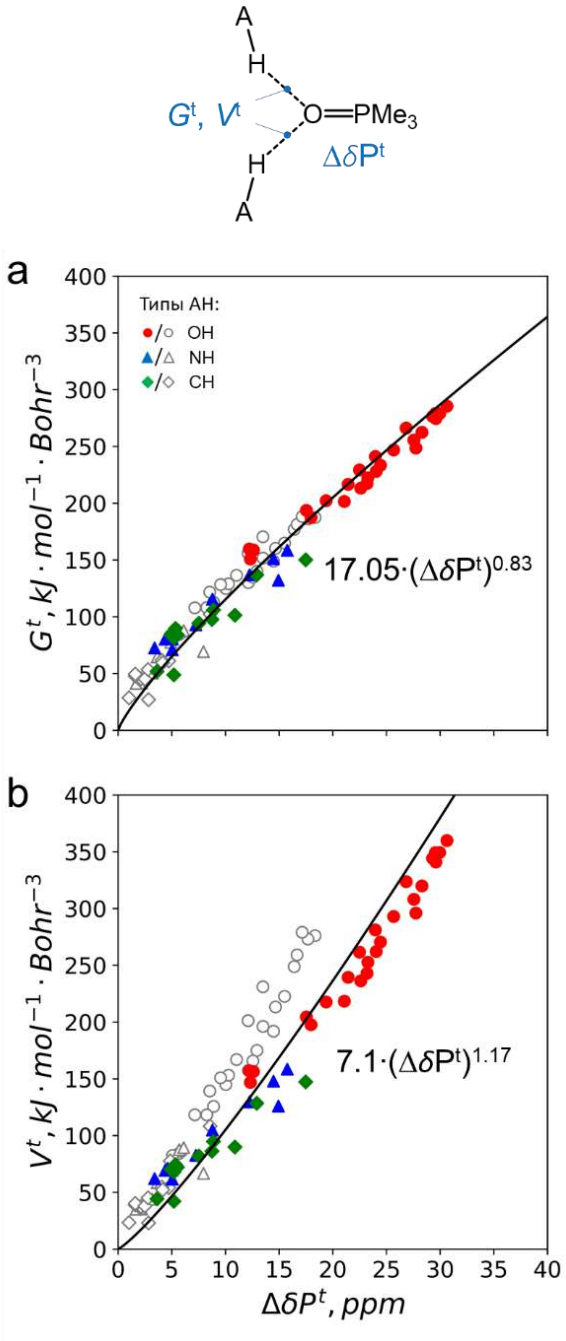

Figure A6. Correlations between $\Delta\delta P^t$ and (a) total local electron kinetic energy density G^t and $\Delta\delta P^t$, (b) total local electron potential energy density V^t and. Solid curves correspond to correlation functions fitted for both 1:1 complexes (open gray symbols) and 1:2 complexes (filled red, blue and green symbols), the power value fixed at 0.83 for $G^t(\Delta\delta P^t)$ and 1.17 for $V^t(\Delta\delta P^t)$ due to the correlations $\Delta E^a(G^a)$ is linear (Figure 2.21a), the correlations $G^a(V^a)$ and $\Delta E^t(\Delta\delta P^t)$ are power functions (Figure 2.21b and Figure 2.23c).

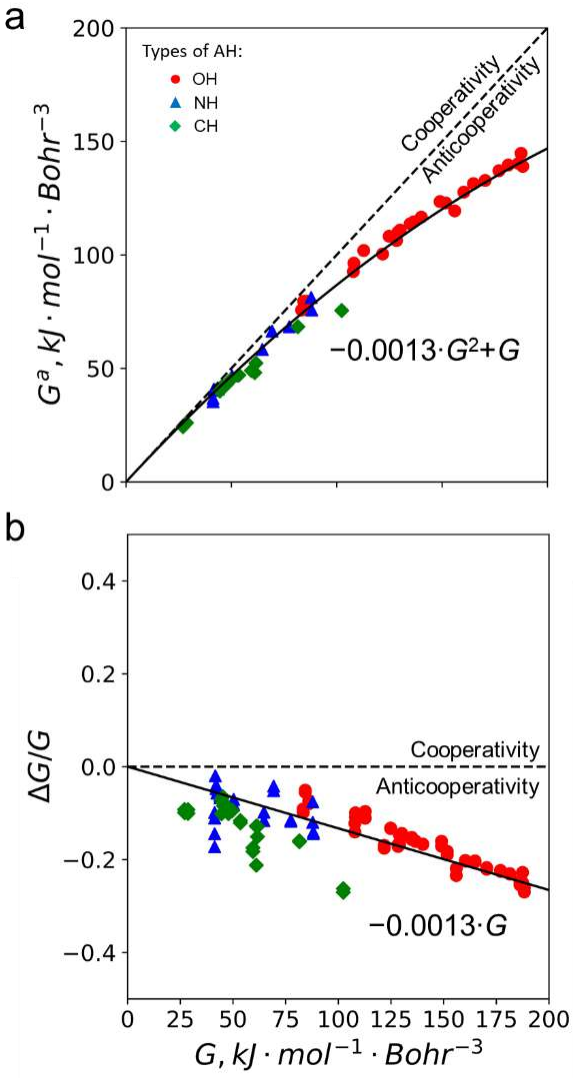

Figure A7. (a) Correlation between G^a and G. (b) Correlation between G and relative hydrogen bond cooperativity on local electron kinetic energy density $\Delta G/G$ ($\Delta G = G^a - G$). Solid curves correspond to correlational equations shown next to the curves. The correlation $\Delta G/G(G)$ seems close to linear with coefficient –0.0013 $kJ^{-1}\cdot mol\cdot Bohr^3$ obtained by least squares fitting. The correlation function for $G^a(G)$ derived from fitting function for correlation between $\Delta G/G$ and G. Dashed lines indicate the boundary between regions of cooperativity and anticooperativity effects.

Table A3. Explicit fitting equations of some correlation functions mentioned in text: $\Delta\Delta\nu_{P=O}(\Delta E)$, $\Delta\Delta\delta H(\Delta E)$, $\Delta\Delta\delta P(\Delta E)$, $r_2^a(r_2)$, $\Delta r_2/r_2(r_2)$, $\Delta\Delta\nu_{P=O}(r_2)$, $\Delta\Delta\delta H(r_2)$, $\Delta\Delta\delta P(r_2)$.

Correlations function	**Figure**	**Explicit fitting function**
$\Delta\Delta\nu_{P=O}(\Delta E)$	Figure 2.25a	$\lvert\Delta\Delta\nu_{P=O}\rvert = 0.284\cdot(2\cdot\Delta E - 0.0039\cdot\Delta E^2)^{1.266} - 0.284\cdot\Delta E^{1.266}$
$\Delta\Delta\delta H(\Delta E)$	Figure 2.25b	$\Delta\Delta\delta H = -0.00065\cdot\Delta E^2$
$\Delta\Delta\delta P(\Delta E)$	Figure 2.25c	$\Delta\Delta\delta P = 0.152\cdot(2\cdot\Delta E - 0.0039\cdot\Delta E^2)^{1.205} - 0.152\cdot\Delta E^{1.205}$
$r_2^a(r_2)$	Figure 2.29a	$r_2^a = 0.96 - 0.426\cdot\ln\left(-0.769\cdot\exp\left(-2\cdot\frac{r_2-0.96}{0.426}\right)+\exp\left(-\frac{r_2-0.96}{0.426}\right)\right)$
$\Delta r_2/r_2(r_2)$	Figure 2.29b	$\Delta r_2/r_2 = r_2^{-1}\cdot\left(0.96 - 0.426\cdot\ln\left(-0.769\cdot\exp\left(-2\cdot\frac{r_2-0.96}{0.426}\right)+\exp\left(-\frac{r_2-0.96}{0.426}\right)\right) - r_2\right)$
$\Delta\Delta\nu_{P=O}(r_2)$	Figure A9a	$\lvert\Delta\Delta\nu_{P=O}(r_2)\rvert = 761\cdot\exp\left(-\frac{r_2^a(r_2)-0.96}{0.307}\right) - 284\cdot\exp\left(-\frac{r_2-0.96}{0.307}\right)$
$\Delta\Delta\delta H(r_2)$	Figure A9b	$\Delta\Delta\delta H(r_2) = 32.85\cdot\exp\left(-\frac{r_2^a(r_2)-0.96}{0.426}\right) - 32.85\cdot\exp\left(-\frac{r_2-0.96}{0.426}\right)$
$\Delta\Delta\delta P(r_2)$	Figure A9c	$\Delta\Delta\delta P(r_2) = 188.3\cdot\exp\left(-\frac{r_2^a(r_2)-0.96}{0.322}\right) - 73.8\cdot\exp\left(-\frac{r_2-0.96}{0.322}\right)$

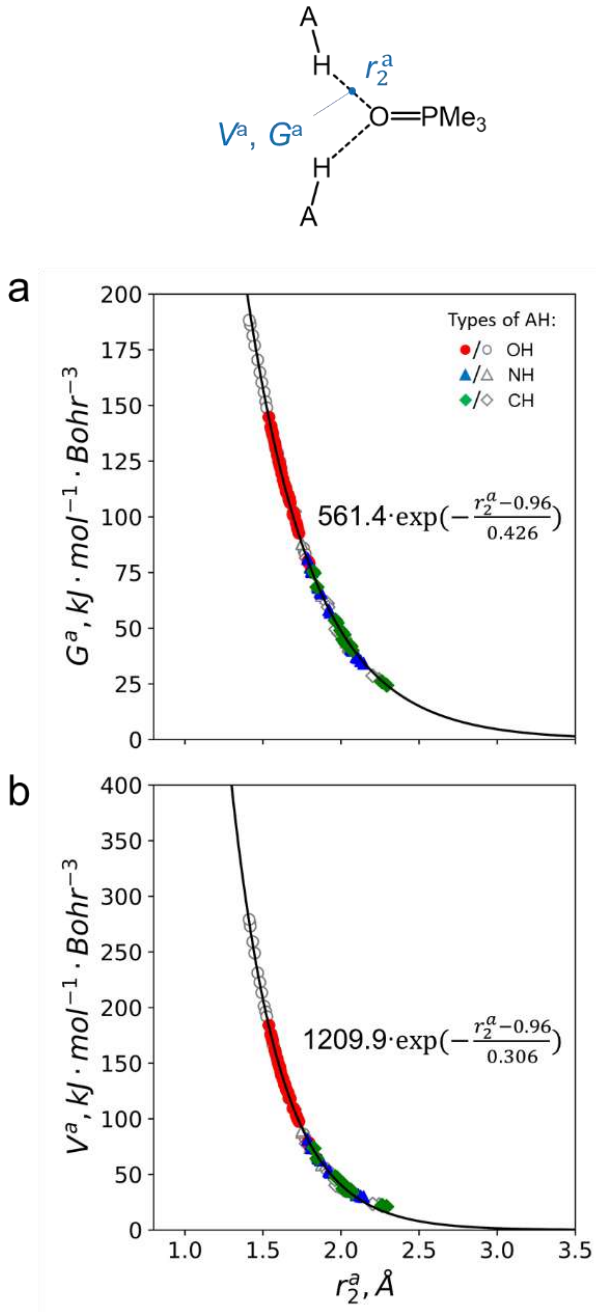

Figure A8. Correlations between hydrogen bond length r_2^a and (a) G^a, (b) V^a for the set of studied Me_3PO complexes with proton donors. Open gray symbols correspond to 1:1 complexes; filled red, blue and green symbols correspond to 1:2 complexes with $Me_3PO\cdots HO$, $Me_3PO\cdots HN$ ($Me_3PO\cdots HN^+$) and $Me_3PO\cdots HC$ types of hydrogen bonds. The solid lines correspond correlation functions $g\cdot\exp(-(r_2^a - r_2^0)/h)$, where coefficients g and h were obtained for $G^a(r_2^a)$ and $V^a(r_2^a)$ by the least squares fitting.

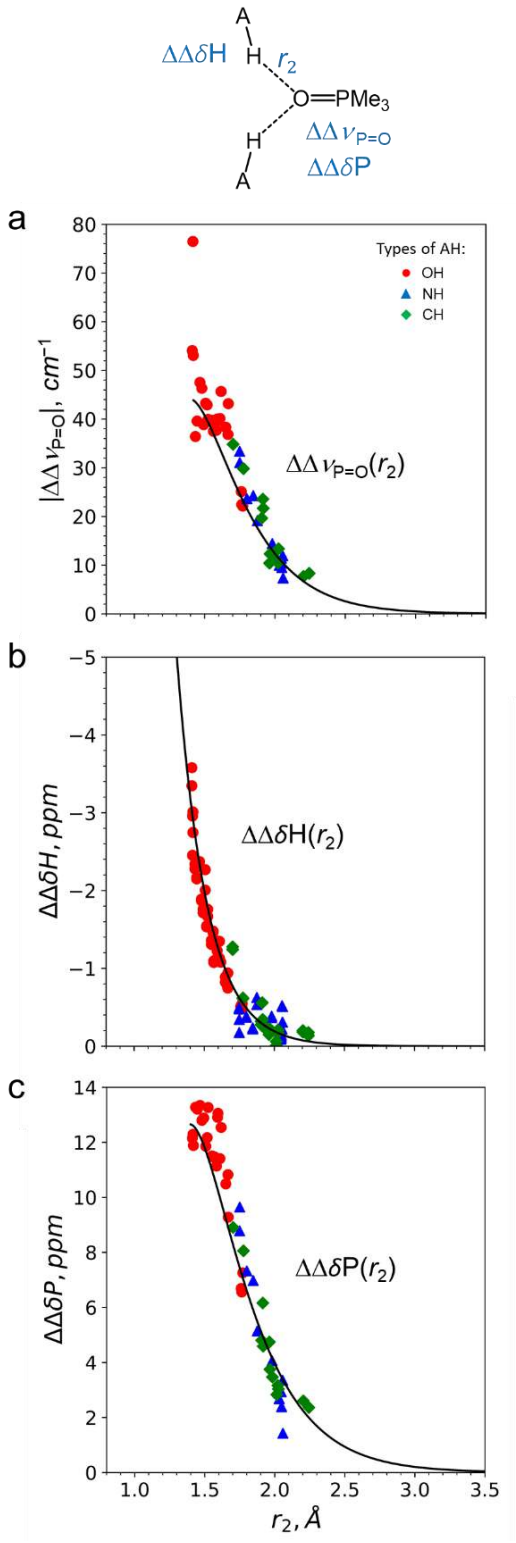

Figure A9. Correlations between r_2 and different parameters described cooperativity on spectral parameters: (a) $\Delta\Delta\nu_{P=O} = \Delta\nu^{t}_{P=O} - \Delta\nu_{P=O}$, (b) $\Delta\Delta\delta H = \Delta\delta H^{a} - \Delta\delta H$ and (c) $\Delta\Delta\delta P = \Delta\delta P^{t} - \Delta\delta P$. Solid curves correspond to correlation functions $|\Delta\Delta\nu_{P=O}|(r_2)$, $\Delta\Delta\delta H(r_2)$ and $\Delta\Delta\delta P(r_2)$ explicitly given in Appendix A, Table A3 (derived from correlations given in Figures 2.28–2.29).

Appendix B. ^{1}H and ^{31}P NMR spectra of free Ph_3PO in CDF_3/CDF_2Cl mixture

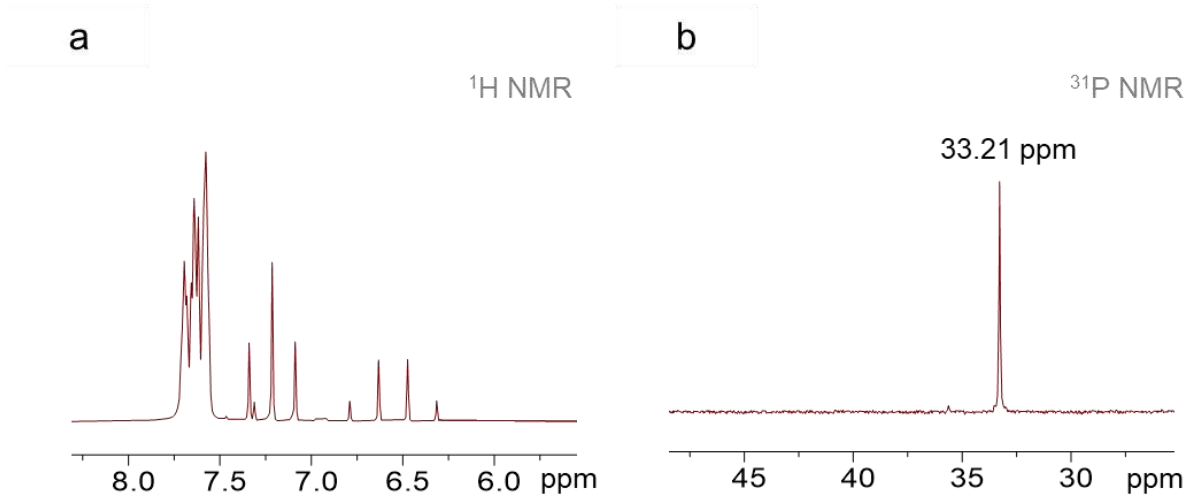

Figure B1. The part of (a) ^{1}H NMR and (b) ^{31}P NMR spectra of free Ph_3PO in solution in mixture of liquefied deuterated freons CDF_3/CDF_2Cl at 100 K.

Appendix C. IR spectra of individual compounds, their complexes in CCl_4 solution

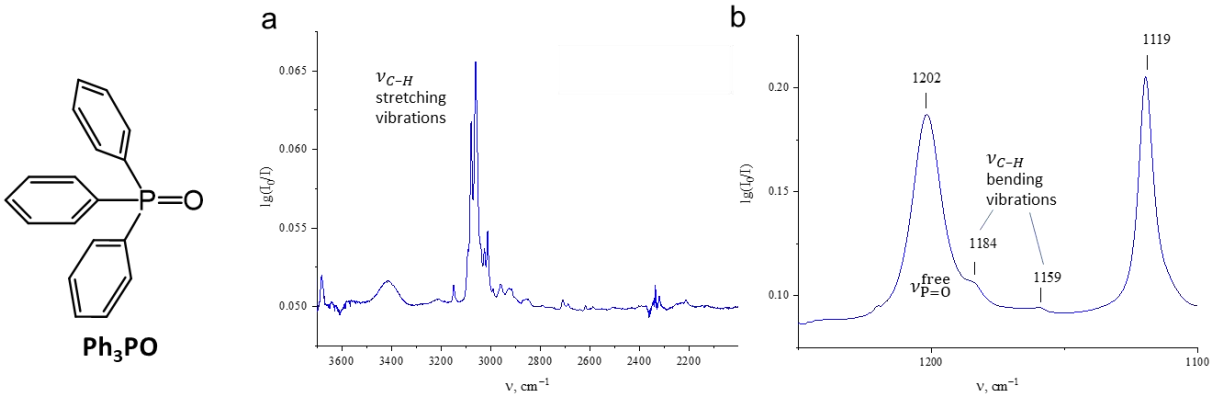

Figure C1. Parts of IR spectrum of ~3.9 mmol·L^{-1} solution of triphenylphosphine oxide (Ph_3PO) in CCl_4 at room temperature. Spectral regions containing (a) O–H stretching band (2000–3700 cm^{-1}) and (b) P=O stretching band (1100–1250 cm^{-1}) of individual compounds and their complexes are shown. The P=O band for free Ph_3PO, $\nu_{P=O}^{free}$, is located at 1202 cm^{-1}.

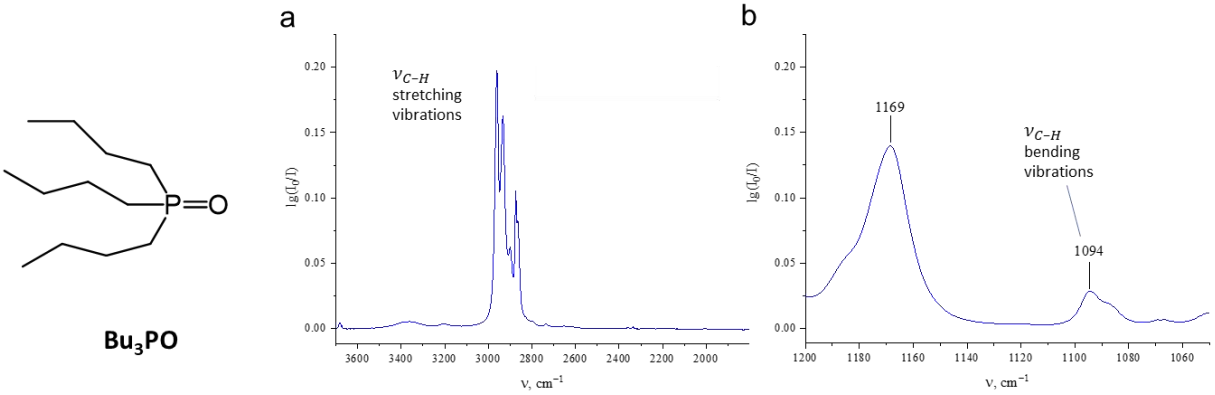

Figure C2. Parts of IR spectrum of ~4.7 mmol·L^{-1} solution of tributylphosphine oxide (Bu_3PO) in CCl_4 at room temperature. Spectral regions containing (a) O–H stretching band (2000–3700 cm^{-1}) and (b) P=O stretching band (1100–1250 cm^{-1}) of individual compounds and their complexes are shown. The P=O band for free Bu_3PO, $\nu_{P=O}^{free}$, is located at 1169 cm^{-1}.

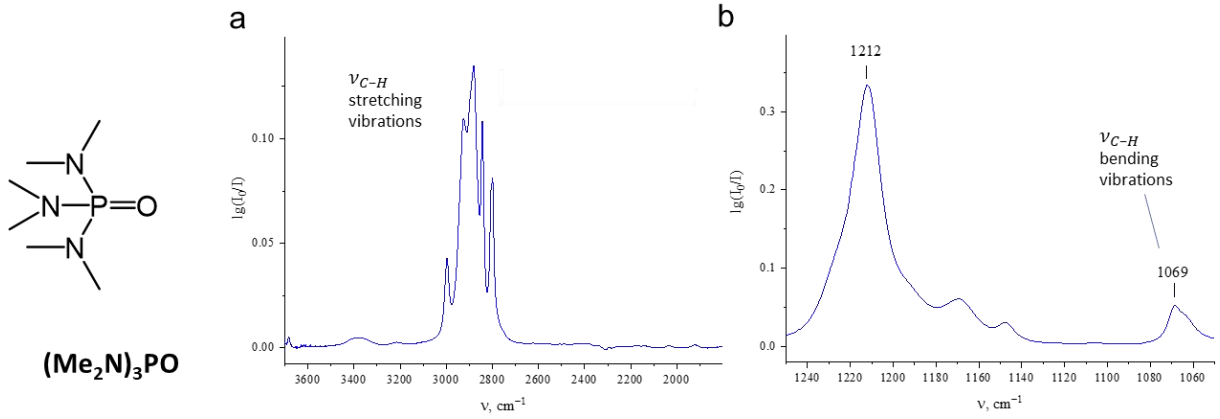

Figure C3. Parts of IR spectrum of ~5.8 mmol·L^{-1} solution of hexamethylphosphoramide ((Me$_2$N)$_3$PO) in CCl_4 at room temperature. Spectral regions containing (a) O–H stretching band (2000–3700 cm^{-1}) and (b) P=O stretching band (1100–1250 cm^{-1}) are shown. The P=O band for free (Me$_2$N)$_3$PO, $\nu_{P=O}^{free}$, is located at 1212 cm^{-1}.

Table C1. The wavenumbers of absorption bands corresponding to stretching vibration of OH group, ν_{OH}^{free}, and P=O group, $\nu_{P=O}^{free}$, of Ph_3PO, Bu_3PO, (Me$_2$N)$_3$PO and proton donors in solutions in CCl_4 at room temperature.

Compound	**The type of vibration**	**The frequency of vibration, in cm^{-1}**
1	ν_{OH}^{free}, stretching	3557
3		3611
5		3613
6		3609
8		3606
15		3594
17		3529
18		3516
19		3519
20		3619
Ph_3PO	$\nu_{P=O}^{free}$, stretching	1202
Bu_3PO		1212
(Me$_2$N)$_3$PO		1169

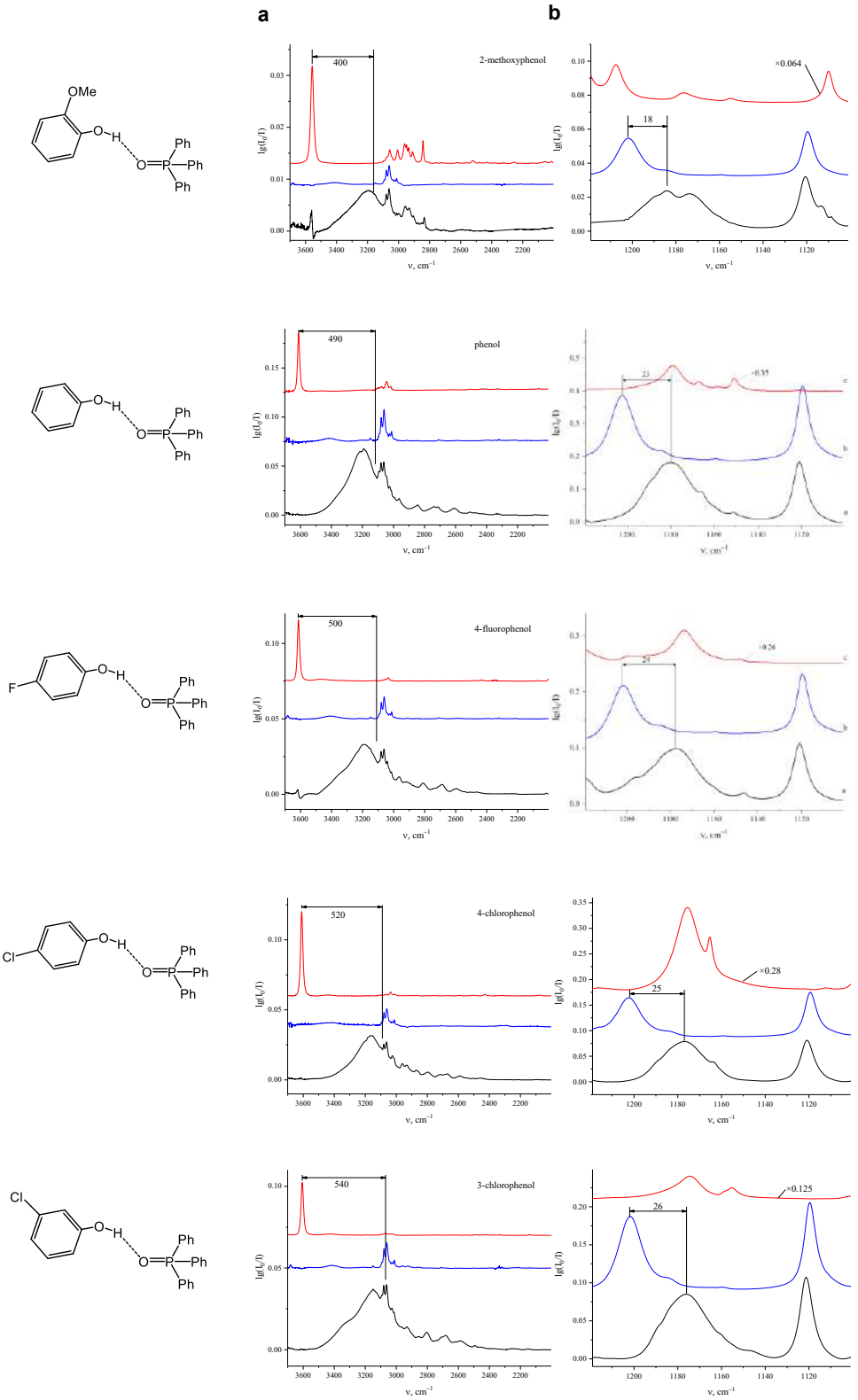

Figure C4. Continued on next page.

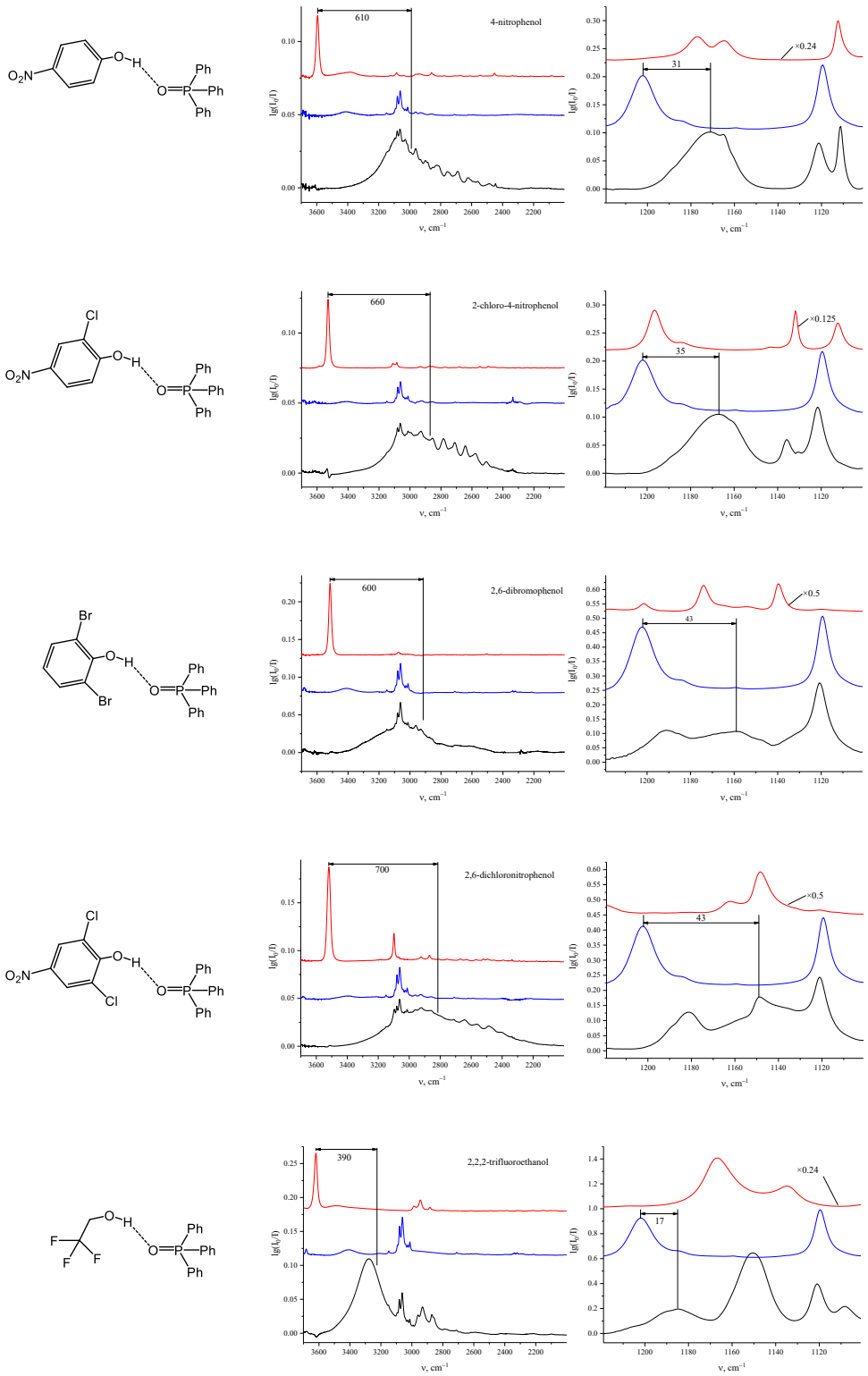

Figure C4. IR spectra of complexes formed by Ph_3PO and proton donors in CCl_4 solution at room temperature in the regions of (a) OH stretching vibrations (b) P=O stretching vibrations. The spectra of free proton donors (red), free Ph_3PO (blue) and their complexes (black) are shown. Vertical bars indicate locations of OH and P=O vibrational bands for individual compounds and their complexes.

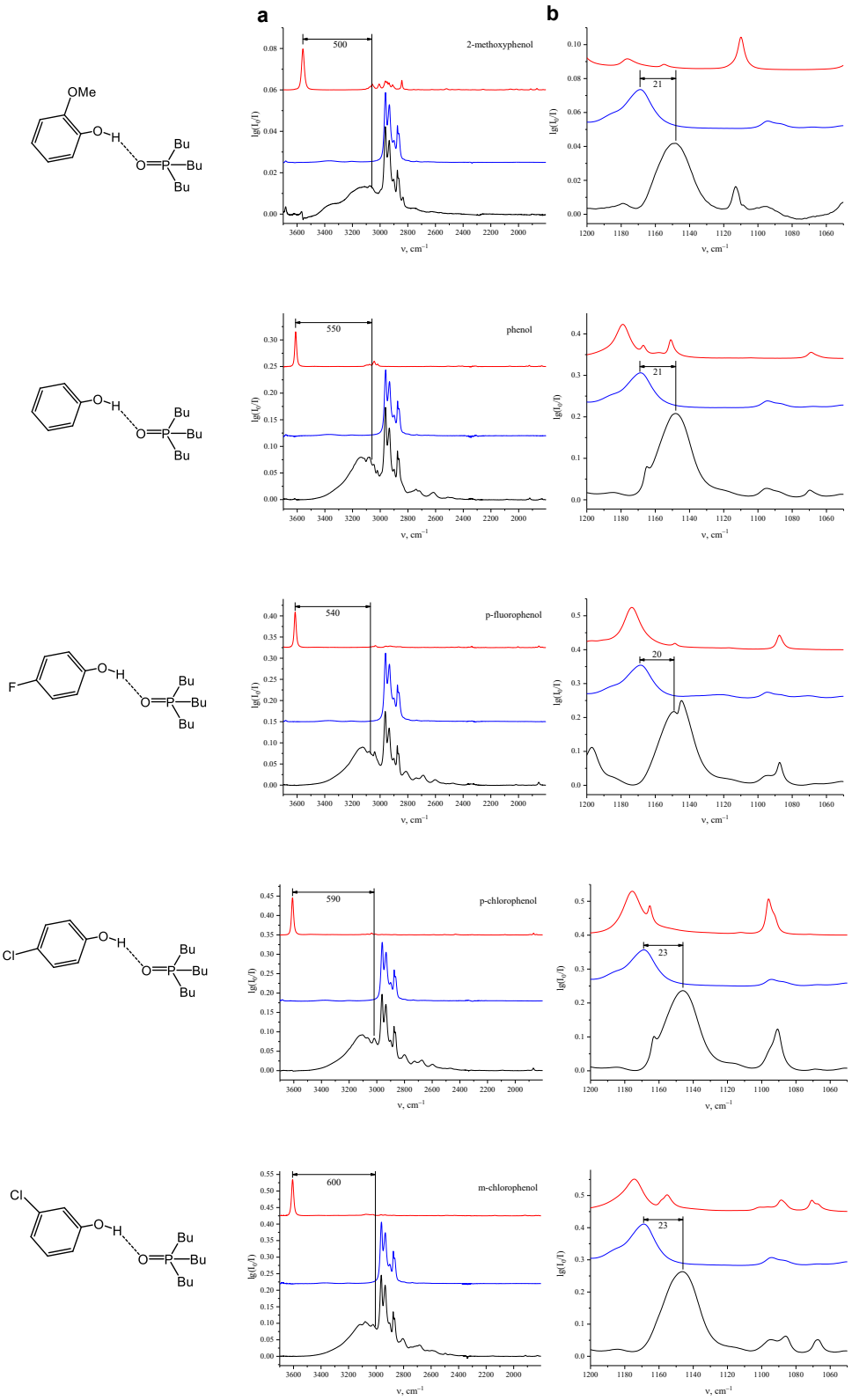

Figure C5. Continued on next page.

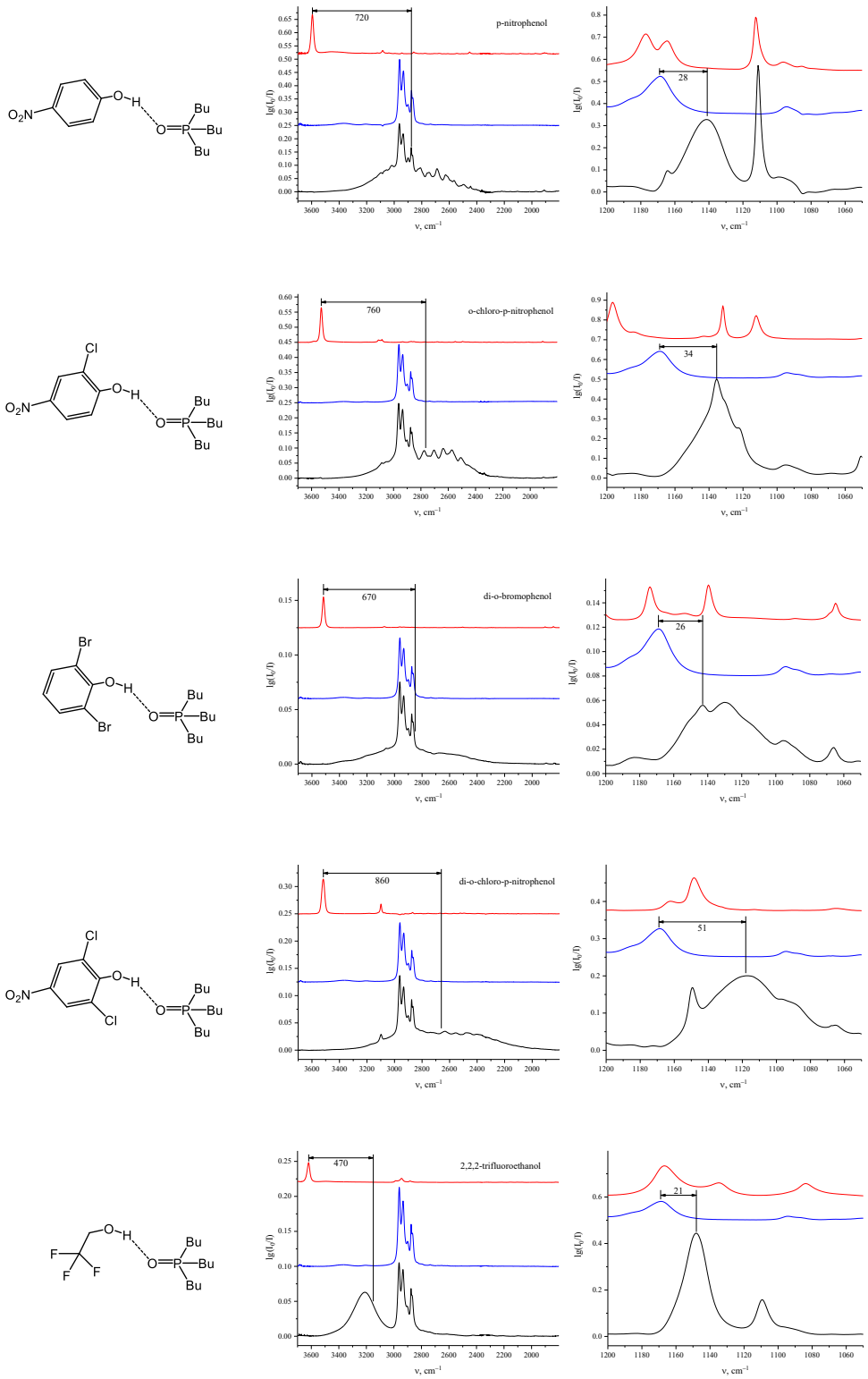

Figure C5. Parts of IR spectra of complexes formed by Bu_3PO and proton donors in CCl_4 solution at room temperature in the regions of (a) OH stretching vibrations (b) P=O stretching vibrations. The spectra of free proton donors (red), free Bu_3PO (blue) and their complexes (black) are shown. Vertical bars indicate locations of OH and P=O vibrational bands for individual compounds and their complexes.

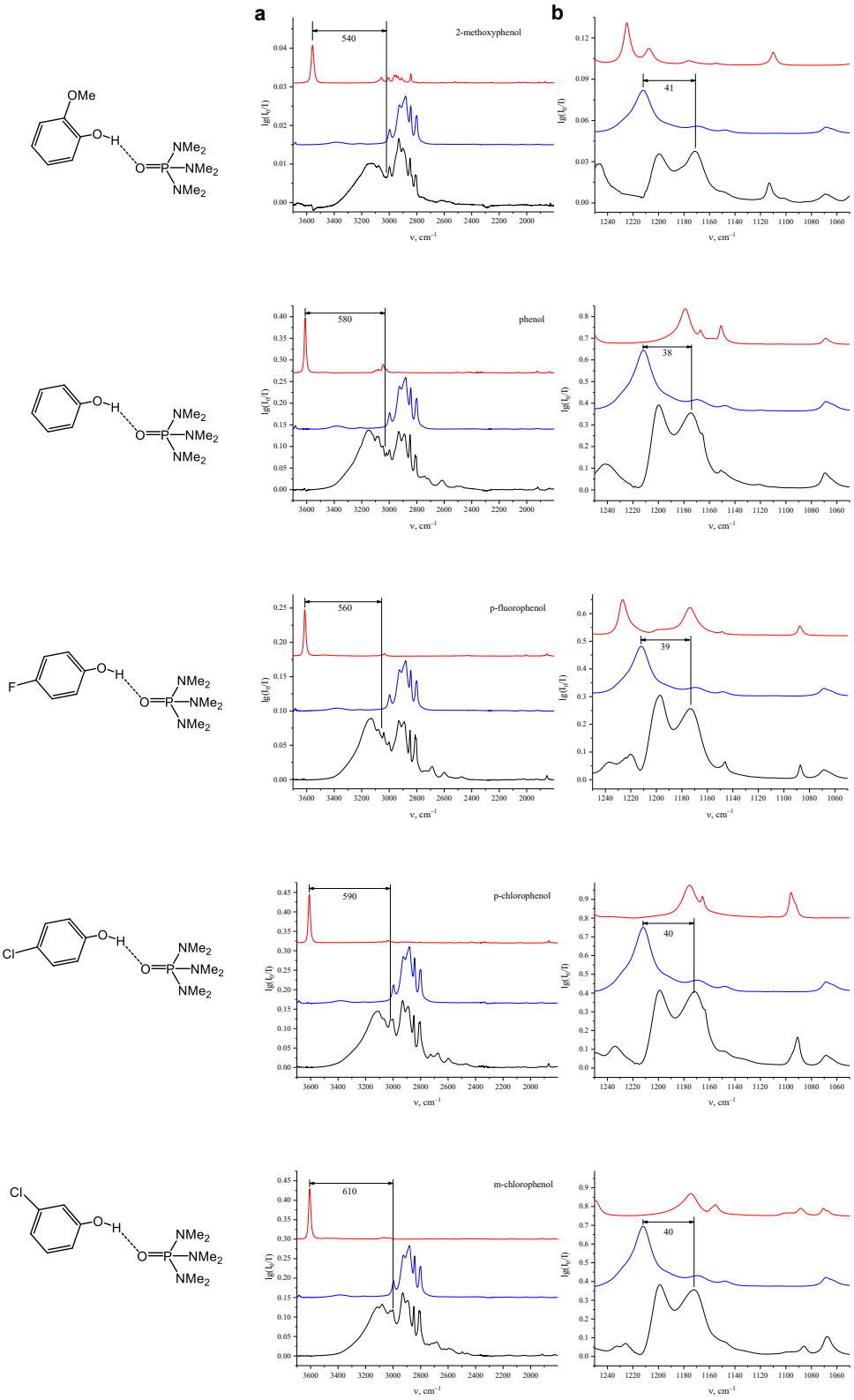

Figure C6. Continued on next page.

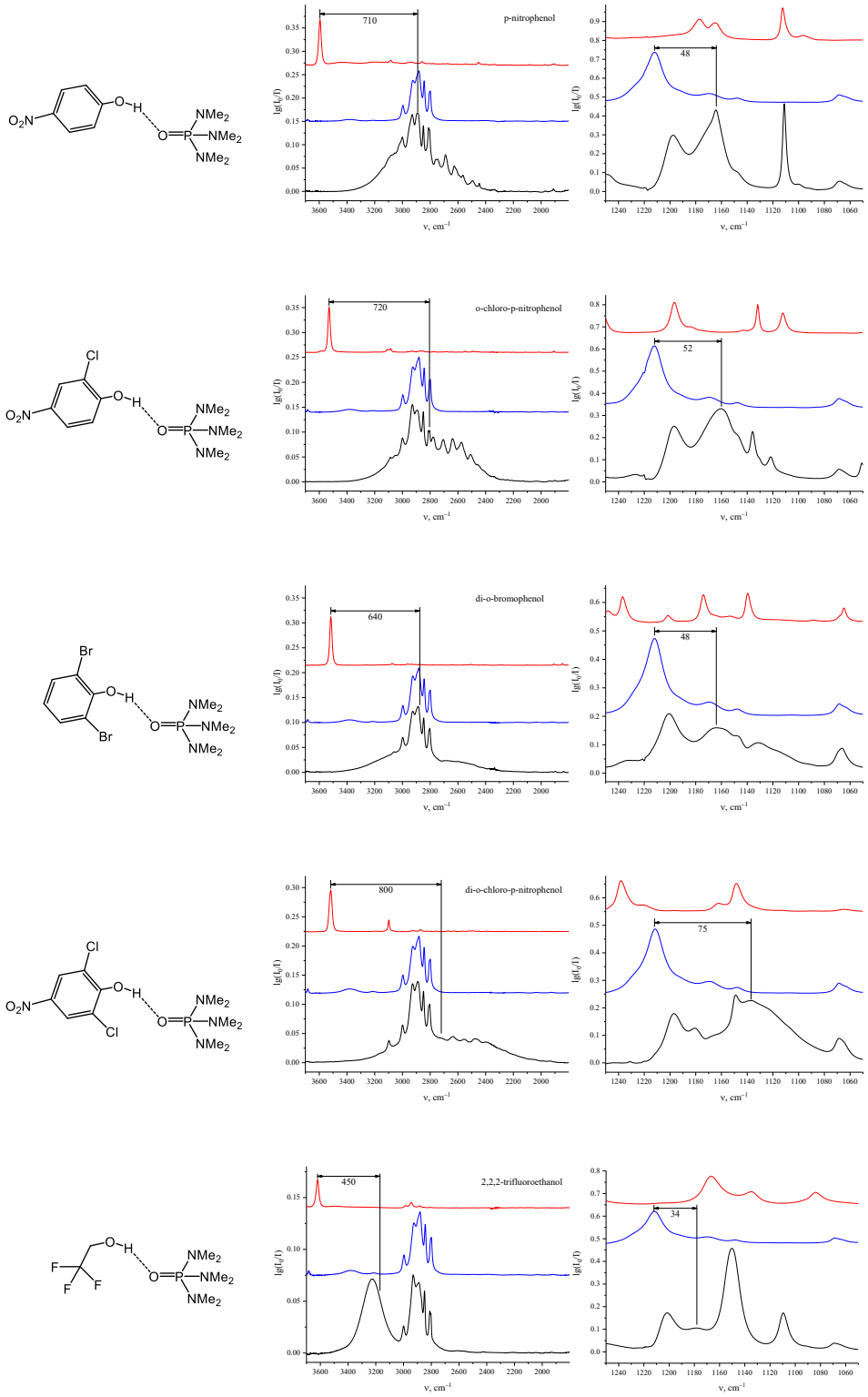

Figure C6. Parts of IR spectra of complexes formed by $(Me_2N)_3PO$ and proton donors in CCl_4 solution at room temperature in the regions of (a) OH stretching vibrations (b) P=O stretching vibrations. The spectra of free proton donors (red), free $(Me_2N)_3PO$ (blue) and their complexes (black) are shown. Vertical bars indicate locations of OH and P=O vibrational bands for individual compounds and their complexes.